UNIVERSITY OF CALIFORNIA SAN DIEGO

Epidermal Sensor System for Monitoring Liquid Swallowing Behavior

A Dissertation submitted in partial satisfaction of the requirements for the degree

Doctor of Philosophy

in

Chemical Engineering

by

Beril Polat

Committee in charge:

Professor Darren J. Lipomi, Chair
Professor Ertugrul Cubukcu
Professor James Friend
Professor Tina Nga Ng
Professor Nisarg Shah

2022

The Dissertation of Beril Polat is approved, and it is acceptable in quality and form for publication on microfilm and electronically.

University of California San Diego

2022

DEDICATION

I dedicate this thesis to my mom and my dad for providing me the opportunity to pursue higher education.

TABLE OF CONTENTS

LIST OF FIGURES

LIST OF TABLES

ACKNOWLEDGEMENTS

The past six years have been very inspiring and empowering in many ways. I was challenged mentally, emotionally, and physically but I persevered and completed the tasks that were ahead of me. This wouldn't have been possible without the help of the people around me. During this time, I learned to ask for help. Thankfully, I was surrounded by mentors, friends, and family who lift me up every single time I needed it.

During the first two years of my Ph.D., I thank all my labmates in Prof. Sirbuly's lab, especially Dr. Yuesong Shi and Dr. Conor Riley. Dr. Shi and I had the same attitude towards solving problems and that enabled us to publish in Nature Protocols together. I appreciated her encouragement and love of Harry Potter. Similarly, Dr. Riley was a mentor to me when I needed to brainstorm ideas or think about my career development. His mini-lectures were always very helpful. Lastly, I thank Prof. Sirbuly for giving me the opportunity to start my Ph.D. at UC San Diego.

Switching to Lipomi Lab was one of the best decisions I made during my six years in graduate school. I came up with the ideas and methods for this thesis in this laboratory. I thank Prof. Laure Kayser, Prof. Charles Dhong, Dr. Sam Root and Dr. Cody Carpenter for introducing me to the lab and helping me start my journey in this lab. They were true mentors and friends inside and outside the laboratory. I thank Dr. Julian Ramirez for being the best coworker, friend, and mentor one can ask for. I appreciated his "let's talk for real" moments when I needed to hear constructive criticism. I always had the best advice from him. I thank Laura Becerra, Tarek Rafeedi, and Dr. Rachel Blau for being my brainstorming buddies and helping me accomplish this work. Their help got me through the deadlines every time. I thank Dr. Rory Runser, Dr. Andrew

Kleinschmidt, and Alex Chen for always being open to proofreading my work and helping with crucial supplemental experiments for my project. Everyone in this lab has helped me get to where I am now so I thank everyone in the Lipomi Lab. Finally, I thank the best mentor, boss, and teacher out there, Prof. Darren Lipomi. I am glad our paths intercepted, and you agreed to mentor me for the rest of my Ph.D. This work truly wouldn't be possible if it wasn't for your mentorship, ideas, and professional connections.

Lastly, I thank all my friends and family who helped me get up and continue researching every day. From the beginning, I was able to keep a healthy work-life balance thanks to the UCSD Triathlon Team members. I thank my family for always being one phone call away to discuss stressful times and assuring me every time. I wouldn't have made it without you.

I also include the following acknowledgments below as required by the University of California, San Diego.

Chapter 1, in part, will be submitted for publication of the material as it may appear in Advanced Healthcare Materials. Beril Polat, Tarek Rafeedi, and Darren J. Lipomi. 2022. The dissertation author was the primary investigator and author of this paper.

Chapter 2 and Appendix A, in full, is a reprint of the material as it appears in ACS Applied Nano Materials, 2021, 4 (8), 8126-8134. Beril Polat, Laura L. Becerra, Po-Ya Hsu, Vineel Kaipu, Patrick P. Mercier, Chung-Kuan Cheng, and Darren J. Lipomi. American Chemical Society, 2021. The dissertation author was the primary investigator and author of this paper.

Chapter 3 and Appendix B, in part, will be submitted for publication of the material as it may appear in Advanced Healthcare Materials. Beril Polat, Tarek Rafeedi, Laura L. Becerra,

Alexander X. Chen, Kuanjung Chiang, Vineel Kaipu, Rachel Blau, Patrick P. Mercier, Chung-Kuan Cheng, and Darren J. Lipomi. 2022. The dissertation author was the primary investigator and author of this paper.

Chapter 4, in part, is under preparation for publication of the material. Beril Polat, Tarek Rafeedi, and Darren J. Lipomi. 2023.

VITA

2015	Bachelor of Science in Chemical and Biomolecular Engineering
	Johns Hopkins University
2016	Master of Science in Chemical and Biomolecular Engineering
	Johns Hopkins University
2022	Doctor of Philosophy in Chemical Engineering
	University of California San Diego

PUBLICATIONS

B, Polat, T. Rafeedi, D. J. Lipomi*, "Materials-Enabled Flexible and Wearable Sensors for Monitoring the Swallowing Activity", In progress. 2022.

B. Polat, T. Rafeedi, L.L. Becerra, A. X. Chen, K. Chiang, V. Kaipu, R. Blau, P.P. Mercier, C.K. Cheng, D.J. Lipomi*, "External Measurement of Swallowed Volume during Exercise Enabled by Stretchable Derivatives of PEDOT:PSS, Graphene, Metallic Nanoparticles, and Machine Learning", In progress. 2022

R. Blau, A. Chen, **B. Polat**, L.L. Becerra, R. Runser, B. Zamanimeymian, K. Choudhary, D.J. Lipomi*, "Intrinsically Stretchable Block Copolymer Based on PEDOT:PSS for Improved Performance in Bioelectronic Applications", *ACS Applied Materials & Interfaces*, 2022, Vol. 14 (4), 4823-4835

B. Polat, L.L. Becerra, P. Hsu, V. Kaipu, P.P. Mercier, C.K. Cheng, D.J. Lipomi*, "Epidermal Graphene Sensors and Machine Learning for Estimating Swallowed Volume", *ACS Applied Nano Materials*, 2021, Vol. 4 (8), 8126-8134

J. Ramirez, **B. Polat**, D.J. Lipomi*, "Metallic Nanoislands on Graphene for Biomechanical Sensing", *ACS Omega*, 2020, Vol. 5 (26), 15763-15770

C.W. Carpenter, M.G. Malinao, T.A. Rafeedi, D. Rodriquez, S.T.M. Tan, N.B. Root, K. Skelil, J. Ramirez, **B. Polat**, S.E. Root, V.S. Ramachandran, D.J. Lipomi*, "Electropneumotactile Stimulation: Multimodal Haptic Actuators Enabled by a Stretchable Conductive Polymer on Inflatable Pockets", *Advanced Materials Technologies*, 2020, Vol. 5 (6), 1901119

Y. Shi†, **B. Polat**†, Q. Huang, D. Sirbuly*, "Nanoscale fiber optic force sensors for mechanical probing at the molecular and cellular level", *Nature Protocols*, 2018, Vol. 13 (11), 2714-2739

Q. Jin, M. Li, **B. Polat**, S. K. Paidi, A. Dai, A. Zhang, J. V. Pagaduan, I. Barman*, D. H. Gracias*, "Mechanical trap surface-enhanced raman spectroscopy for three-dimensional surface molecular imaging of single live cells", *Angewandte Chemie International Edition,* 2017, Vol. 56, pg. 1-5

K. Malachowski, M. Jamal, Q. Jin, **B. Polat**, C. J. Morris, D. H. Gracias*, "Self-folding single cell grippers", *Nano Letters,* 2014, Vol. 14, pg. 4164-4170. *Highlighted in Nature and Nature Nanotechnology.*

† Co-first author

* Corresponding author

ABSTRACT OF THE DISSERTATION

Epidermal Sensor System for Monitoring Liquid Swallowing Behavior

by

Beril Polat

Doctor of Philosophy in Chemical Engineering

University of California San Diego, 2022

Professor Darren J. Lipomi, Chair

Assessment of liquid intake is necessary to obtain a complete picture of an individual's hydration status. Measurements using state-of-the-art wearable devices have been demonstrated, but none of these devices have combined high sensitivity, unobtrusiveness, and automated estimation of volume, i.e., using machine learning. Such a capability would have immense value in a variety of medical contexts, such as monitoring patients with dysphagia or the performance of athletes. This dissertation first surveys the literature for existing materials-enabled sensors used to detect and/or monitor swallowing activity. Next, a new epidermal sensor platform is introduced to address the issues that still exist in this field. This epidermal sensor platform is combined with machine learning to measure swallowed liquid volume based on signals obtained from the surface of the skin. The key sensors of the device are a composite piezoresistive sensor consisting of single-layer graphene decorated with gold nanoislands and coated with a highly plasticized form of the conductive polymer poly(3,4-ethylenedioxythiophene):poly(styrenesuflonate) (PEDOT:PSS) and a surface electromyography (sEMG) sensor comprised of PEDOT that is electrostatically bound to poly(styrenesulfonate)-*b*-poly(poly(ethylene glycol) methyl ether acrylate) (PSS-*b*-PPEGMEA). The use of strain and sEMG measurements together both (1) improve the accuracy of estimated swallowed volumes and (2) permit the differentiation of swallowing from motion artifacts. Finally, the performance of this sensor platform is tested with two cohort studies where participants are in a resting position or exercising during a swallow. The combined measurements of strain and sEMG from these studies—processed by the machine learning algorithm—can estimate unknown swallowed volumes cumulatively between 5 to 30 mL of water. Ultimately, this system holds promise for numerous applications in sports medicine, rehabilitation, and the detection of nascent dysfunction in swallowing.

Chapter 1 Materials-Enabled Flexible and Wearable Sensors for Monitoring the Swallowing Activity

Abstract

Swallowing is an integral process of water and nutrient intake. Swallowing difficulties or abnormalities can severely impact a person's immediate health causing dehydration, malnutrition, aspiration pneumonia, weight loss, anxiety, or even death by asphyxia. To detect the onset of swallow disorders, it is imperative to regularly monitor those who are at risk of developing it. The emerging field of wearable sensors has lent itself to understanding the nature of deglutition behavior in non-invasive and unobtrusive ways. The published work in this field so far strives to come closer to having a remote monitoring system where the travel time and cost of clinics can be reduced to a minimum. In this review, we specifically survey the newest literature on materials-enabled wearable devices that are aimed to detect and/or monitor swallowing behavior. We examine both proof-of-concept and cohort study experiments while focusing on the novel materials and mechanisms used for sensing. We also discuss some advantages and disadvantages of these non-invasive monitoring sensors and future work that needs to be done.

1.1 Introduction

Oropharyngeal swallowing, scientifically known as deglutition, is a physiological process where the neck and throat muscles move a portion of the food or liquid from mouth to stomach. The process starts with a voluntary initiation and continues with a series of involuntary reflexes of the muscles.[1] There are different models described for solid and liquid food swallows. For liquid swallow, the Four Stage Model is used whereas for the solid swallow, the Process Model of Feeding is used.[2,3] With the help of these established models, monitoring swallow function has been a popular field of interest for the diagnosis and therapy of swallowing disorders such as dysphagia. Although the condition of dysphagia can be treated with speech and language therapy, it isn't always completely curable.[4,5,6,7] Patients develop this condition as a result of obstructive or damaged tissue from injury or surgery, or it could be neurological or muscular in origin as an effect of aging.[5,8,9,10] There are different exercise maneuvers that are designed to prevent the further development of this condition[11,12,13,14,15,16,17,18,19,20,21,22,23,24,24], however, once dysphagia advances, it becomes very difficult to regain the swallowing ability for the patients.[25,26] If left untreated, it can cause aspiration pneumonia, weight loss, and anxiety over the nutritional intake.[27,28,29] The current gold standard methods of dysphagia diagnosis include videofluoroscopy[30,31,32,33] and endoscopy[34,35,36] which are expensive and both require clinicians to operate the equipment. Additionally, videofluoroscopy exposes patients to radiation through X-ray and barium-modified boluses. The details on these clinical methods of monitoring swallowing are out of this review's scope.

In this review, we will start with a brief overview of the anatomy involved in swallowing and measurable signals during a swallow. After that, we will introduce different sensing modalities used for detecting and monitoring swallowing activity which include strain, pressure,

electromyography (EMG), and acoustic sensors. Within each sensing modality, we will survey different novel materials used to achieve these sensor types and how they are used to detect swallowing behavior. In the end, we will discuss the challenges and opportunities in these materials-enabled sensors for monitoring swallowing activity. We will keep the focus of this review on the novelty of the sensors that are materials-enabled for monitoring oropharyngeal swallowing. The esophageal phase of swallowing is beyond the focus of this review.

1.2 Swallowing Physiology

Swallowing is a physiological process starting with a voluntary act and continuing with the precise coordination of more than 30 pairs of muscles.[37] It recruits different layers of the central nervous system from the cerebral cortex to the medulla oblongata.[38] The anatomy of swallowing involves many structures starting with the oral cavity, pharynx, larynx, and esophagus (**Figure 1.1a**).[2,39,40] Along with these structures, other muscles, bones, cartridges, and saliva glands work in coordination to move the bolus from the oral cavity to the esophagus. The physiology of swallowing is described differently for liquid and solid boluses. For swallowing liquids, the Four Stage Model is used, whereas for swallowing solids, the Process Model is used.[3,41,42]

The Four Stage Model consists of four phases during a swallow (**Figure 1.1b**). The first phase is called the Oral Preparatory stage and it starts after a liquid bolus is taken into the mouth by a cup or straw. The bolus is held on the tongue surface while the anterior and posterior of the oral cavity are sealed to prevent leakage into the oropharynx. The second phase is called the Oral Propulsive stage where the tongue propels the bolus from the anterior of the oral cavity to the posterior into the pharynx. The next phase, the Pharyngeal stage, happens to overlap with the Oral Propulsive stage for the liquids. For the solids, the Process Model provides more information

before the Pharyngeal stage. After ingestion of the solid, the Stage Transport stage begins where the tongue carries the bolus to the post-canine region onto the lower teeth for chewing. Immediately after the first transport stage, the Food Processing stage starts. This is when the food particles are reduced in size until the food size is optimal for swallowing. During the processing stage, the cyclic jaw movement is established with the coordination of the tongue, cheek, soft-palate, and hyoid bone.[3,43] Unlike liquid swallow, the posterior oral cavity isn't completely sealed during this phase allowing air with the food aroma to be pushed through the pharynx to the chemoreceptors in the nose.[44,45,46] In Stage II Transport, very similar to the Oral Propulsive Stage, the soft food gets pushed into the oropharynx by the tongue. For both the liquids and solids, the next phase is the Pharyngeal Stage which is a rapid movement within a second. This stage is crucial in propelling food through the pharynx into the esophagus while keeping the airway protected by insulating the larynx and trachea from the pharynx. With the elevation of the soft palate and tongue base retraction, the bolus is pushed against the pharyngeal walls and squeezed downwards. In order to protect the airways, the vocal folds are closed to seal the glottis.[47,48] The arytenoids are tilted forward to contact the epiglottic base while the hyoid bone and larynx are pulled upward by the contraction of the suprahyoid muscles and thyrohyoid muscle. At this step, the epiglottis tilts backward to seal the laryngeal vestibule and the upper esophageal sphincter (UES) opens up to allow the bolus to pass into the esophagus.[49,50,51] Once the bolus is in the UES, the Esophageal Stage starts. During this stage, the bolus is moved from UES to the lower esophageal sphincter (LES) and eventually into the stomach via peristaltic wave motion of the tubular esophagus structure.

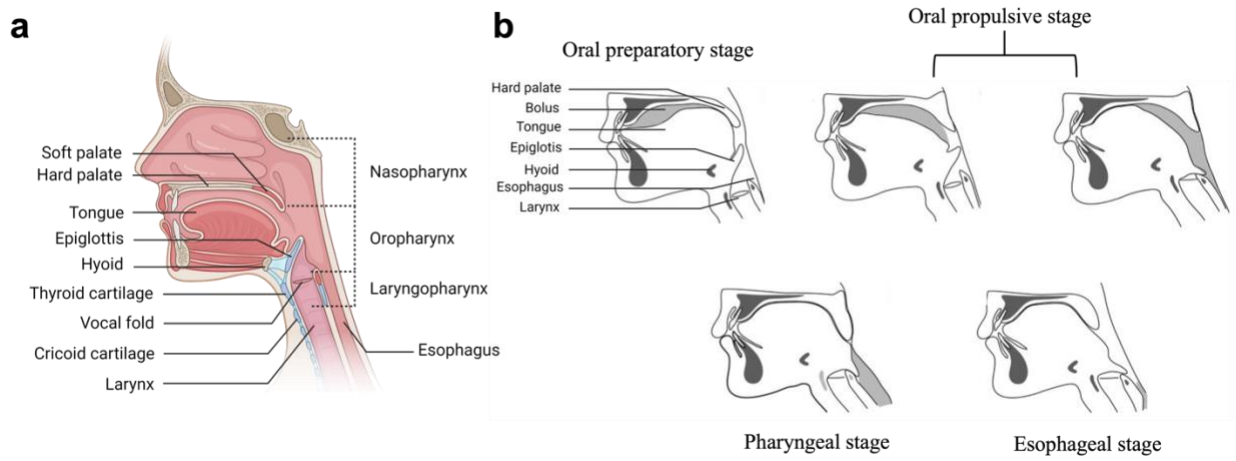

Figure 1.1. Swallowing anatomy and physiology. **(a)** A schematic diagram of the human head anatomy is shown. The diagram shows all the main structures involved in swallowing. **(b)** A schematic shows the different stages of a liquid swallow. Reproduced with permission.[2]

The coordination of the muscles contracting, and relaxing is an important aspect of swallowing. It aids with bolus transportation throughout the process. Hence, it has been studied extensively using electromyography methods. The muscle groups that are studied in detail include the jaw and perioral muscles, submandibular/suprahyoid muscles, tongue muscles, laryngeal, and pharyngeal muscles, and cricopharyngeal (CP) muscle of the UES.[38,52] For the jaw, perioral, and submandibular muscles, it is easier to pick up muscle EMG signals superficially with an epidermal electrode, whereas for the tongue, laryngeal, pharyngeal, and CP muscles, needle EMG electrodes or intralaminar catheter EMG electrodes are required.

In addition to neuromuscular activities extracted using EMG, which are electrical in nature, the literature examines mechanical motion resulting from this neural signal. The common targets of mechanical detection are the submental muscle contraction and the vertical motion of the larynx (laryngeal excursion). In the literature on dysphagia, according to Clave and Shaker, slow or delayed laryngeal vestibule closure, which is assisted by the larynx's motion, is indicative of

swallow abnormalities.[4] Studies done using sEMG show that submental muscle contractions were longer in duration for dysphagic subjects compared to non-dysphagic controls.[53] As shown in some studies in the review, such difference in muscle contraction is detectable by superficial probing of skin deformation.

The scope of this review will be the activation of submandibular muscles during the swallow. The studies using surface EMG electrodes for the submandibular muscles are vast. They include different volumes of boluses to see the activation potential differences in the muscles. It is important to understand the anatomy and physiology of swallowing before designing novel sensors. There are many structures on the mouth, neck, and throat that play a role in swallowing, and it is essential to know which part of this highly coordinated process the sensors will be collecting information from. The newer sensing modalities can shed light onto unknown parts of this process and there exist a few different ways to do so.

1.3 sEMG-Based Wearable Sensors

Surface electromyography (sEMG) is widely applied in wearable biosensors. It has been used in applications such as tremor diagnosis, wireless monitoring of exercise activity, aiding muscle rehabilitation, gait assessment, and detection of bruxism among other applications.[54,55,56,57,58] sEMG wearable sensors also show promise in detecting and characterizing seizures.[59] In this section we discuss sEMG electrodes for their role in swallow assessment and detection of dysphagia.

In general terms, the sEMG electrodes need to be used as a pair since they measure the voltage difference between each electrode. This voltage difference occurs due to the action potential that travels from the nerve cell to the muscle to induce a contraction. This creates a

depolarization zone that shifts along with the muscle fiber as a "motor unit action potential (MUAP)". If electrodes are on the muscle, the measured signal shows the depolarization and the subsequent repolarization phase which form a bipolar voltage change. The raw signal can later be pre-processed to extract frequency features for determining the timing, force, and fatigue of the muscle.

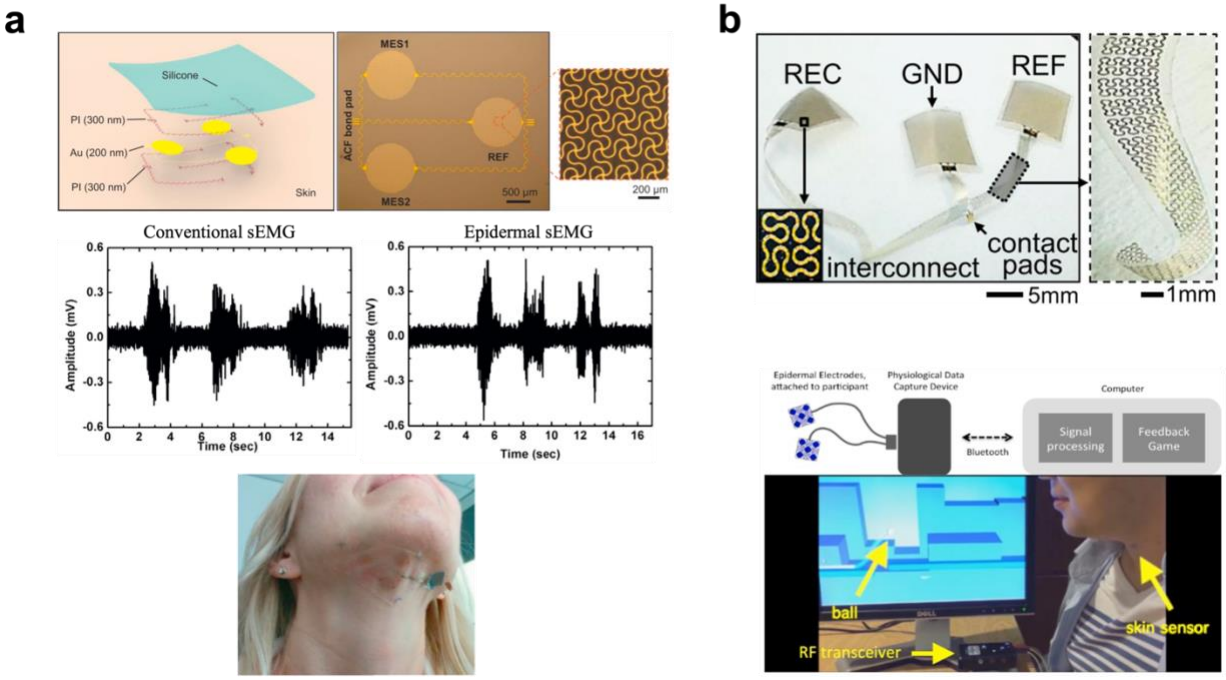

Figure 1.2. The sEMG-based electrodes designed for the detection of swallowing behavior. **(a)** One of the first applications of epidermal metal films used to detect swallowing by Constantinescu et al. Reproduced with permission.[60] **(b)** Another gold thin film epidermal sEMG sensor was used by Nicholls et al. to create a feedback game using the swallowing signals collected from the sensor patch. The epidermal sensor figure[61] and the feedback game[62] schematic are both reproduced with permission.

The most commonly used sEMG electrode for monitoring swallow has been the conventional Ag/AgCl electrodes with wet conductive gels. These electrodes exhibit very stable electrical properties and are thus preferred in clinical conditions and research. Despite their desired electrode-skin impedance values, over time these gel electrodes dry out and coagulate eventually

becoming unusable for long-term purposes. Therefore, the field has moved to search for dry electrodes with similar electrical and mechanical properties.[63] As one of the first groups, Constantinescu et al. demonstrated a pilot study for detecting different swallowing maneuvers using thin, light, and conformal gold electrodes in a mesh design support on a silicon substrate (**Figure 1.2a**).[60] They used three gold electrodes (200 nm thick) in a mesh filamentary serpentine design (two for sensing, one for reference). The mesh electrodes had a 20 μm width and a radius of curvature of 45 μm. The mesh design and the polyimide support layer under the gold electrodes allowed this sensor to achieve over 30% elasticity. They conducted the swallow experiments while the participants were seated near a desk since the cable connection was needed to collect signals. The comparison of a conventional sEMG adhesive patch and their epidermal sEMG patch showed very similar signal amplitudes for a saliva swallow proving the efficacy of the new electrodes. A year later, Nicholls et al. demonstrated "skin-like electronics" being used to measure electrophysiological signals (sEMG) using a similar fabrication process to Constantinescu et al (**Figure 1.2b**).[62] Their skin-like electrode was also made from a gold nano-membrane electrode (300 nm thick) with a fractal design integrated onto two types of soft elastomeric membranes (silicone) with 5 μm thickness. The electrode fabrication included a series of photolithography steps and was previously used to make electrodes for electroencephalography (EEG) to study human brain activity.[61] Although the electrodes were not novel, their experimental procedures were. They utilized the collected sEMG data from the epidermal electrodes to create a swallow feedback-based game. After transferring the data to a computer via Bluetooth, they applied upper and lower thresholds to the signal amplitude and assigned a ball to jump when there was a swallow detected in a video game. Even as a proof-of-concept, this novel approach encouraged participants to engage with the swallowing experiments. The same group published a more in-depth analysis

of this “human-computer interaction” within the same year to demonstrate the clinical feasibility of treating swallowing disorders.[64] At this point, research groups understood the need for a sensor platform with an additional sensing modality to confirm the sEMG swallow signals from the motion artifacts. Towards this goal, Kim et al. designed the first combined epidermal sEMG and strain patch to detect the swallowing event (**Figure 1.3a).**[65] The patch had an interconnect base in a honeycomb design with two sets of sEMG electrodes and a commercially available piezoresistive strain gauge strip. The interconnects consisted of a 13 μm thick polyimide sheet with a 9 μm thick copper film and were encapsulated with two soft elastomers (10 μm thick Silbione and 5 μm thick EcoFlex) with a core/shell layout. Later, they electroplated the skin exposed sEMG electrode area with gold (500 nm) to ensure biocompatibility. The honeycomb shape and the elastomers allowed this patch to have robust electrical and mechanical properties as well as adhesiveness to the skin. The group tested the sensor patch on a healthy subject as well as a dysphagia patient to compare the swallowing behaviors. They were able to confirm the detection of swallow in each case and suggested that this platform can be reusable between subjects. This work also utilized a Bluetooth data transmission unit which made the platform more desirable for clinical settings. Later, the same group conducted a validation study with forty healthy adults to confirm their results.[66]

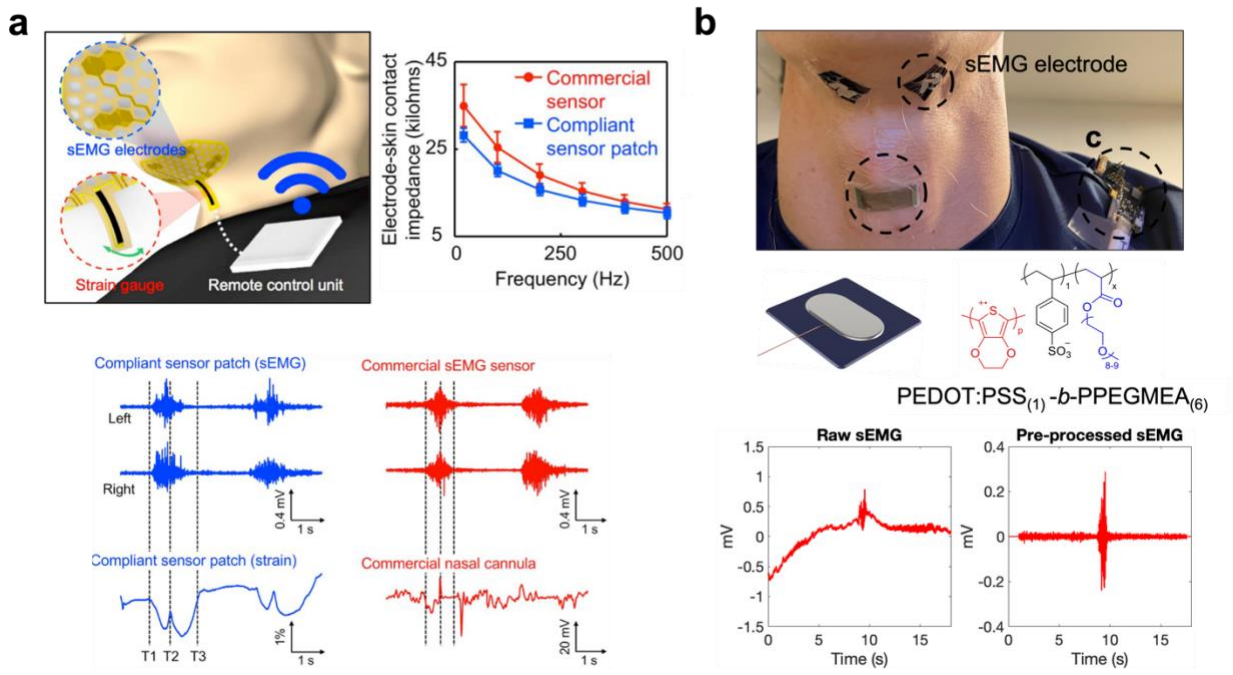

Figure 1.3. The sEMG-based electrodes designed for the detection of swallowing behavior. **(a)** An epidermal sensor patch integrated both with metal thin film sEMG electrodes and a commercial strain gauge strip (reproduced with permission).[65] **(b)** PEDOT:PSS-based sEMG electrode used for detection of swallow.

Metal thin films have been the material choice for the electrodes until conductive polymers started gaining more attention in the field. The advantages of the conductive polymers included their machinability, tunability of electrical and mechanical properties, and biocompatibility. Among them, poly(ethylenedioxythiophene):poly(styrenesulfonate) (PEDOT:PSS) has become a very popular one to use as a dry sEMG electrode. Without any modifications, PEDOT:PSS is not very stretchable or adhesive to the skin. However, Blau et al. were able to formulate and synthesize PEDOT:PSS$_{(1)}$-*b*-PPEGMEA$_{(6)}$ block copolymer[67] with great success, and Polat et al. tested sEMG films made from this polymer for detection of swallowing on the throat (**Figure 1.3b**). Even though this was the only conductive polymer used in detecting sEMG signals from the swallowing behavior, there exist many other conductive polymers that were used for different muscle groups in the body. However, these are out of the topic range of this review.

1.4 Strain-Based Wearable Sensors

Strain gauges are defined as materials that experience a change in electrical resistance when they are mechanically deformed. In recent years, strain gauges have been applied to many wearable devices for healthcare monitoring, prosthetics, sports, and entertainment. Recent developments in organic and inorganic materials and nanocomposites have led to a plethora of application studies on wearable strain gauges. From applications in electronic skin to heartrate monitoring, strain gauges offer a range of sensitivity, stretchability, and scale.[68,69,70,71] Their performance as a sensor is defined by the term "gauge factor" (GF) which gives a relative change in electrical resistance of material over an applied strain.[72] Strain sensors placed on the throat typically incur bending or tensile strain under the mechanical forces exerted by swallow action, generating a signal. One of the first materials-enabled strain sensors used to detect swallowing as well as small motions on the face was from Roh et al.[73] They reported a novel three-layer stacked strain sensor made up of single-wall carbon nanotubes (SWCNTs), PEDOT:PSS, and polyurethane (PU) (**Figure 1.4a**). All the individual materials were water-soluble which made the fabrication of the strain sensor relatively easy. This nanohybrid structure had tunable stretchability (over 100%), optical transparency (~63%), strain sensitivity, and stability. Different concentrations of SWCNTs in the mix enabled them to have different gauge factor values due to the increased conductivity and sensitivity to strains. In general, 1 mg/ml SWCNTs concentration exhibited gauge factors between 39.4 to 837.1 for strains 1.6 to 3.5% and had a stable resistivity response to cyclic strain measurements over 200 cycles. From the same group, Hwang et al. low-density silver nanowires (AgNWs) with PEDOT:PSS/PU to fabricate a strain sensor (**Figure 1.4b**).[74] Similarly, this sensor showed high optical transparency (~75.3%), stretchability (up to 100%), and sensitivity to strain

(GF = 12 for 2% strain). In addition to its physical properties, this sensor was driven by a supercapacitor (SC) that was charged by a triboelectric nanogenerator (TENG). Both electrodes in the SC and TENG layer used the same materials that were used in the strain sensor layer, namely AgNWs/PEDOT:PSS/PU. The conductivity and the stretchability of this stacked material composite worked well for all the different layers and allowed them to experiment detection of small motions on a participant's neck including saliva swallowing and eating. They demonstrated some of these experiments when the strain sensor was powered by the supercapacitor. Both papers proved that a fine-tuned mix of conductive nanoparticles with conductive polymers was sensitive and stable enough to make a strain sensor that can detect a small motion such as swallowing.

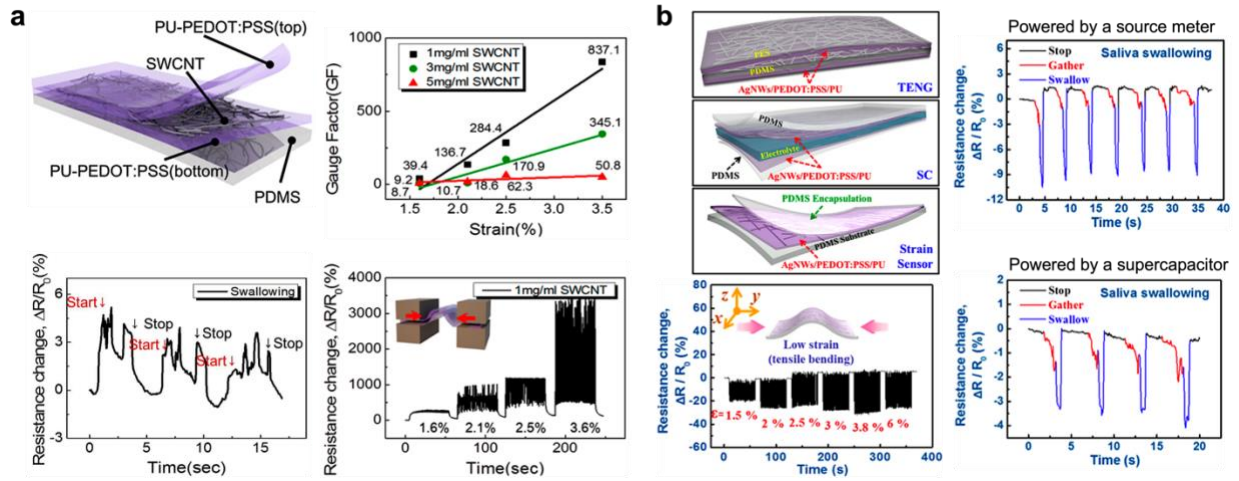

Figure 1.4. Carbon nanotube (CNT) and silver nanowire (AgNW)-based elastomeric strain sensor designs for detection of swallowing behavior. **(a)** Roh et al. used SWCNTs with the elastomeric PEDOT:PSS/PU mix as a strain sensor to detect saliva swallowing as a demonstration. Reproduced with permission.[73] **(b)** Hwang et al. adopted the same elastomeric base but mixed with AgNWs and stacked it up with a layer of SC and TENG for power consumption. They also demonstrated detection of saliva swallow when the strain sensor was powered by a conventional source meter and by the SC. Reproduced with permission.[74]

Another use of conductive nanoparticles as a strain sensor was by Zhu et al. to monitor human motions including swallowing (**Figure 1.5a**).[75] They opted to use copper nanowires

(CuNWs) because of the abundance of copper, its low cost, and excellent electrical conductivity. However, CuNWs get oxidized in the air over time, so they embedded CuNWs into water-dispersible modified graphene (WGP) sheets to form an even more conductive film. After sandwiching this hybrid film with an elastomer, polydimethylsiloxane (PDMS), they characterized the electrical and mechanical properties as well as demonstrations on swallowing detection. As they increased the WGP concentration to 33.3 wt% in the hybrid film, they observed an increase in the electrical conductivity up to 3.02 x 10^4 S/m but the concentrations above 34 wt% WGP showed a decrease in the electrical conductivity. They hypothesized that the CuNWs were acting like a conducting bridge between the WGP sheet junctions at low WGP density and thus enhancing the overall conductivity. When the density of WGP increased, the CuNWs were getting more disconnected from each other and thus exhibiting lower conductivities. However, the sensitivity at 2% strain was exceptionally good with a GF value of ~175,000. The overall PDMS-encapsulated strain sensor had a tensile fracture strain of 120% and thus even after the cyclic strain-relaxation testing, the sensor maintained its original electrical properties. Graphene was also used by another group to construct a conductive material composite for a strain sensor. Ramirez et al. investigated a piezoresistive strain sensor comprising palladium nanoislands (PdNIs) on single-layer graphene (Gr) to detect swallowing differences between healthy and dysphagic patients using machine learning (**Figure 1.5b**).[76] It is reported that graphene alone does not exhibit exceptional piezoresistivity. However, when ultra-thin films of metals (<10 nm) are evaporated on top of the graphene, it has been observed that instead of a continuous film, they form island-like structures.[72] This was believed to be due to the changes in the electronic band structure of graphene during the initial stages of metallization. This composite material strain sensor had very high resolution and sensitivity at a low strain regime (GF = ~17 for 0.0001% or 1 ppm and GF = 125 for 0.001%, 10

ppm) and was easily transferrable to any substrate of choice. The group chose to transfer Gr/PdNIs onto Kapton tape to make a flexible strain sensor and detected swallowing differences between healthy and dysphagic subjects as well as different types of boluses. Later, a custom-crafted machine learning algorithm was used to classify the swallowing signals as healthy or dysphagic for future determination of dysphagia onset. Similarly, Polat et al. used the same graphene/ metallic nanoisland composite to predict different swallowed liquid volumes using machine learning (**Figure 1.5c**).[77] They used 8 nm thick gold nanoislands (AuNIs) on top of a single graphene layer due to the ultra-sensitivity at a low strain regime and the near-zero temperature coefficient of the gold nanoislands at that thickness. Instead of Kapton tape, they transferred the Gr/AuNIs onto the PDMS substrate and coated the AuNIs with a highly plasticized conductive polymer, PEDOT:PSS, mixed with dimethylsiloxane with Triton-X, so-called "PEDOT:PSS dough". This PEDOT:PSS dough acted as another layer for electron transport if the Gr/AuNI film experienced any tears. Without the conductive polymer, Gr/AuNI film stretched only up to 2% strain but after spray-coating the polymer, they reached up to 86% stretchability. Due to the ultra-sensitivity of the Gr/AuNI/PEDOT:PSS dough strain sensor, they were able to detect minute signal differences in different water volumes (5 to 30 ml, in 10 ml increments) and later were able to predict the testing volumes using a machine learning algorithm.

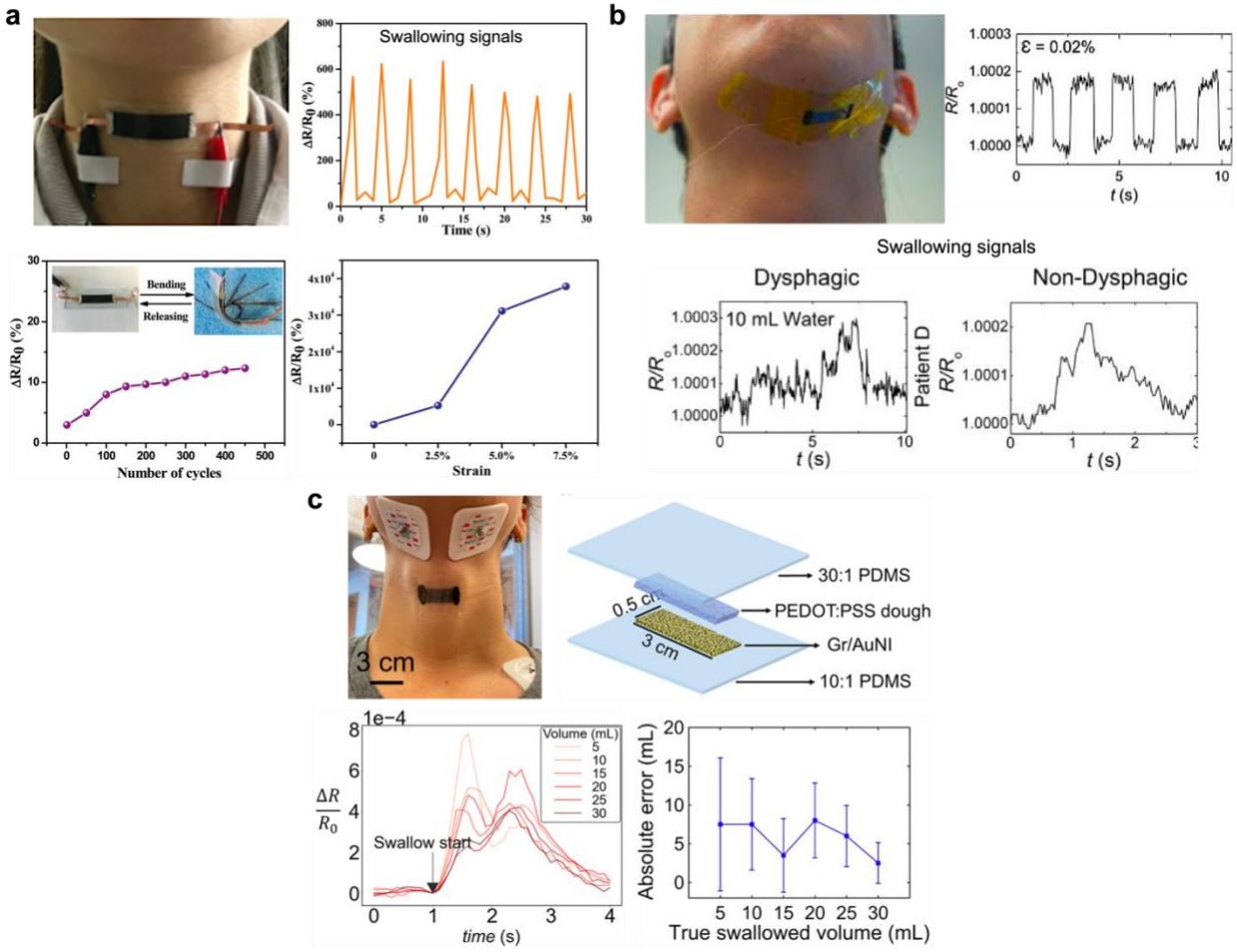

Figure 1.5. Graphene and metallic nanoparticles-based strain sensors for detection and monitoring of swallowing. **(a)** Zhu et al. demonstrated a mix of CuNWs and WGP on a PDMS substrate to show detection of swallowing on the neck. Reproduced with permission.[75] **(b)** Ramirez et al. utilized thin PdNIs on graphene transferred onto a Kapton tape to demonstrate the detection of swallowing differences between healthy and dysphagic subjects using machine learning. Reproduced with permission.[76] **(c)** Polat et al. used a composite of AuNIs on graphene-coated with PEDOT:PSS dough transferred onto PDMS substrate to demonstrate the detection sensitivity of the Gr/AuNI/PEDOT:PSS dough strain sensor between different swallowed water volumes. Reproduced with permission.[77]

The fiber-based strain sensors were also used for swallow detection. For example, Huang et al. used an ultra-thin, flexible, and elastic PU yarn that was dip-coated with graphene nanoplatelets and carbon black (CB)/SWCNTs (**Figure 1.6a**).[78] This sensor was stretchable up to 350% with little hysteresis, had a low detection limit of 0.5%, and had long-term stability (over 2400 cycles). It showed a GF value of 2 for 2.5% strain. In addition to the characterization, they

detected repeated swallowing signals on a subject's neck. Similarly, Zang et al. used a commercial and highly elastic fiber that had a PU core with two layers of helically-wound polyester (PE) fibers (**Figure 1.6b**).[79] They dip-coated their fiber with graphene oxide (GO) and then reduced GO chemically with hydrobromic acid (HBr) to get reduced GO (RGO). The strain sensor had a GF value of ~240 for 5% strain, the conductivity of 1.31 S/m, and was able to detect differences between effortful swallowing versus slow swallowing.

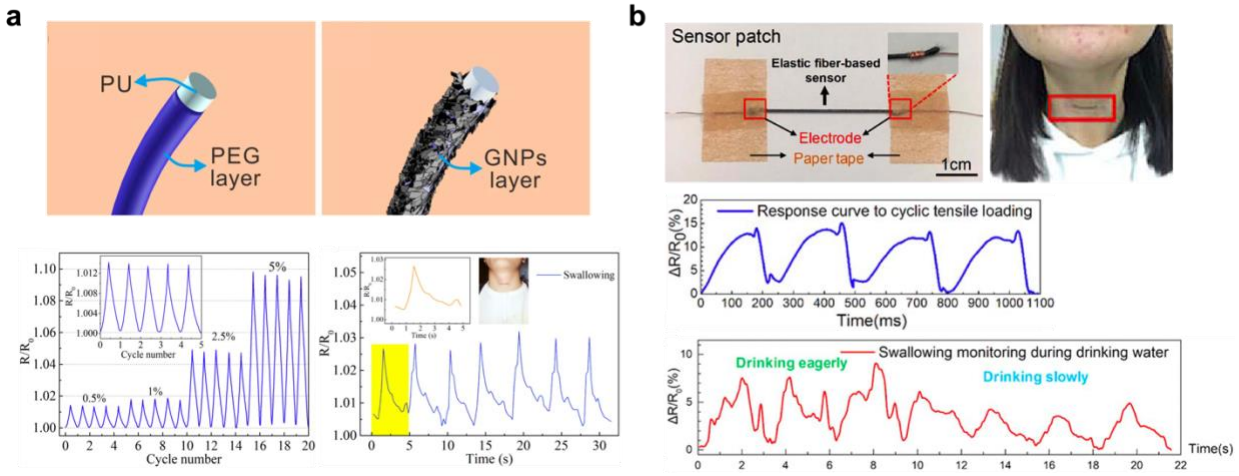

Figure 1.6. Fiber-based strain sensors are dip-coated with conductive materials. **(a)** Huang et al. used a PU fiber to dip-coat graphene nanoplatelets and CB/SWCNTs and made a strain sensor that was able to detect repeated swallowing behavior. Reproduced with permission.[78] **(b)** Zang et al. also used RGO to coat their PU/PE fiber. They were able to detect swallowing differences when it was effortful versus when it was slow and controlled. Reproduced with permission.[79]

As a different approach, Zhang et al. opted to use ionic liquids as a base for their strain sensor (**Figure 1.7).**[80] Specifically, they used 1-ethyl-3-methylimidazolium bis(trifluoromethylsulfonylmide) ([EMIM][TFSI]) as the ionic liquid (IL) encapsulated with PDMS and Eco-Flex elastomeric substrates. They achieved a GF value of 7.9 within 5% strain with a low detection limit of 0.1% strain.

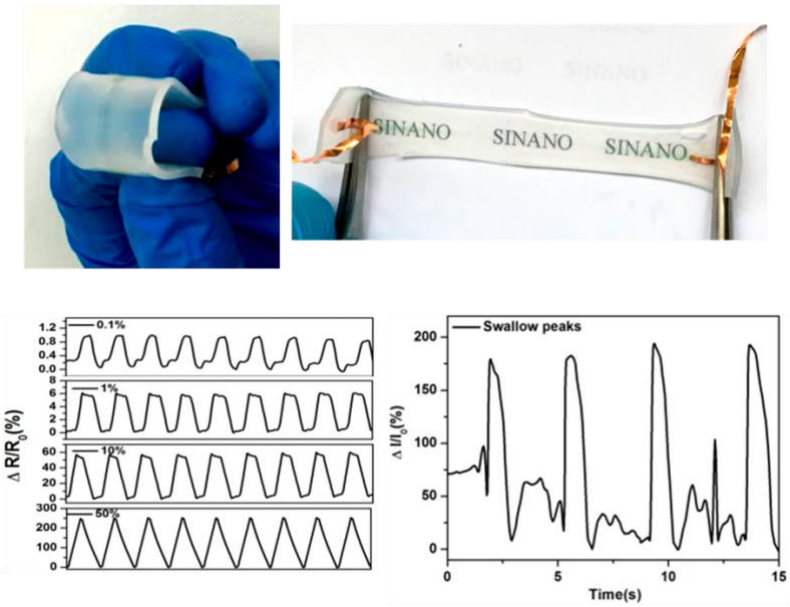

Figure 1.7. Other mixed conductive materials are used as strain sensors for swallowing detection. Zhang et al. demonstrated the use of ILs embedded in the elastomeric substrate as excellent strain sensors for minute human motions such as swallowing. Reproduced with permission.[80]

Lastly, there has been quite an amount of attention on modified hydrogels to be used as strain sensors for the detection of swallowing. Even though it is a challenging task to use hydrogels that are intrinsically brittle, there were a few research groups who found ways to change that. For example, Sun et al. synthesized a conductive nanocomposite hydrogel comprised of oxidized multi-walled carbon nanotubes (oxCNTs) and polyacrylamide (PAAm) (**Figure 1.8a**).[81] They hypothesized that the oxCNTs formed conductive pathways in the hydrogel network and contributed to the strain sensitivity. They used a very high bond (VHB) tape to sandwich the hydrogel before detection of swallowing on a subject's neck. This PAAm-oxCNTs hydrogel had a stretchability up to 600%, a high tensile strength (0.71 MPa), excellent durability (over 300 cycles), and self-recovery efficiency (90%) that was time-dependent. The conductivity was measured to be 0.067 S/m. The GF values varied from 1.5 - 3.39 for 0-250% strain. Another group,

Wang et al., combined two conducting hydrogels, polyaniline (PANI) and aramid nanofiber-polyvinyl alcohol (ANF-PVA), to make their strain sensor (**Figure 1.8b**).[82] PANI/ANF-PVA hydrogel network had an elongation at break of 140% and tensile strength of 2.4 MPa. The strain sensitivity was excellent for the detection of swallowing activity and had a GF value of 16 for the tensile strain range of 0-100%. Additionally, the strain detection stability was confirmed over 500 cycles of bending. Recently, Xu et al. synthesized another conductive organohydrogel by introducing MXene nanosheets into gluten networks that were derived from edible wheat flour dough (**Figure 1.8c**).[83] Due to the amino acid residues in the gluten network, the created composite ($GMOH_x$) showed high flexibility (elongation at break ~600%) and self-adhesiveness. The conductivity was measured to be 0.0005 S/m and the GF value was 3.2 for the strain range 0-300%. Durability was also confirmed over 4000 cycles under 50% strain. In addition, this biocompatible and biodegradable organohydrogel was able to detect swallowing activity repeatedly.

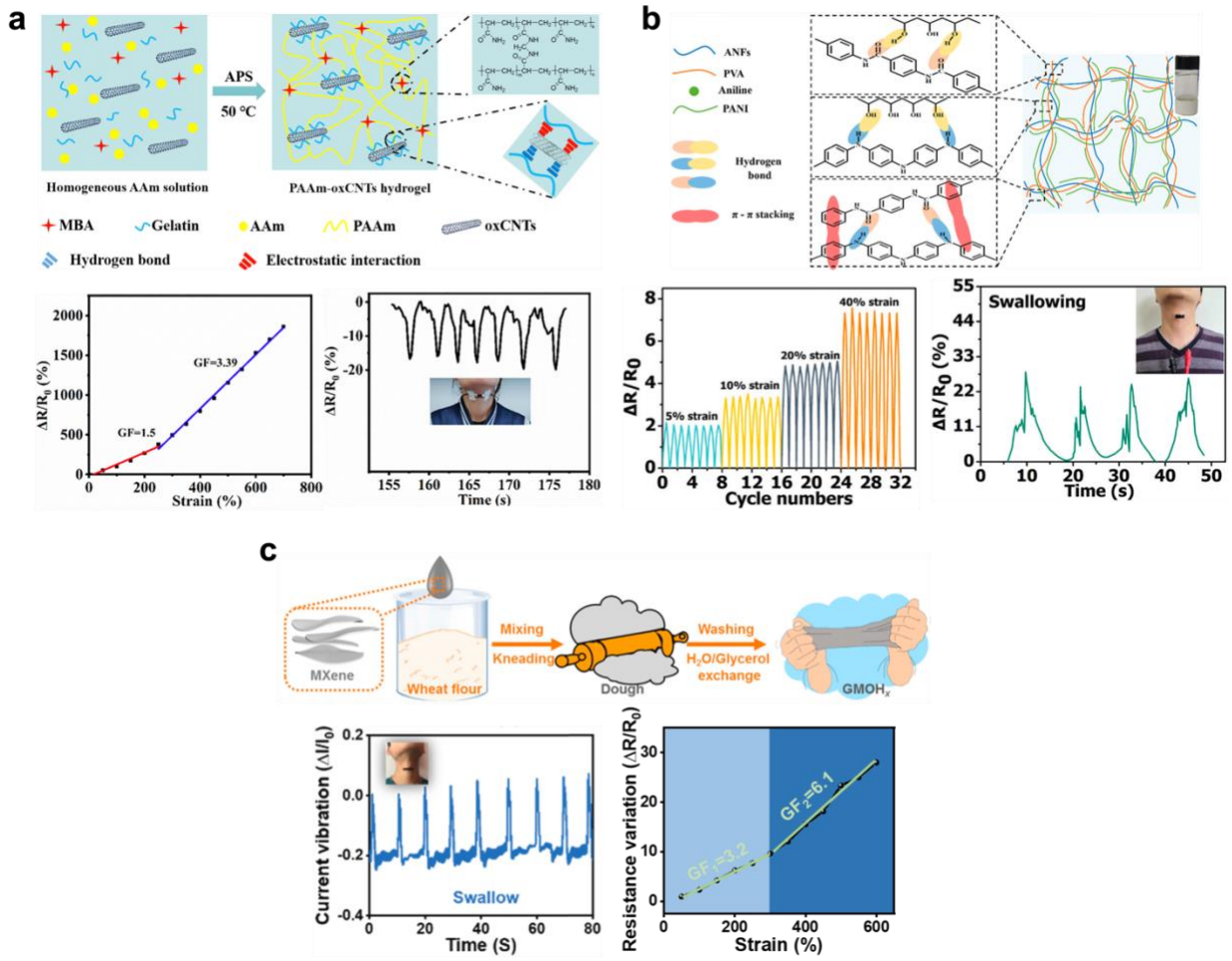

Figure 1.8. Conductive hydrogels exhibit strain sensing abilities to be used to detect swallowing. **(a)** Sun et al. used synthesized PAAm-oxCNTs hydrogels to detect swallowing motion. Reproduced with permission.[81] **(b)** Wang et al. demonstrated PANI/ANF-PVA hydrogel network as a strain sensor that can also detect swallowing motion. Reproduced with permission.[82] **(c)** Xu et al. incorporated MXene nanosheets into gluten networks to make the strain sensor that was used to also detect swallowing. Reproduced with permission.[83]

1.5 Pressure-Based Wearable Sensors

Another modality of swallow assessment is the monitoring of pressure signals exerted onto a sensor. Unlike strain sensing, the source of the generated signal is typically the compression of the active materials or architectures due to a net force normal to the skin surface. The applications of wearable pressure sensor are similar to those seen for strain sensors as demonstrated in several review article.[84,85,86,87,88] Reported pressure sensors for swallow detection can be parsed into

groups by their mechanism of transduction such as capacitive, optical, piezoelectric, or piezoresistive. On capacitive sensors, the literature reports several permutations of materials for the electrodes and the dielectric medium with various mechanical and electrical properties. For example, Kou et al. described a wireless system developed around an NH_4HCO_3/Gr/PDMS dielectric sponge capacitor (**Figure 1.9a**).[89] The sensor showed a low detection limit of 5 Pa with a rapid response time for accurate biomechanical sensing. The capacitive sensor was built into a patch and an antenna allowing for wireless and onboard-battery-free transmission. The authors demonstrated that the resonant frequency of the patch decreased like the square root of the capacitance of the patch. In another work by Xia et al., the dielectric material of the capacitive sensor was a colloidal gel that functioned as an optical sensor by color indication, giving the sensor a dual response to pressure change (**Figure 1.9b**).[90] The dielectric material of the device consisted of free-radically polymerized N-isopropyl acrylamide (NIPAm), N, N' – methylenebisacrylamide (Bis), and acrylic acid (AAc) creating gel particles (approximate size range 0.45 µm – 1.1 µm) which had also been treated with sodium hydroxide for improved capacitance.

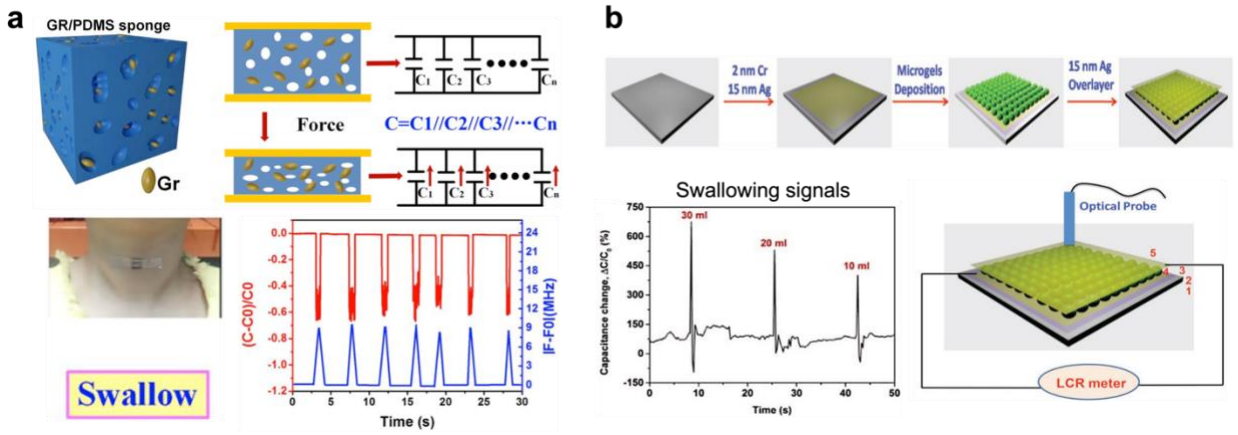

Figure 1.9. Examples of pressure-based sensors for detection of swallow. **(a)** Kou et al. demonstrated a pressure sensor made up of NH_4HCO_3/Gr/PDMS to detect human motions like swallowing. Reproduced with permission.[89] **(b)** Xia et al. sandwich a layer of microgels between silver layers to create a capacitive sensor for detecting swallowing. Reproduced with permission.[90]

A more direct optical approach had been attempted by Maeda et al. where they used a hetero-core fiber optic pressure sensor embedded in a silicone rubber housing (**Figure 1.10a**).[91] The device was placed above the laryngeal prominence (LP) and examined optical loss due to pressure on the fiber optic when a swallow was initiated. Piezoelectric materials were also a promising candidate for swallow pressure sensing. The use of the common piezoelectric polymers such as polyvinylidene fluoride (PVDF) was demonstrated in a paper by Iizuka et al. where a urethane sheet was lined with piezoelectric sensors and placed near the LP (**Figure 1.10b**).[92] The work characterized the mean rising and lowering the velocity of the larynx motion. Another group had the unique idea of a conductive material to be used as a strain sensor to assess swallowing disorders. Natta et al. patterned ultra-thin, and flexible aluminum nitride (AlN) film onto a soft Kapton tape coupled with sticky PDMS-polyethyleneimine (PEIE) to get a sensor that was 26 μm thick (**Figure 1.11a**).[93] Using this sensor, they were able to extract certain important factors from the data such as the duration of the swallowing act, frequency of spontaneous saliva deglutition, and latency. They also utilized wireless Bluetooth technology to transfer the collected sensor data into a phone app. The authors also highlighted the superiority of AlN's non-toxicity, biocompatibility, and superiority over PVDF piezoelectrics which degrade under heat exposure. Lee et al. proposed a pressure sensor comprised of ionic polymer-metal composite (IPMC) material for recognizing throat movements during a swallow (**Figure 1.11b**).[94] Essentially, a pressure applied to the IPMC induces cations and water molecules to move from high to low-stress regions and create a charge distribution while forming a dielectric potential layer. The metal of choice was gold because of its non-corrosive nature in the air. They also utilized a machine learning algorithm, a support vector model (SVM), to calculate the performance of throat

movement detection of their sensor. Although more commonly used in the strain modality, piezoresistivity can be used to sense pressure exerted by laryngeal motion. Guan et al. used a molybdenum diselide/ multi-walled carbon nanotubes ($MoSe_2$/MWNTs) composite capped with PDMS and copper foil electrodes on either side. Among the biosensing demonstrations in this work, the authors placed the sensor above the laryngeal prominence of a male subject and observed swallowing signals as reduction in the resistance of the sensor.[95]

Although these works share a similar mechanical operation principle, the signals they generate are dependent on the placement of the sensor and the mechanism of signal generation. More physiological understanding of skin deformation during a swallow is required to move beyond an empirical framework for sensor architecture and design a more targeted one.

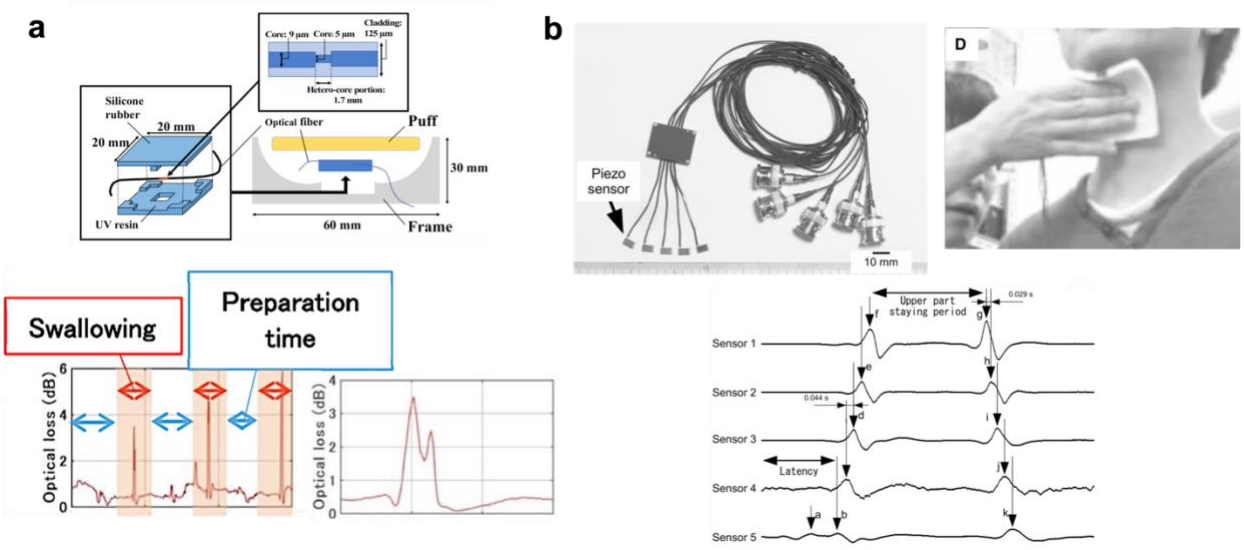

Figure 1.10. Other capacitive sensor demonstrations for detection of swallow. **(a)** Maeda et al. used a hetero-core fiber optic pressure sensor to monitor the movement of LP during swallowing. Reproduced with permission.[91] **(b)** Iizuka et al. used small piezo pressure sensors on the neck to obtain certain swallowing parameters. Reproduced with permission.[92]

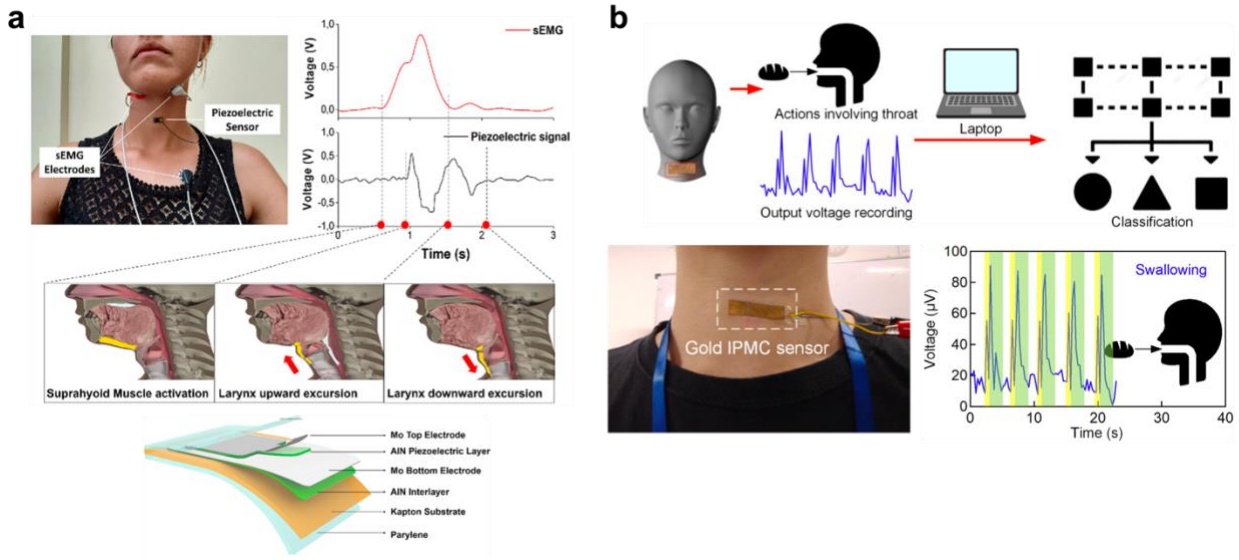

Figure 1.11. A few examples of unique pressure-based sensors for swallow detection**. (a)** Natta et al. demonstrated a pressure sensor comprised of AlN on Kapton tape backed sandwiched with parylene sheets for swallow detection. Reproduced with permission.[93] **(b)** Lee et al. used IPMC with gold as their sensor for tracking throat movement during a swallow and using a machine learning model on the collected data. Reproduced with permission.[94]

1.6 Acoustic-Based Wearable Sensors

In our bodies, mechanical waves constantly propagate through the tissue and fluids of the body rooting from the natural physiological events of the body. Depending on the frequency of the waves, they reveal characteristic signatures of an individual event such as vocal fold vibrations (~100 Hz), cardiac contractions (~10 Hz), and respiration (~0.1 Hz). Many of these mechano-acoustic (MA) signals greatly attenuate at the skin-air interface hence there has been a search for mechano-acoustic sensors that can capture these sound signatures of certain events over the skin. Tao et al. utilized a laser-induced graphene film that could generate and detect sounds from the skin (**Figure 1.12**).[96] Unconventionally, their MA sensor didn't utilize the piezoelectric effect but rather used direct laser writing (450 nm) of polyimide (PI) into porous graphene films.[97] This

porous film structure allowed the detection of weak vibrations which was suitable for sound detection. When placed on the throat, this sensor was able to detect the mechanical vibrations of throat cords during a swallowing activity.

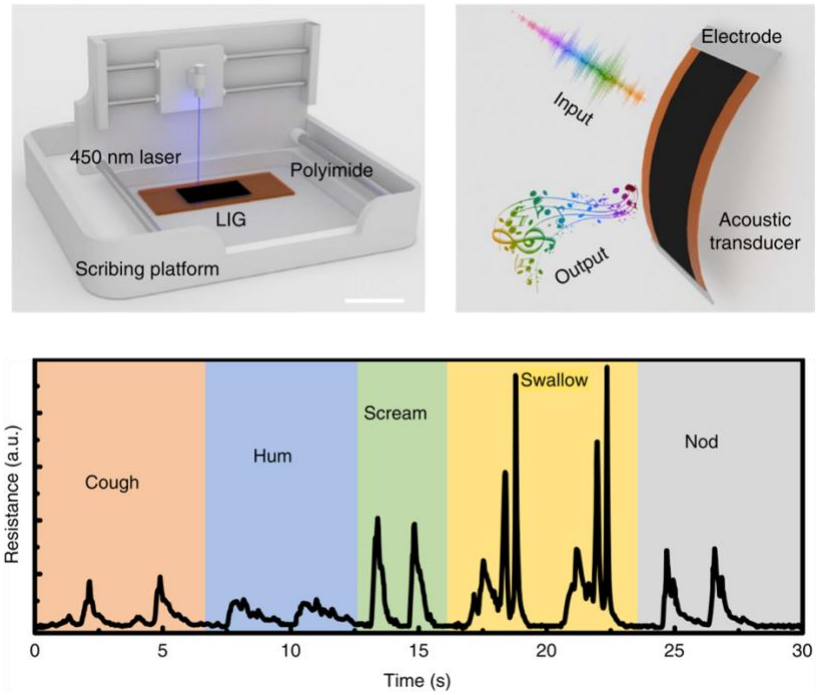

Figure 1.12. A novel and materials-enabled MA sensor for detection of throat movement during a swallow. Tao et al. demonstrated the use of LIG films as MA sensors to generate and detect sound signals from the skin. Reproduced with permission.[96]

Designing new materials for MA sensors hasn't been a large field of study when detecting swallow activities. However, a lot of studies were done using commercial accelerometers and microphones (and new designs to put all the sensors in one patch) to detect sound signals during a swallow.[98,99,100,101,102,103] These studies also worked towards applying deep learning to the collected data to be able to understand the physiology of swallowing a little better. Some of these studies are shown in **Figure 1.13** for reference. It is worthwhile to mention the work that has been done to design unobtrusive wearable devices to detect sound signals during a swallow and use this

data to model a machine learning algorithm to extract important features and learn from this physiological event.

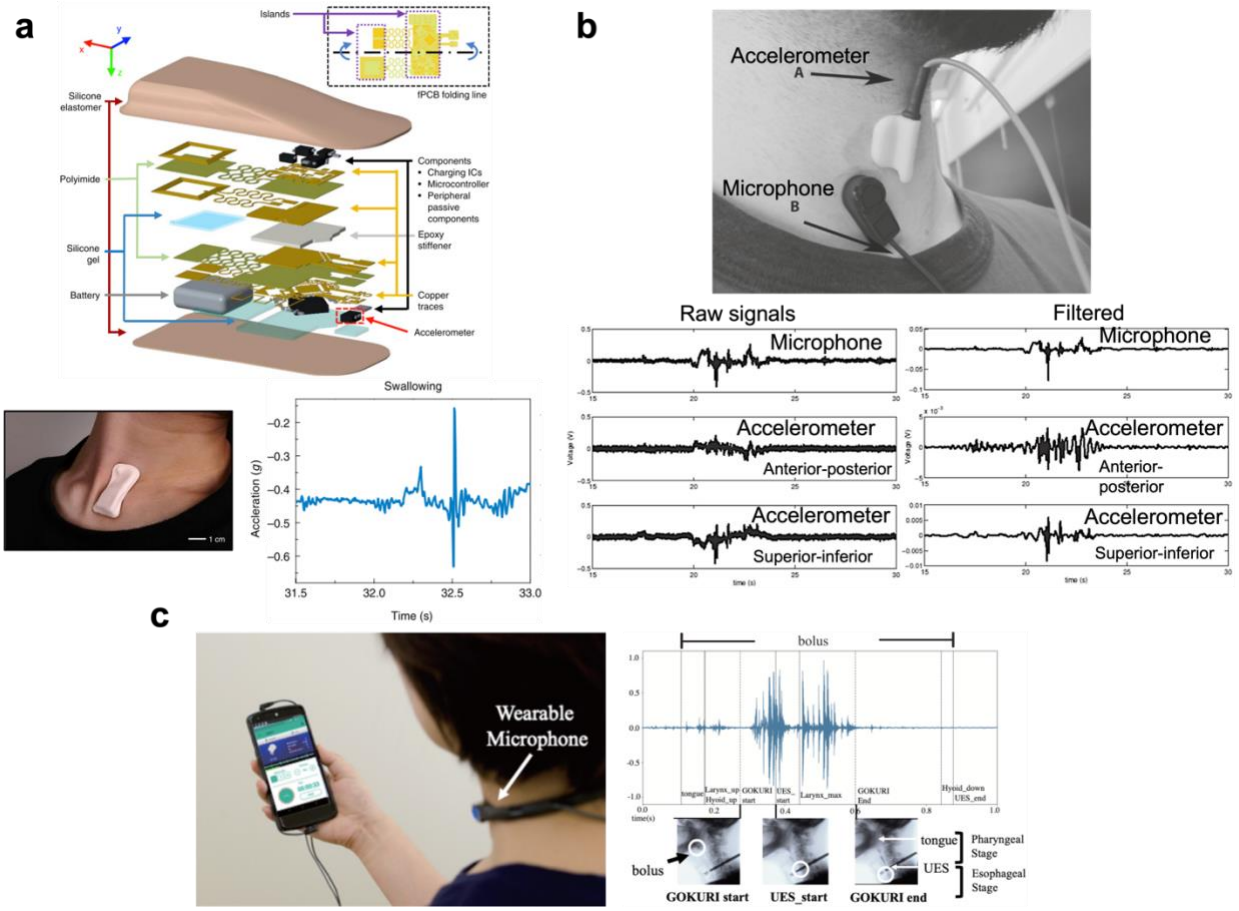

Figure 1.13. Other studies used commercial accelerometers and microphones for detecting swallowing sounds. **(a)** Lee et al. designed a flexible, wireless, and soft caging for an accelerometer to detect swallowing when placed on the suprasternal notch. Reproduced with permission.[98] **(b)** Dudik et al. used both a microphone and an accelerometer to detect swallowing signals and conducted feature analysis from the signals. Reproduced with permission.[99] **(c)** Kuramoto et al. showed a smartphone-based wearable microphone device to monitor the swallowing behavior changes over time. Reproduced with permission.[100]

1.7 Challenges and Future Opportunities

Overall, the field of wearable swallow sensors is looking for an unobtrusive, wearable, skin conformable, sensitive, and wireless sensor platform for swallow detection and monitoring. All the discussed literature examples addressed at least one of these requirements. Still, there is much

to be improved and much to be experimented with to achieve an at-home wearable technology. For example, all the studies discussed in this review performed swallowing experiments while the participants were in a resting position with no other bodily movement present. This certainly kept the motion artifacts to a minimum and provided ease in the data processing. However, most potential patients and customers of an epidermal sensor device for swallowing will be moving around or not going to be completely stationary. There needs to be more investigation towards identifying these motion artifacts coming from the user's body motion and using appropriate filters to remove them from the raw data. Additionally, user engagement during swallowing therapies is crucial for preventing swallowing disorders. Therefore, haptic feedback systems (visual or physical) should be investigated for incorporating the user's engagement with the device and therapy. This can be possible via novel haptic materials that are up and coming. With these shortcomings addressed, we can reach a more effective sensor platform that can perform detection and engagement of a user.

1.8 Conclusion

The importance of monitoring the swallowing behavior has gained more attention over the years, especially after the literature on dysphagia has increased in numbers. This awareness of a problem that is so prevalent in life encouraged a field of study that focused on designing sensor platforms that use different sensing modalities to detect swallowing activity. Many studies used conventional sensors to detect and monitor swallowing, but some used novel materials to tap into better sensitivities and conformabilities to skin. We surveyed different materials-enabled studies in this review separated by the sensing modalities they used. The major fields were sEMG, strain, pressure, and acoustic-based wearable sensors with each having a different set of materials used

as the sensor core. Sensor characteristics and performances were discussed while comparing the signals they detected from a swallow. Finally, we discussed the untapped areas in this field and places of improvement. We foresee this review to give a big picture of where we are at as a field in terms of swallow detection using novel materials.

Acknowledgments

This work was supported by a gift from PepsiCo & the Gatorade Sports Sciences Institute. Additional support was provided by the member companies of the Center for Wearable Sensors in the Jacobs School of Engineering at the University of California, San Diego, including Dexcom, Gore, Honda, Huami, Instrumentation Laboratory, Kureha, Merck KGaA, PepsiCo, Roche, Samsung, and Sony. This work was performed in part at the San Diego Nanotechnology Infrastructure (SDNI), a member of the National Nanotechnology Coordinated Infrastructure, which is supported by the National Science Foundation (Grant ECCS-1542148).

Chapter 1, in part, will be submitted for publication of the material as it may appear in Advanced Healthcare Materials. Beril Polat, Tarek Rafeedi, and Darren J. Lipomi. 2022. The dissertation author was the primary investigator and author of this paper.

References

1. Jones, B. *Normal and Abnormal Swallowing*. (Springer, New York, NY, 2003). doi:https://doi.org/10.1007/978-0-387-22434-3.

2. Matsuo, K. & Palmer, J. B. Anatomy and Physiology of Feeding and Swallowing: Normal and Abnormal. *Phys. Med. Rehabil. Clin. N. Am.* **19**, 691–707 (2008).

3. Hiiemae, K. M. & Palmer, J. B. Food Transport and Bolus Formation during Complete

Feeding Sequences on Foods of Different Initial Consistency. *Dysphagia* **14**, 31–42 (1999).

4. Clavé, P. & Shaker, R. Dysphagia: Current reality and scope of the problem. *Nat. Rev. Gastroenterol. Hepatol.* **12**, 259–270 (2015).

5. Eisbruch, A. *et al.* Dysphagia and aspiration after chemoradiotherapy for head-and-neck cancer: Which anatomic structures are affected and can they be spared by IMRT? *Int. J. Radiat. Oncol. Biol. Phys.* **60**, 1425–1439 (2004).

6. Cooper, J. S., Fu, K., Marks, J. & Silverman, S. Late effects of radiation therapy in the head and neck region. *Int. J. Radiat. Oncol. Biol. Phys.* **31**, 1141–64 (1995).

7. Nguyen, N. P. *et al.* Dysphagia following chemoradiation for locally advanced head and neck cancer. *Ann. Oncol.* **15**, 383–388 (2004).

8. Roden, D. F. & Altman, K. W. Causes of dysphagia among different age groups: A systematic review of the literature. *Otolaryngol. Clin. North Am.* **46**, 965–987 (2013).

9. Hutcheson, K. A. *et al.* Late dysphagia after radiotherapy-based treatment of head and neck cancer. *Cancer* **118**, 5793–5799 (2012).

10. Garon, B. R., Sierzant, T. & Ormiston, C. Silent Aspiration - Results of 2,000 Video Fluoroscopic Evaluations. *J. Neurosci. Nurs.* **41**, 178–185 (2009).

11. Caudell, J. J. *et al.* Factors Associated With Long-Term Dysphagia After Definitive Radiotherapy for Locally Advanced Head-and-Neck Cancer. *Int. J. Radiat. Oncol. Biol. Phys.* **73**, 410–415 (2009).

12. Hutcheson, K. A. *et al.* Eat and exercise during radiotherapy or chemoradiotherapy for pharyngeal cancers: Use it or lose it. *JAMA Otolaryngol. - Head Neck Surg.* **139**, 1127–1134 (2013).

13. Roe, J. W. G., Drinnan, M. J., Carding, P. N., Harrington, K. J. & Nutting, C. M. Patient-reported outcomes following parotid-sparing intensity-modulated radiotherapy for head and neck cancer. How important is dysphagia? *Oral Oncol.* **50**, 1182–1187 (2014).

14. Tubiana, M. & Eschwege, F. Conformal radiotherapy and intensity-modulated radiotherapy - Clinical data. *Acta Oncol. (Madr).* **39**, 555–567 (2000).

15. Feng, F. Y. *et al.* Intensity-modulated chemoradiotherapy aiming to reduce dysphagia in patients with oropharyngeal cancer: Clinical and functional results. *J. Clin. Oncol.* **28**, 2732–2738 (2010).

16. King, S. N., Dunlap, N. E., Tennant, P. A. & Pitts, T. Pathophysiology of Radiation-Induced Dysphagia in Head and Neck Cancer. *Dysphagia* **31**, 339–351 (2016).

17. Burkhead, L. M., Sapienza, C. M. & Rosenbek, J. C. Strength-training exercise in dysphagia rehabilitation: Principles, procedures, and directions for future research. *Dysphagia* **22**, 251–265 (2007).

18. Lazarus, C. Tongue strength and exercise in healthy individuals and in head and neck cancer patients. *Semin. Speech Lang.* **27**, 260–267 (2006).

19. Smith, B. G. & Lewin, J. S. Lymphedema management in head and neck cancer. *Curr. Opin. Otolaryngol. Head Neck Surg.* **18**, 153–158 (2010).

20. Carnaby-Mann, G., Crary, M. A., Schmalfuss, I. & Amdur, R. 'Pharyngocise': Randomized controlled trial of preventative exercises to maintain muscle structure and swallowing function during head-and-neck chemoradiotherapy. *Int. J. Radiat. Oncol. Biol. Phys.* **83**, 210–219 (2012).

21. Mashhour, K., Abdelkader, R., Abdelkader, L., El Hadary, S. & Hashem, W. Swallowing exercises: Will they really help head and neck cancer patients? *Asian Pacific J. Cancer Prev.* **19**, 797–801 (2018).

22. Van Der Molen, L. *et al.* A randomized preventive rehabilitation trial in advanced head and neck cancer patients treated with chemoradiotherapy: Feasibility, compliance, and short-term effects. *Dysphagia* **26**, 155–170 (2011).

23. Kotz, T. *et al.* Prophylactic swallowing exercises in patients with head and neck cancer undergoing chemoradiation: A randomized trial. *Arch. Otolaryngol. - Head Neck Surg.* **138**, 376–382 (2012).

24. Kulbersh, B. D. *et al.* Pretreatment, preoperative swallowing exercises may improve dysphagia quality of life. *Laryngoscope* **116**, 883–886 (2006).

25. Martin-Harris, B. *et al.* Respiratory-swallow training in patients with head and neck cancer. *Arch. Phys. Med. Rehabil.* **96**, 885–893 (2015).

26. Ciarambino, T., Sansone, G., Para, O. & Giordano, M. Dysphagia: what we know? A minireview. *J. Gerontol. Geriatr.* **69**, 188–194 (2021).

27. Høxbroe Michaelsen, S., Grønhøj, C., Høxbroe Michaelsen, J., Friborg, J. & von Buchwald, C. Quality of life in survivors of oropharyngeal cancer: A systematic review and meta-analysis of 1366 patients. *Eur. J. Cancer* **78**, 91–102 (2017).

28. Nguyen, N. P. *et al.* Aspiration rate following chemoradiation for head and neck cancer: An underreported occurrence. *Radiother. Oncol.* **80**, 302–306 (2006).

29. Eisbruch, A. *et al.* Objective assessment of swallowing dysfunction and aspiration after radiation concurrent with chemotherapy for head-and-neck cancer. *Int. J. Radiat. Oncol. Biol. Phys.* **53**, 23–28 (2002).

30. Palmer, J. B., Kuhlemeir, K. V., Tippett, D. C. & Lynch, C. A protocol for the videofluorographic swallowing study. *Dysphagia* **8**, 209–214 (1993).

31. Logemann, J. A. *Manual for the Videofluorographic Study of Swallowing*. (PRO-ED, 1993).

32. Logemann, J. A. Role of the modified barium swallow in management of patients with dysphagia. *Otolaryngol. - Head Neck Surg.* **116**, 335–338 (1997).

33. Martin-Harris, B., Logemann, J. A., McMahon, S., Schleicher, M. & Sandidge, J. Clinical utility of the modified barium swallow. *Dysphagia* **15**, 136–141 (2000).

34. Badenduck, L. A. *et al.* Fiber-optic endoscopic evaluation of swallowing to assess swallowing outcomes as a function of head position in a normal population. *Otolaryngol. Neck Surg.* **43**, (2014).

35. Langmore, S. E., Schatz, K. & Olsen, N. Fiberoptic endoscopic examination of swallowing safety: a new procedure. *Dysphagia* **2**, 216–219 (1988).

36. Bastian, R. W. Videoendoscopic evaluation of patients with dysphagia: an adjunct to the modified barium swallow. *Otolaryngol. Neck Surg.* **104**, 339–350 (1991).

37. Shaw, S. M. & Martino, R. The Normal Swallow: Muscular and Neurophysiological Control. *Otolaryngol. Clin. North Am.* **46**, 937–956 (2013).

38. Ertekin, C. & Aydogdu, I. Neurophysiology of swallowing. *Clin. Neurophysiol.* **114**, 2226–2244 (2003).

39. Logemann, J. A. *Evaluation and treatment of swallowing disorders*. (PRO-ED, 1998).

40. Dodds, W. J., Stewart, E. T. & Logemann, J. A. Physiology and Radiology of the Normal Oral and Pharyngeal Phases of Swallowing. *Am. J. Roentgenol.* **154**, 953–963 (1989).

41. Palmer, J. B., Rudin, N. J., Lara, G. & Crompton, A. W. Coordination of mastication and swallowing. *Dysphagia* **7**, 187–200 (1992).

42. Dua, K. S., Ren, J., Bardan, E., Xie, P. & Shaker, R. Coordination of deglutitive glottal function and pharyngeal bolus transit during normal eating. *Gastroenterology* **112**, 73–83

(1997).

43. Matsuo, K., Hiiemae, K. M. & Palmer, J. B. Cyclic motion of the soft palate in feeding. *J. Dent. Res.* **84**, 39–42 (2005).

44. Buettner, A., Beer, A., Hannig, C. & Settles, M. Observation of the swallowing process by application of videofluoroscopy and real-time magnetic resonance imaging-consequences for retronasal aroma stimulation. *Chem. Senses* **26**, 1211–1219 (2001).

45. Hodgson, M., Linforth, R. S. T. & Taylor, A. J. Simultaneous real-time measurements of mastication, swallowing, nasal airflow, and aroma release. *J. Agric. Food Chem.* **51**, 5052–5057 (2003).

46. Palmer, J. B. & Hiiemae, K. M. Eating and breathing: interactions between respiration and feeding on solid food. *Dysphagia* **18**, 169–178 (2003).

47. Shaker, R., Dodds, W. J., Dantas, R. O., Hogan, W. J. & Arndorfer, R. C. Coordination of deglutitive glottic closure with oropharyngeal swallowing. *Gastroenterology* **98**, 1478–1484 (1990).

48. Ohmae, Y., Logemann, J. A., Kaiser, P., Hanson, D. G. & Kahrilas, P. J. Timing of glottic closure during normal swallow. *Head Neck* **17**, 394–402 (1995).

49. Logemann, J. A. *et al.* Closure mechanisms of laryngeal vestibule during swallow. *Am. J. Physiol. Liver Physiol.* **262**, G338–G344 (1992).

50. Cook, I. J. *et al.* Opening mechanisms of the human upper esophageal sphincter. *Am. J. Physiol. Liver Physiol.* **257**, G748–G759 (1989).

51. Ertekin, C. & Aydoğdu, I. Electromyography of human cricopharyngeal muscle of the upper esophageal sphincter. *Muscle Nerve* **26**, 729–739 (2002).

52. Argov, Z. & de Visser, M. Dysphagia in adult myopathies. *Neuromuscul. Disord.* **31**, 5–20 (2021).

53. Sakai, K. *et al.* Submental muscle activity and its role in diagnosing sarcopenic dysphagia. *Clin. Interv. Aging* **15**, 1991–1999 (2020).

54. Vescio, B., Quattrone, A., Nisticò, R., Crasà, M. & Quattrone, A. Wearable Devices for Assessment of Tremor. *Front. Neurol.* **12**, 1–7 (2021).

55. Iqbal, S. M. A., Mahgoub, I., Du, E., Leavitt, M. A. & Asghar, W. Advances in healthcare wearable devices. *npj Flex. Electron.* **5**, 1–14 (2021).

56. Sethi, A., Ting, J., Allen, M., Clark, W. & Weber, D. Advances in motion and electromyography based wearable technology for upper extremity function rehabilitation: A review. *J. Hand Ther.* **33**, 180–187 (2020).

57. Tao, W., Liu, T., Zheng, R. & Feng, H. Gait analysis using wearable sensors. *Sensors* **12**, 2255–2283 (2012).

58. Yamaguchi, T. *et al.* Portable and wearable electromyographic devices for the assessment of sleep bruxism and awake bruxism: A literature review. *Cranio - J. Craniomandib. Pract.* **00**, 1–9 (2020).

59. Beniczky, S., Arbune, A. A., Jeppesen, J. & Ryvlin, P. Biomarkers of seizure severity derived from wearable devices. *Epilepsia* **61**, S61–S66 (2020).

60. Constantinescu, G. *et al.* Epidermal electronics for electromyography: An application to swallowing therapy. *Med. Eng. Phys.* **38**, 807–812 (2016).

61. Norton, J. J. S. *et al.* Soft, curved electrode systems capable of integration on the auricle as a persistent brain-computer interface. *Proc. Natl. Acad. Sci. U. S. A.* **112**, 3920–3925 (2015).

62. Nicholls, B., Ang, C. S., Efstratiou, C., Lee, Y. & Yeo, W. H. Swallowing detection for game control: Using skin-like electronics to support people with dysphagia. *2017 IEEE Int. Conf. Pervasive Comput. Commun. Work. PerCom Work. 2017* 413–418 (2017) doi:10.1109/PERCOMW.2017.7917598.

63. Fu, Y., Zhao, J., Dong, Y. & Wang, X. Dry electrodes for human bioelectrical signal monitoring. *Sensors (Switzerland)* **20**, 1–30 (2020).

64. Lee, Y. *et al.* Soft electronics enabled ergonomic human-computer interaction from swallowing training. *Sci. Rep.* **7**, 1–12 (2017).

65. Kim, M. K. *et al.* Flexible submental sensor patch with remote monitoring controls for management of oropharyngeal swallowing disorders. *Sci. Adv.* **5**, 1–10 (2019).

66. Kantarcigil, C. *et al.* Validation of a novel wearable electromyography patch for monitoring submental muscle activity during swallowing: A randomized crossover trial. *J. Speech, Lang. Hear. Res.* **63**, 3293–3310 (2020).

67. Blau, R. *et al.* Intrinsically Stretchable Block Copolymer Based on PEDOT:PSS for Improved Performance in Bioelectronic Applications. *ACS Appl. Mater. Interfaces* **14**, 4823–4835 (2022).

68. Amjadi, M., Kyung, K. U., Park, I. & Sitti, M. Stretchable, Skin-Mountable, and Wearable Strain Sensors and Their Potential Applications: A Review. *Adv. Funct. Mater.* **26**, 1678–1698 (2016).

69. Afsarimanesh, N. *et al.* A review on fabrication, characterization and implementation of wearable strain sensors. *Sensors Actuators, A Phys.* **315**, 112355 (2020).

70. Souri, H. *et al.* Wearable and Stretchable Strain Sensors: Materials, Sensing Mechanisms, and Applications. *Adv. Intell. Syst.* **2**, 2000039 (2020).

71. Athavale, Y. & Krishnan, S. Biosignal monitoring using wearables: Observations and

opportunities. *Biomed. Signal Process. Control* **38**, 22–33 (2017).

72. Ramírez, J. *et al.* Exploring the limits of sensitivity for strain gauges of graphene and hexagonal boron nitride decorated with metallic nanoislands. *Nanoscale* **12**, 11209–11221 (2020).

73. Roh, E., Hwang, B. U., Kim, D., Kim, B. Y. & Lee, N. E. Stretchable, Transparent, Ultrasensitive, and Patchable Strain Sensor for Human-Machine Interfaces Comprising a Nanohybrid of Carbon Nanotubes and Conductive Elastomers. *ACS Nano* **9**, 6252–6261 (2015).

74. Hwang, B. U. *et al.* Transparent Stretchable Self-Powered Patchable Sensor Platform with Ultrasensitive Recognition of Human Activities. *ACS Nano* **9**, 8801–8810 (2015).

75. Zhu, Y. *et al.* Enhanced oxidation resistance and electrical conductivity copper nanowires-graphene hybrid films for flexible strain sensors. *New J. Chem.* **41**, 4950–4958 (2017).

76. Ramírez, J. *et al.* Metallic Nanoislands on Graphene for Monitoring Swallowing Activity in Head and Neck Cancer Patients. *ACS Nano* **12**, 5913–5922 (2018).

77. Polat, B. *et al.* Epidermal Graphene Sensors and Machine Learning for Estimating Swallowed Volume. *ACS Appl. Nano Mater.* **4**, 8126–8134 (2021).

78. Huang, Y. *et al.* Highly stretchable strain sensor based on polyurethane substrate using hydrogen bond-assisted laminated structure for monitoring of tiny human motions. *Smart Mater. Struct.* **27**, (2018).

79. Zang, S., Wang, Q., Wan, J., Huang, X. & Ren, X. A flexible and skin-mountable elastic fiber-based sensor patch for healthcare monitoring. *Biomed. Phys. Eng. Express* **5**, (2019).

80. Zhang, S. H. *et al.* Wearable wide-range strain sensors based on ionic liquids and monitoring of human activities. *Sensors (Switzerland)* **17**, 1–10 (2017).

81. Sun, X. *et al.* Carbon nanotubes reinforced hydrogel as flexible strain sensor with high stretchability and mechanically toughness. *Chem. Eng. J.* **382**, 122832 (2020).

82. Wang, J., Lin, Y., Mohamed, A., Ji, Q. & Jia, H. High strength and flexible aramid nanofiber conductive hydrogels for wearable strain sensors. *J. Mater. Chem. C* **9**, 575–583 (2021).

83. Xu, H. *et al.* Conductive and eco-friendly gluten/MXene composite organohydrogels for flexible, adhesive, and low-temperature tolerant epidermal strain sensors. *Colloids Surfaces A Physicochem. Eng. Asp.* **636**, 128182 (2022).

84. Pan, H. & Lee, T. W. Recent Progress in Development of Wearable Pressure Sensors Derived from Biological Materials. *Adv. Healthc. Mater.* **10**, 1–17 (2021).

85. Wang, H. *et al.* Flexible capacitive pressure sensors for wearable electronics. *J. Mater. Chem. C* **10**, 1594–1605 (2022).

86. Chen, W. & Yan, X. Progress in achieving high-performance piezoresistive and capacitive flexible pressure sensors: A review. *J. Mater. Sci. Technol.* **43**, 175–188 (2020).

87. He, J. *et al.* Recent advances of wearable and flexible piezoresistivity pressure sensor devices and its future prospects. *J. Mater.* **6**, 86–101 (2020).

88. Li, R. *et al.* Research progress of flexible capacitive pressure sensor for sensitivity enhancement approaches. *Sensors Actuators, A Phys.* **321**, 112425 (2021).

89. Kou, H. *et al.* Wireless wide-range pressure sensor based on graphene/PDMS sponge for tactile monitoring. *Sci. Rep.* **9**, 1–7 (2019).

90. Xia, X., Zhang, X., Serpe, M. J. & Zhang, Q. Microgel-Based Devices as Wearable Capacitive Electronic Skins for Monitoring Cardiovascular Risks. *Adv. Mater. Technol.* **5**, 1–8 (2020).

91. Maeda, M. *et al.* Non-invasive swallowing examination device using hetero-core fiber optic pressure sensor. *LifeTech 2021 - 2021 IEEE 3rd Glob. Conf. Life Sci. Technol.* 315–316 (2021) doi:10.1109/LifeTech52111.2021.9391794.

92. Iizuka, M. *et al.* A new flexible piezoelectric pressure sensor array for the noninvasive detection of laryngeal movement during swallowing. *J. Physiol. Sci.* **68**, 837–846 (2018).

93. Natta, L. *et al.* Conformable AlN Piezoelectric Sensors as a Non-invasive Approach for Swallowing Disorder Assessment. *ACS Sensors* **6**, 1761–1769 (2021).

94. Lee, J. H., Chee, P. S., Lim, E. H. & Tan, C. H. Artificial intelligence-assisted throat sensor using ionic polymer–metal composite (IPMC) material. *Polymers (Basel).* **13**, (2021).

95. Guan, J., Zhang, D. & Li, T. Flexible Pressure Sensor Based on Molybdenum Diselide/Multi-Walled Carbon Nanotubes for Human Motion Detection. *IEEE Sens. J.* **21**, 10491–10497 (2021).

96. Tao, L. Q. *et al.* An intelligent artificial throat with sound-sensing ability based on laser induced graphene. *Nat. Commun.* **8**, 1–8 (2017).

97. Lin, J. *et al.* Laser-induced porous graphene films from commercial polymers. *Nat. Commun.* **5**, 5–12 (2014).

98. Lee, K. H. *et al.* Mechano-acoustic sensing of physiological processes and body motions via a soft wireless device placed at the suprasternal notch. *Nat. Biomed. Eng.* **4**, 148–158 (2020).

99. Dudik, J. M., Jestrović, I., Luan, B., Coyle, J. L. & Sejdić, E. A comparative analysis of swallowing accelerometry and sounds during saliva swallows. *Biomed. Eng. Online* **14**, 1–15 (2015).

100. Kuramoto, N. *et al.* Deep Learning-Based Swallowing Monitor for Realtime Detection of Swallow Duration. *Proc. Annu. Int. Conf. IEEE Eng. Med. Biol. Soc. EMBS* **2020-July**,

4365–4368 (2020).

101. O'Brien, M. K. *et al.* Advanced Machine Learning Tools to Monitor Biomarkers of Dysphagia: A Wearable Sensor Proof-of-Concept Study. *Digit. Biomarkers* **5**, 167–175 (2021).

102. Khalifa, Y., Coyle, J. L. & Sejdić, E. Non-invasive identification of swallows via deep learning in high resolution cervical auscultation recordings. *Sci. Rep.* **10**, 1–13 (2020).

103. Movahedia, F., Kurosub, A., Coyleb, J. L., Pererac, S. & Sejdić, E. A comparison between swallowing sounds and vibrations in patients with dysphagia. *Comput. Methods Programs Biomed.* **144**, 179–187 (2017).

Chapter 2 Epidermal Graphene Sensors and Machine Learning for Estimating Swallowed Volume

Abstract

Assessment of liquid intake is necessary to obtain a complete picture of an individual's hydration status. Measurements using state-of-the-art wearable devices have been demonstrated, but none of these devices have combined high sensitivity, unobtrusiveness, and automated estimation of volume, i.e., using machine learning. Such a capability would have immense value in a variety of medical contexts, such as monitoring patients with dysphagia or the performance of athletes. Here, an epidermal sensor platform is combined with machine learning to measure swallowed liquid volume based on signals obtained from the surface of the skin. The key component of the device is a composite piezoresistive sensor consisting of single-layer graphene decorated with metallic nanoislands and coated with a highly plasticized form of the conductive polymer poly(3,4-ethylenedioxythiophene):poly(styrenesuflonate) (PEDOT:PSS). Surface electromyography (sEMG) signals obtained with conventional electrodes are used in concert with the strain measurements. The use of strain and sEMG measurements together both (1) improve the accuracy of estimated volumes and (2) permit the differentiation of swallowing from motion artifacts. In a cohort consisting of 11 participants, the combined measurements of strain and sEMG—processed by the machine learning algorithm—were able to estimate unknown swallowed volumes cumulatively between 5 to 30 mL of water with greater than 92% accuracy. Ultimately, this system holds promise for numerous applications in sports medicine, rehabilitation, and the detection of nascent dysfunction in swallowing.

2.1. Introduction

Despite the importance of water consumption and hydration for homeostasis, there are no well-established methods of reliably measuring the intake of liquids.[1–4] Individuals from many groups and with different conditions are at risk of dehydration and its adverse effects, including children, the elderly, adults living and working in hot climates, survivors of head and neck cancer, and athletes. Graduated drinking bottles provide a visual measure to track consumed volume. However, this method is highly unreliable because it does not account for spillage and sharing. Moreover, it requires constant attention from the subject or the examiner. There is thus a need for a more practical, unobtrusive method of tracking swallowed volume, for example, by using a simple wearable sensor. This paper describes an epidermal strain sensor, combined with conventional sEMG measurements, which can accurately measure swallowed volumes based on the movement of the skin and electrical activity of the swallowing muscles. When the data obtained from this system is analyzed using a machine learning algorithm, the system is capable of estimating cumulative swallowed volume with an accuracy of more than 92%.

The literature encompasses a variety of methods to measure swallowed volume, each of which is subject to various constraints. For example, videofluoroscopy[5–8], endoscopy[9–11], and acoustic sensors (i.e., microphones)[12,13] have the ability to provide accurate measurements, but require bulky, specialized equipment and can rarely be performed during exercise or even regular activity. Mobile devices offer the ability to obtain these measurements without laboratory equipment. Over approximately the last 15 years, the advent of epidermal sensors has led to many impressive measurements of various physiological quantities from different groups.[14–23,24,25] Swallowing activity in particular has been the subject of a subset of these studies.[26–30] For example, a device described by Roh et al. was composed of strain sensors based on a nanocomposite

comprising single-wall carbon nanotubes, a conductive polymer (PEDOT:PSS), and polyurethane. This device was able to distinguish events in the neck associated with swallowing from movements of the skin.[31] By replacing the carbon nanotubes with silver nanowires, the same group later demonstrated a self-powered version of the device. This device, which was nearly transparent owing to the use of silver nanowires, was able to detect minute deflections of the skin, including those associated with the motion of drinking water.[32] Using a different piezoresistive system, namely an ionic liquid embedded in an elastomer, Zhang et al. were able to capture body motions ranging from 0.1% to 400% strain including the swallowing behavior.[33] However, these systems still required classification of signals by the (human) experimenters. Moreover, the studies did not demonstrate automated, quantitative estimation of swallowed volume, an essential metric for assessing hydration status.

Toward the goal of sensing and automated analysis of swallowing activity, there have been a small number of notable studies. Kim et al. described a wearable sensor that included both sEMG electrodes and a commercial strain gauge on the same patch and allowed remote data transmission and power by connecting the patch to a wireless unit using a ribbon cable and anisotropic conductive film.[34] Previous studies in our group by Ramirez et al. have reported a nanocomposite strain sensor consisting of single-layer graphene decorated with metallic nanoislands.[35] When the strain data from the neck was combined with signals obtained from commercial sEMG electrodes, a machine learning algorithm was able to correctly identify materials swallowed in a bolus on the basis of consistency: water, yogurt, or a chewed cracker.[35] Furthermore, this platform was also able to distinguish swallowing patterns obtained from dysphagic and non-dysphagic individuals. Despite these successes, the device possessed a high mechanical stiffness and was unable to stretch with natural movements of the skin. To overcome barriers associated with mechanical stiffness,

including discomfort and strong awareness of the participant, it was necessary to re-engineer the nanocomposite strain gauge to make it compatible with a stretchable, epidermal form factor. Moreover, in this study, the automated classification using machine learning was based on large differences in swallowing signals (i.e., water vs. yogurt, normal swallowing vs. dysphagic swallowing). Ultimately, monitoring hydration status would require classifying signals with much finer variance.

Toward the goal of automated classification of swallowing signals, Schultheiss et al. described an algorithm to reliably detect the swallowing patterns from the other bodily movements (head movements, talking, and chewing) using two different measurements (sEMG and bioimpedance).[36] After collecting both measurement signals during a swallow, the authors used a combination of physiological criteria and classifiers to accurately differentiate swallows from non-swallows. Similarly, Farooq and Sazonov preferred to use multiclass classification to lessen the influence of unwanted motion artifacts which confound the signals arising from eating solid foods.[37] The authors used data from a piezoelectric strain sensor and an accelerometer and processed it using a two-stage multiclass classification approach. The participants were directed to eat solid food items in both sedentary and active states (i.e., walking), and using their classification method, the authors achieved a weighted average of precision of 99.85% in detecting the solid food intake. In another example, Shieh et al. used three separate sensors—a nasal cannula, sEMG electrodes, and a force sensor (FSR) on the neck—to collect temporally resolved parameters during swallowing and analyze the coordination between respiration and swallowing.[38] The authors designed an algorithm to detect the onset and the offset of a swallow from the sEMG, nasal airflow, and FSR sensors. Analysis of this combination of measurements was able to differentiate the swallowing events from respiration and find a correlation between them to understand the

effects of long-term smoking on swallowing function. Despite these successes, it is nevertheless the case that a nanomaterial-enabled, minimally obtrusive device has never been coupled to a machine learning algorithm capable of detecting minute differences in swallowed volume.

Here, we describe a non-invasive, minimally obtrusive patch-like sensor for monitoring swallowed volume (**Figure 2.1**). The sensor is worn on the neck and operates by recording strain and sEMG signals, which originate from deformation of the skin and activation of the swallowing muscles. The strain sensor is composed of single-layer graphene decorated with a film of metallic nanoislands and coated with a highly plasticized conductive polymer. The graphene-nanoisland film confers exceptional resolution, on the order of 0.0001% strain, and sensitivity with a gauge factor of 100 for 0.0001% strain (as shown in reference 39) while the highly plasticized conductive polymer confers stretchability commensurate with the skin, with a high dynamic range up to 10% strain (as described in reference 40).[39,40] In parallel, we developed a machine-learning algorithm using features from the strain signal to estimate the volume of boluses of unknown size. The application of an epidermal strain gauge and machine learning to the problem of swallowing volume provides the opportunity to differentiate signals from continuously varying biomechanical cues in an automated manner. Ultimately, we expect technologies such as this one to find broad use in many health-related fields, including sports medicine, mobile healthcare, and physical therapy.

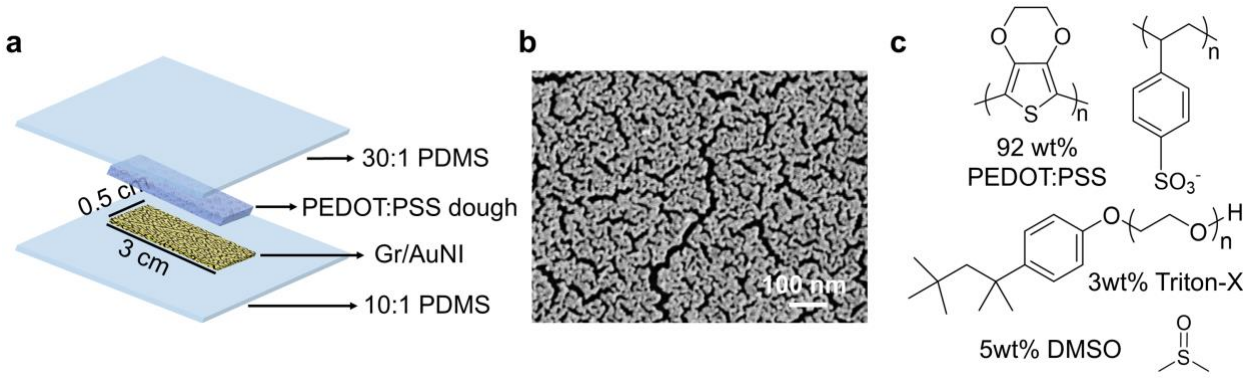

Figure 2.1. Materials and structure of the sensor. **(a)** A layer-by-layer representation of the strain sensor. **(b)** A scanning electron micrograph of the AuNIs. **(c)** Chemical structures of the PEDOT:PSS, Triton-X and DMSO which make up the PEDOT:PSS dough.

2.2 Experimental design

2.2.1 Composition of the strain sensor

The strain sensor comprises a sheet of monolayer graphene decorated with thermally evaporated metallic nanoislands (**Figure 2.1a**). We formed a morphology of metallic nanoislands by thermal evaporation of gold onto a film of graphene on copper. The gold was evaporated at a rate of 0.03 Å/s and the resulting nanoisland film had a low nominal thickness (8 nm). The nanoisland structure forms as a consequence of a balance between two characteristic energies: the binding energy of the gold atom to the graphene (~0.09 eV) and its diffusion barrier on graphene (~0.4 eV). Due to this interplay of energies, the evaporation of gold on graphene is biased towards island-like growth at low nominal thicknesses. The details of this process are discussed elsewhere.[39,41] The graphene-metal composite film is overlayed with a thin film of a highly plasticized conductive polymer, poly(3,4-ethylenedioxythiophene):poly(styrenesulfonate) (PEDOT:PSS). The thinness and stretchability of the sensor permits it to be transferred onto many types of substrate.[41] One potential issue associated with most types of nanoparticle-based strain gauge is unwanted sensitivity to temperature. In previous work, Marin et al. found that it was

possible to achieve a near-zero temperature coefficient of resistance in the type of graphene-metal composites explored here with precise tuning of the nominal thickness of the metal. In the case of gold, the optimal thickness was 8 nm (**Figure 2.1b**).[42] When used alone, the graphene/gold nanoisland (Gr/AuNI) film is mechanically brittle, and fails at approximately 2% strain. To increase the dynamic range of the sensor, we spray coated them with PEDOT:PSS "dough" (**Figure 2.1c**), a treatment which has been shown, in previous work, to extend the stretchability of the sensor up to approximately 80% (**Figure 2.2**).[40] While PEDOT:PSS "dough" has found wide use in bioelectronic applications when used alone,[43–48] its purpose here is to serve as a conductive bridge between the nanoislands in the event of fracture of the graphene film.[40]

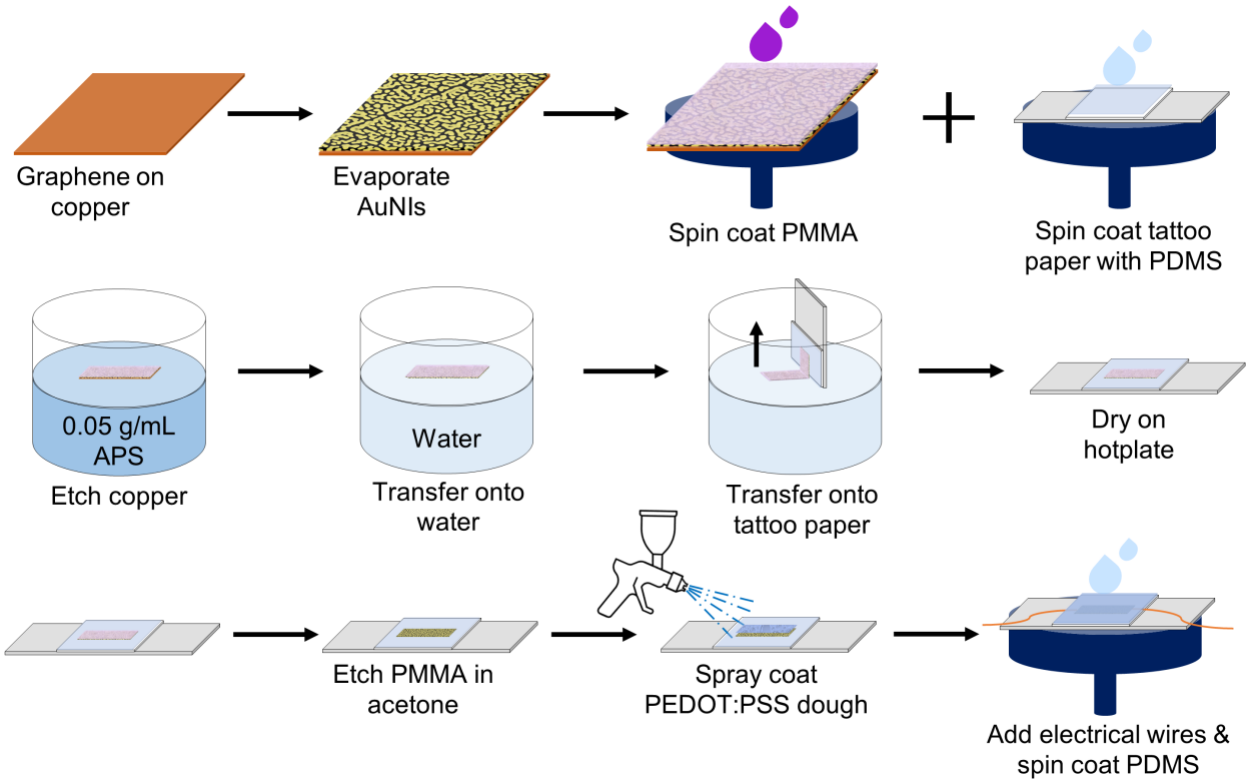

Figure 2.2. Schematic summary of the process used to fabricate the Gr/AuNI thin film coated with highly plasticized PEDOT:PSS

Each one of the three materials of which our composite strain sensor is composed exhibits sensitivity to strain individually. For example, single-layer graphene has piezoresistive properties arising from both a change in electronic band structure due to the elongation of C-C bonds and electron scattering caused by the defects in graphene. Ultrathin metallic films show piezoresistive properties due to nanoscale cracks that occur upon mechanical strain. Lastly, a highly plasticized conductive polymer film possesses piezoresistivity at high strains due to the granular structure of the film, where contractions and elongations can cause denser packing of the grains and thus change the electrical conduction. The mechanisms involved in sensing small strains for the Gr/AuNI structure are hypothesized to be the scattering of electrons in the densely packed regions, cracks formed in the film due to strain, and quantization of electrons due to physical confinement in the thickness of the film. The tunneling of electrons between unpercolated metal regions was ruled out as the dominant mechanism for the Gr/AuNI sensors via use of hexagonal boron nitride as the 2D substrate instead of graphene.[39] The addition of PEDOT:PSS "dough" added mechanical stability to Gr/AuNI film and strain sensitivity at high strain region.[40]

Measurement of strain alone can be confounded by motion artifacts: movement of the skin arising from coughing, sneezing, head turning, yawning, and talking. By combining measurements of strain with measurements of electrical muscle activity (sEMG), it is possible to differentiate the true swallowing from the motion artifacts. While it would be ideal to incorporate sEMG sensors on the same patch which contains the strain sensors, for the sake of experimental simplicity, we decided to use commercial sEMG electrodes in this prototype. For a further treatment of how sEMG and strain measurements can be combined to eliminate motion artifacts by machine learning, see Ramirez et al.[35]

2.2.2 Machine learning algorithm

We used machine learning for two purposes in our study. The first was to differentiate swallowing from artifacts of other types of motion. The second purpose was to estimate the volume of the swallowed water. In our study, we performed the swallowed-water-volume estimation through three steps: signal processing, feature extraction, and algorithm development. In the first step, we removed the noise in the sEMG and strain raw data (**Figure 2.3a**). In the second step, we identified the features in the swallow patterns in the strain data to build the volume estimation algorithm. We did this by first selecting two peak points and two valley points around the two swallowing peaks as fiducial points. Using these selected fiducial points, the algorithm was able to calculate additional features such as the durations, magnitudes, slopes, curvatures, and kernels of the swallowing peaks which represent the physiology of the moving muscles during a voluntary swallow. In addition to the strain data, we added the area underneath the curve from the processed sEMG data as a feature. In the last step, we trained the algorithm for each participant individually, using three-fold cross-validation tests on a total of 60 swallows per participant, to evaluate the performance of the trained algorithm **(Figure 2.3b)**.

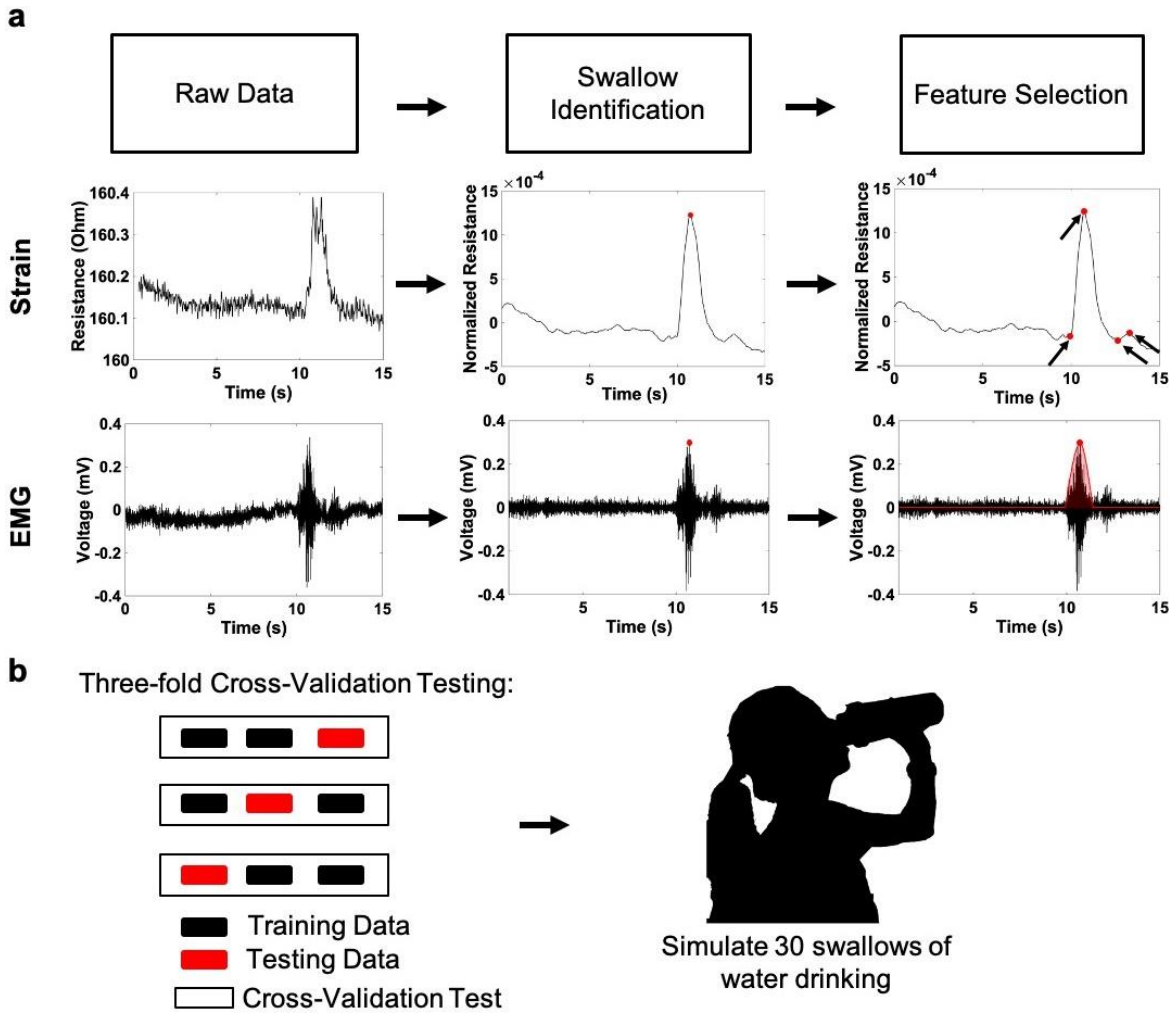

Figure 2.3. Schematic representation of the machine learning approach. **(a)** The workflow of the data processing and construction of the algorithm. First, the raw data from the strain and sEMG sensors is processed by removal of the baseline noise and filtering. Next, the algorithm is trained to identify the peak arising from swallowing and to look for the unique features around the peak. **(b)** The algorithm is trained and tested with a three-fold cross-validation method and used in estimation studies simulating 30 independent swallows of water by the participant.

2.3 Experimental Methods

2.3.1 Fabrication of the graphene-based strain gauge

The nanocomposite strain gauges were fabricated by modifying a previously published procedure.[40] Briefly, we thermally evaporated 8 nm gold at a rate of 0.03 Å/s on a 7.5 cm x 7.5 cm piece of copper foil with single-layer graphene (GrollTex, Inc.) grown on both sides using an Orion

System (AJA International). We recorded the temperature of the main chamber to be 26-27ºC during the evaporation process. The conductivity of the graphene film before the metal evaporation was ~2 kΩ. After evaporation of the metal, the resistance decreased to ~300-400 Ω.[40] We observed another increase in conductivity after spray-coating the PEDOT:PSS "dough" (~100-200 Ω). In the design of a strain gauge, the resolution, sensitivity, and signal-to-noise ratio are more important than the absolute conductivity. After deposition, we etched the back side of the piece in the air plasma cleaner for 5 min at 30 W at 250 mTorr to remove the excess graphene layer. We then spin-coated the side bearing the gold nanoislands with a 200 nm film of 4 wt% poly(methylmethacrylate) (PMMA, Alfa Aesar) dissolved in anisole (Acros Organics) at 4000 rpm with 1000 rpm/s for 60 s, and annealed it on a hotplate at 150 °C for 10 min. In this form, the Gr/AuNI films were ready to be transferred (**Figure 2.2**).

To make the epidermal film onto which we would transfer the strain gauges, we cut a 5 cm x 5 cm piece from a temporary tattoo paper (Duradecal, Laser Temporary Tattoo - carrier sheets) and placed it onto a glass slide (76 mm x 52 mm). We taped the edges of the tattoo paper to the glass slide using 1 mil (25 μm thick) polyimide (Kapton) tape; the tape covered the whole top surface and the edges of the back surface. Then we spin-coated polydimethylsiloxane (Sylgard 184 PDMS, 10:1 base-to-curing agent ratio, 1 MPa) onto the tattoo paper at 1000 rpm with 500 rpm/s for 60 s and cured the PDMS on a hotplate at 150 °C for 10 min. We etched the copper support of a 3 cm x 0.75 cm strain sensor patch piece in 0.05 g/mL ammonium persulfate solution (APS, Acros Organics), transferred it onto the tattoo paper, and allowed it to dry in air for 12 h. Later, we etched off the PMMA support in an acetone bath for 1 min at 50 °C, rinsed the piece with isopropyl alcohol, and gently dried it with a stream of compressed air.

For the elastomeric conductive polymer layer, we used a highly plasticized poly(3,4-ethylenedioxythiophene) polystyrene sulfonate (PEDOT:PSS) "dough" recipe that was 92 wt% PEDOT:PSS (Clevios PH 1000, 1.2 wt% in water), 3 wt% Triton X-100 (Sigma Aldrich), and 5 wt% dimethyl sulfoxide (DMSO, Sigma Aldrich).[46] We further diluted this stock solution in deionized water in a ratio of 1:3 (stock:water). We spray-coated the PEDOT:PSS solution using a custom stencil mask to cover everywhere on the sensor patch except the Gr/AuNI sensor area. We placed the sensor piece on a hotplate at 150 °C and sprayed 8 x 1 s intervals as a primer, 4 x 10 s spray intervals, then 4 x 20 s spray intervals waiting about 1 min between each spray interval and rotating the piece 90° for an even coverage. After spray deposition of the polymer, we added copper wiring (36 gauge) to each sensor and connected it with carbon paint (Ted Pella, Inc.). We let the carbon paint dry for 12 h (to obtain a stable readout of resistance), and later, we spin-coated PDMS (30:1 base-to-curing agent ratio, 0.15 MPa) onto the whole assembly at 1000 rpm with 500 rpm/s for 60 s. We cured the PDMS on a hotplate at 150 °C for 10 min.

2.3.2 On-body experiments

We performed on-body experiments with 11 healthy participants (ages between 21-30 years old, 3 female, 8 male) with no history of swallowing disorders. We used an approved protocol reviewed by the Internal Review Board at the University of California San Diego Human Research Protections Program (Project # 191950S) and collected signed consent forms from each participant prior to the study.

The placement of the sensor and adhesion to the skin were critical factors in the collection of high-quality data. Thus, the male participants were directed to shave their necks for better

adhesion of the sensors. The participants sat comfortably in a chair, while we placed two sEMG electrodes underneath their chin on the upper throat area, and a reference electrode on the left collarbone (**Figure 2.4a**). We then applied the strain sensor to the skin by transferring it from the tattoo paper. The long axis of the sensor was positioned perpendicular to the neck, on the center of the throat, just below the sEMG electrodes **(Figure 2.4a)**. The horizontal orientation of the strain sensor was more favorable than the vertical orientation due to available space on the participant's throat and nearly similar estimation results **(Figure A.1)**. After this, we removed the backing of the tattoo paper with a wet paper towel. The sEMG electrodes and wires from the strain sensor were connected to the MAX30001 Evaluation kit for data acquisition. Finally, we immobilized the wiring with Scotch tape. With regard to biocompatibility, all of the components are encapsulated in PDMS, which is well known to be biocompatible.[49,50,51,52] That is, instances of contact dermatitis are rare. Also, the commercial electrodes used for sEMG are ubiquitous in professional healthcare settings.

Once we verified the correct placement of the sensor by visually confirming that the strain sensor lied directly underneath the sEMG electrodes and on the middle of the throat, we asked the participants to sit in a chair in an upright but relaxed position **(Figure 2.4b)**. Before each swallow recording, the participants were given a small cup of water of a known volume (5 mL, 10 mL, etc.) and were asked to hold the liquid volume in their oral cavity until they were directed to swallow (**Figure 2.4c**). Once the recording started, the participants remained still for 10 s, then swallowed the water, and then waited for another 10 s after which the recording was stopped. We tested volumes starting from 5 mL to 30 mL, increasing in 5 mL increments for each participant (5 mL, 10 mL, 15 mL, 20 mL, 25 mL, 30 mL). The volumes were given in random order. We repeated

each volume swallow 10 times, yielding 60 swallows per participant in total. During this time, the participants were allowed to take as many breaks as needed.

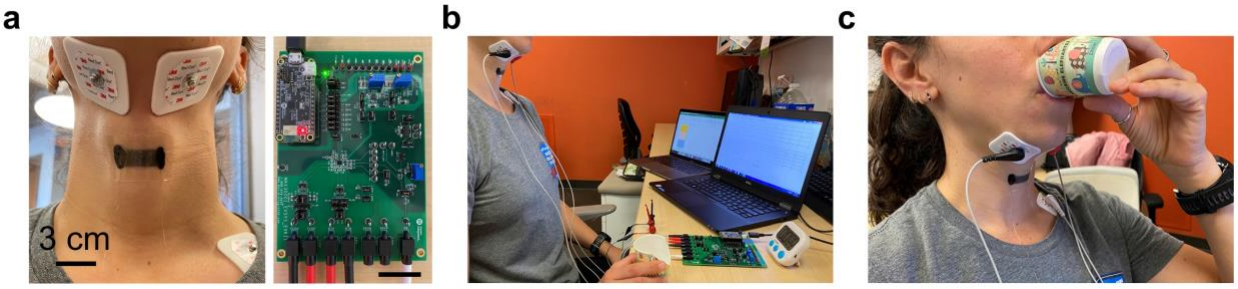

Figure 2.4. On-body experimental set-up. **(a)** A close-up image of the strain and sEMG sensors on the throat of the participant and the MAX30001 Evaluation kit used in the experiments. Scale bar is 3 cm. **(b)** The photograph shows the testing set-up where the sensors are connected to the Evaluation kit which is connected to a laptop, and the participant is seated in a relaxed position before instructed to swallow water from the cup. **(c)** The image captures the participant being instructed to swallow the known volume of water.

2.3.3 Data acquisition

To measure and collect sEMG and strain signals from the sensors, we used the commercially available "MAX30001 Evaluation System" (MAX30001EVSYS) This evaluation system includes the MAX30001 Evaluation kit and a corresponding GUI system software for configuring and saving the data from the kit. This Evaluation kit can measure up to one channel of ECG data (output data in mV) and one channel of Bioimpedance data (output data in mΩ). For this project, we connected the sEMG electrodes to the ECG channel (the sEMG signals' magnitude and spectral content are similar to ECG signals) and the strain sensor wires to the Bioimpedance (BioZ) channel of the Evaluation kit. The external lead biasing was used for both the channels for which the reference electrode, placed on the collarbone, was connected to the Body Bias pin of the kit. The ECG channel used for the sEMG signals was configured to have a gain of 20 V/V and a

sampling rate of 512 samples/s. On the other hand, the BioZ channel used for the strain signals was configured to have a gain of 10 V/V, with a current of 32 μA at 80 kHz, and a sampling rate of 64 samples/s. To preserve the full spectral content and have the flexibility to post-process the data at a later stage, all the digital filters post-ADC were bypassed (**Figure A.2**).

2.3.4 Construction of the volume estimation model

We began constructing the volume estimation model by processing the raw data from the sensors (**Figure 2.3a**). First, we cleaned the raw data from the sEMG and strain sensors, which were composed of 660 trials/sensor in total from 11 participants. For each trial, the swallowing data was a one-dimensional temporal signal. The data output rates were 64 samples/s for the strain sensor and 512 samples/s for the sEMG sensor. The strain data was cleaned with a three-order Savitzky-Golay filter with the span of 1 s in each filter kernel. For the sEMG data, we removed the low-frequency baseline drift noise lower than 10 Hz.

Next, we extracted the swallowing signal features from the sEMG and strain data. For the features in the sEMG signal arising from swallowing, we calculated the area under the peak versus time by integrating a time interval of 0.4 s that centered at the peak of the swallow. For the strain signal features, we first identified the swallowing peak with our algorithm and then applied the fiducial point method to quantify the features of interest. We identified the swallow peak by searching for the maximum positive differentiation value in the swallowing data. The pseudocode of the swallowing peak detection algorithm is shown in **Figure A.3**. Using this approach, we empirically selected two valleys and two peaks in the strain data as illustrated in **Figure 2.3a**. The first of the two peaks belonged to the swallowing peak, whereas the next one was attributed to

motion due to recovery from the swallow. The two valleys were present right before and after the swallow peak. Using the fiducial points, we extracted additional features by fitting three-order polynomial curves. These additional features included the durations, magnitudes, slopes, curvatures, and kernels constructed by the curves enclosed within the fiducial points in the strain data, and area under the curve in the sEMG data (**Table A.1**).

Lastly for the machine learning, we applied canonical correlation analysis to build the swallowing volume estimation algorithm. Canonical correlation analysis is a technique that seeks the optimal linear combination of the input features to fit the output swallow volume. We used the canonical correlation analysis to find the features for the most optimal linear combination. In our case, the input of the algorithm was the extracted features, and the output was the swallowed water volumes by the participants. We evaluated the built algorithm using three-fold cross-validation tests on the training data for each participant by randomly splitting the 60 trials into three groups, with each group having 20 trials. Next, we trained the swallow volume estimation algorithm with the data from two groups, while using the third group for testing the model. We iterated through all three-fold computations and evaluated the accuracy of the estimations while accumulating the swallowed volume each run. For example, from 60 tested trials from one participant, we randomly selected 30 trials and summed the predicted volumes (**Figure 2.3b**). Finally, we computed the accuracy of the algorithm by comparing the estimated swallow volume to the exact swallow volume. It is important to note that the algorithm estimations were calculated one participant at a time, therefore making the results specific to each participant.

2.4 Results and Discussion

Swallowed volume had a strong influence on the strain present at the surface of the skin. In particular, the volume appeared to be closely related to the ratios between the heights of the two peaks in the signal (**Figure 2.5**). As the liquid volume increased, the first peak became smaller in magnitude whereas the second peak became larger, possibly due to the large displacement of the hyoid bone to allow for the epiglottis to open enough for a larger volume to pass.

It is worthwhile to consider the physiological origins of the features in the data. Such an understanding can lead to improved design of devices and can inform interpretation of the volume estimation algorithm. The sEMG data reflected muscle activity in the submental region, whereas the strain waveforms arose from movement of the skin over the laryngeal/thyroid notch during swallowing. The strain waveforms for each participant showed two peaks due to the tensile strain experienced by the skin during a swallow. The first tensile strain peak represented the start of the oral propulsive stage during a liquid bolus swallow, described by the Four Stage Model.[53,54] During this stage, the tongue rises upward to meet the top of the mouth and open the back of the oral cavity to squeeze the liquid bolus back into the pharynx. The second tensile strain peak represented the pharyngeal stage. During this stage, the hyoid bone and the larynx are displaced upward and forward, causing the suprahyoid and thyrohyoid muscles to contract as the epiglottis tilts backward to allow the bolus to travel in a downward motion.[55–57] Once the bolus was pushed down, all structures reverted to their original positions, resulting in the relaxation behavior that appeared after the second tensile strain peak.

Due to the low viscosity of a liquid bolus, it has been observed that the pharyngeal stage begins during the oral propulsion stage. The first peak in the strain signal arises from the first phase of the swallowing event where the muscles on the throat open the way to esophagus; the second

peak is from the relaxation of the structures back into their original positions. In our previous work, the peaks in the strain signal and the phases of the swallow were identified by X-ray videofluoroscopy using a radio-opaque bolus.[35] In this experiment, one of the patients was given a barium-containing paste, and the swallow and was recorded by video X-ray imaging. The patient performed an identical swallow while wearing the strain sensor.

According to our observations, the height and duration ratios of these two tensile strain peaks varied between individuals but were always present. These features enabled our estimation results using the machine learning algorithm in the later stages, regardless of how different the swallowing behaviors were for each participant.

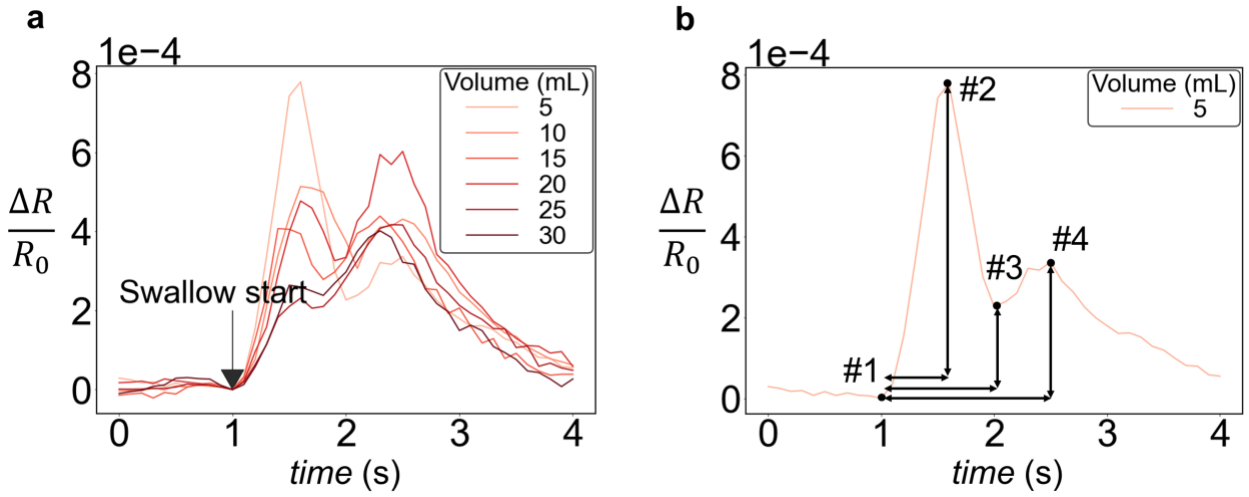

Figure 2.5. Evolution in strain signals as a function of swallowed volume for one participant. Vertical axes show the change in resistance normalized by the baseline resistance and the horizontal axes show the time in seconds. **(a)** All the volumes are plotted for comparison for one participant. Data are plotted after data processing. Each line is the average of 10 swallows. **(b)** The plot shows a representative swallow from the strain sensor for 5 mL and some of the features that are extracted by the machine learning algorithm. Four fiducial points are labeled from 1-4. The features include the distance between these points, the amplitudes, the slopes between the points as shown on the plot.

Lastly, we developed a machine learning algorithm to automate the detection of a swallow in a strain signal and identify the features that aid the estimation of an unknown swallowed volume by an individual. We used the strain and sEMG signals from the cohort study to train the algorithm and validate it using a three-fold cross-validation method. Each fold in the validation method split the 60 total swallows by a participant into 3 groups of 20 swallows and assigned two of them to be the training data and one of them to be the testing data. The accuracy of the estimation of the true volumes of the testing data is shown in **Figure 2.6**. The average accuracy of the estimations of all the cohorts was higher than 92%, reaching as high as 98%, as seen in **Figure 2.6a**. The absolute error for estimation of each tested volume was on average 5 mL and decreased as swallow volume increased (**Figure 2.6b**). Using the estimation results, we plotted a calibration curve to compare the true observed volumes and the estimation volumes. Except for one participant, all of our cohort data estimations followed closely to the true volumes (**Figure 2.6c**).

Statistically, more training data results in better performance of the algorithm and thus better volume estimation. In our studies, the machine learning algorithm estimated cumulative swallowed volumes with higher accuracy than the volume of a single swallow because of the law of averages. Each cumulative swallowed volume was the sum of 30 swallows randomly selected out of 60 total swallows collected from the participants. Thus, having more data per estimation increased the accuracy of the algorithm. In addition, the algorithm was able to estimate the volumes of larger swallows with more accuracy than the volumes of smaller swallows. This can be explained from our observations throughout the experiments with different participants. Most of our participants described 5 mL as too small to swallow, implying that the 10-30 mL range is more comparable to quantities swallowed for everyday hydration. Hence, there were more variations between each trial for 5 mL than any other volume. Related to this limitation is the amount of

water we asked participants to swallow throughout the experiment. Each seated participant drank roughly 1.05 L of water, which was the maximum amount the participants could drink comfortably during the experiment. Due to this limitation, we did not collect more than 10 trials per volume. Lastly, we observed that the placement of the strain sensor was crucial for the validity and reproducibility of the data. If the strain sensor was placed in an off-center position or could not conform well with the participant's skin, the estimation results were less reliable, which was the case for Participant 8. Nevertheless, we included the Participant 8's data in our volume estimation studies to test the adaptability and robustness of our sensor system. After all, even with the sensor placement issue, the estimation results were very promising and proved the robustness of our overall sensor system.

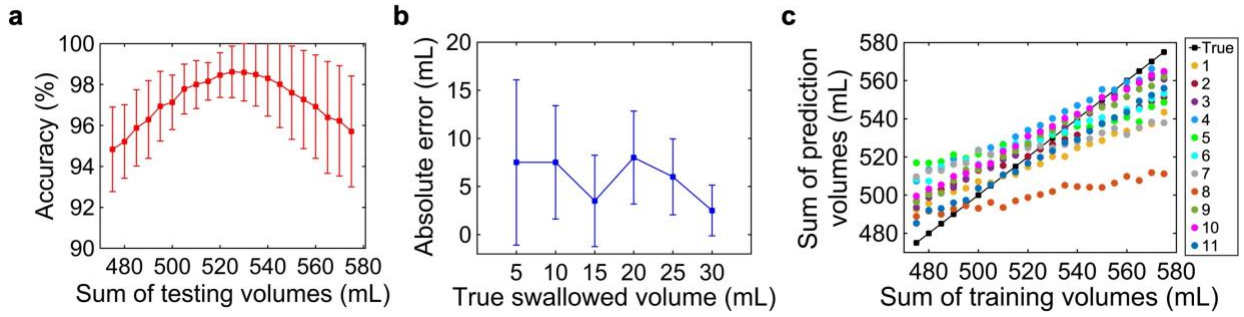

Figure 2.6. Swallowed water volume estimation results. **(a)** The plot shows the accuracy of the predicted cumulative volumes. **(b)** The plot shows the absolute error in milliliters for each tested volume. **(c)** The plot shows a calibration curve between the predicted cumulative volumes and the training cumulative volumes for each tested participant.

2.5 Conclusions

In this work, we have demonstrated the use and application of coupling a highly sensitive strain sensor with a machine learning algorithm to perform an accurate estimation of swallowed

volume. The nanomaterial-enabled device permits minimally obtrusive measurements, which may facilitate the assessment of hydration state, or be used to monitor swallowing function over time for the prevention of disease. Nevertheless, in its current state, our system has some limitations. For example, the sensor platform was tested while the participants were seated. In real-world conditions—i.e., sports medicine—measurement will necessarily take place while participants are in motion. To solve this problem, the form factor of the supporting electronics will have to be miniaturized, and the sEMG electrodes will have to be integrated into the epidermal patch. Our current work is moving toward a flexible custom PCB that wirelessly transfers data to a phone app during exercise. Another limitation to our current system is the fact that the machine learning algorithm is run on a single participant basis. In order to accommodate for this problem, we are working towards collecting more swallowing data from different participants to add into the training pool of the algorithm. Eventually with all the accumulated swallowing data, the algorithm will be able to estimate any swallowed volume with high accuracy for any new participant.

We are also expanding the type of liquid boluses whose volumes can be measured. For example, the range of properties represented by water, energy drinks, carbonated beverages, protein shakes, and chewed food pose challenges for measurement using our system, but not insurmountable ones. In previous work, we have shown that it is possible for a system similar to the one described here to differentiate water, yogurt, and a cracker with high accuracy. The ability to identify the food bolus and also estimate its volume could have implications in monitoring food intake to treat obesity. Given the centrality of swallowing to essentially all aspects of human health, we believe there is significant potential for the device and methodology described here in the fields of sports medicine, rehabilitation, nutrition science, and speech-language pathology.

Acknowledgements

This work was supported by a gift from PepsiCo & the Gatorade Sports Sciences Institute. Additional support was provided by the member companies of the Center for Wearable Sensors in the Jacobs School of Engineering at the University of California, San Diego, including Dexcom, Gore, Honda, Huami, Instrumentation Laboratory, Kureha, Merck KGaA, PepsiCo, Roche, Samsung, and Sony. L.B. acknowledges the support provided by the National Science Foundation Graduate Research Fellowship Program under Grant DGE-2038238. This work was performed in part at the San Diego Nanotechnology Infrastructure (SDNI), a member of the National Nanotechnology Coordinated Infrastructure, which is supported by the National Science Foundation (Grant ECCS-1542148). Lastly, the authors thank Rory Runser for helpful discussions.

Chapter 2 and Appendix A, in full, is a reprint of the material as it appears in ACS Applied Nano Materials, 2021, 4 (8), 8126-8134. Beril Polat, Laura L. Becerra, Po-Ya Hsu, Vineel Kaipu, Patrick P. Mercier, Chung-Kuan Cheng, and Darren J. Lipomi. American Chemical Society, 2021. The dissertation author was the primary investigator and author of this paper.

References

(1) Popkin, B. M.; D'Anci, K. E.; Rosenberg, I. H. Water, Hydration, and Health. *Nutr. Rev.* **2010**, *68* (8), 439–458. https://doi.org/10.1111/j.1753-4887.2010.00304.x.

(2) Jéquier, E.; Constant, F. Water as an Essential Nutrient: The Physiological Basis of Hydration. *Eur. J. Clin. Nutr.* **2010**, *64* (2), 115–123. https://doi.org/10.1038/ejcn.2009.111.

(3) Sawka, M. N.; Cheuvront, S. N.; Carter III, R. Human Water Needs. *Nutr. Rev.* **2005**, *63* (6), 30–39. https://doi.org/10.1301/nr.2005.jun.S30–S39.

(4) Gandy, J.; Martinez, H.; Guelinckx, I.; Moreno, L. A.; Bardosono, S.; Salas-Salvad, J.; Kavouras, S. A. Relevance of Assessment Methods for Fluid Intake. *Ann. Nutr. Metab.* **2016**, *68* (2), 1–5. https://doi.org/10.1159/000446197.

(5) Palmer, J. B.; Kuhlemeir, K. V.; Tippett, D. C.; Lynch, C. A Protocol for the Videofluorographic Swallowing Study. *Dysphagia* **1993**, *8*, 209–214. https://doi.org/https://doi.org/10.1007/BF01354540.

(6) Logemann, J. A. *Manual for the Videofluorographic Study of Swallowing*, 2nd ed.; PRO-ED: Austin, TX, 1993.

(7) Logemann, J. A. Role of the Modified Barium Swallow in Management of Patients with Dysphagia. *Otolaryngol. - Head Neck Surg.* **1997**, *116* (3), 335–338. https://doi.org/10.1016/S0194-5998(97)70269-9.

(8) Martin-Harris, B.; Logemann, J. A.; McMahon, S.; Schleicher, M.; Sandidge, J. Clinical Utility of the Modified Barium Swallow. *Dysphagia* **2000**, *15* (3), 136–141. https://doi.org/10.1007/s004550010015.

(9) Langmore, S. E.; Schatz, K.; Olsen, N. Fiberoptic Endoscopic Examination of Swallowing Safety: A New Procedure. *Dysphagia* **1988**, *2* (4), 216–219. https://doi.org/10.1007/BF02414429.

(10) Bastian, R. W. Videoendoscopic Evaluation of Patients with Dysphagia: An Adjunct to the Modified Barium Swallow. *Otolaryngol. Neck Surg.* **1991**, *104* (3), 339–350. https://doi.org/10.1177/019459989110400309.

(11) Badenduck, L. A.; Matthews, T. W.; McDonough, A.; Dort, J. C.; Wiens, K.; Kettner, R.; Crawford, S.; Kaplan, B. J. Fiber-Optic Endoscopic Evaluation of Swallowing to Assess Swallowing Outcomes as a Function of Head Position in a Normal Population. *Otolaryngol. Neck Surg.* **2014**, *43* (9). https://doi.org/https://doi.org/10.1186/1916-0216-43-9.

(12) Amft, O.; Gerhard, T. Methods for Detection and Classification of Normal Swallowing from Muscle Activation and Sound. *IEEE* **2006**, No. In 2006 Pervasive Health Conference and Workshops, 1–10.

(13) Sazonov, E.; Stephanie, S.; Lopez-Meyer, P.; Makeyev, O.; Sazonova, N.; Melanson, E. L.; Neuman, and M. Non-Invasive Monitoring of Chewing and Swallowing for Objective Quantification of Ingestive Behavior. *Physiol. Meas.* **2008**, *29* (5), 525–541. https://doi.org/http://dx.doi.org/10.1088/0967-3334/29/5/001.

(14) Li, W.; Guo, J.; Fan, D. 3D Graphite–Polymer Flexible Strain Sensors with Ultrasensitivity and Durability for Real-Time Human Vital Sign Monitoring and Musical Instrument Education. *Adv. Mater. Technol.* **2017**, *2* (6), 1–9. https://doi.org/10.1002/admt.201700070.

(15) Zhu, Y.; Hu, Y.; Zhu, P.; Zhao, T.; Liang, X.; Sun, R.; Wong, C. P. Enhanced Oxidation Resistance and Electrical Conductivity Copper Nanowires-Graphene Hybrid Films for Flexible Strain Sensors. *New J. Chem.* **2017**, *41* (12), 4950–4958. https://doi.org/10.1039/c7nj00246g.

(16) Fan, J. A.; Yeo, W. H.; Su, Y.; Hattori, Y.; Lee, W.; Jung, S. Y.; Zhang, Y.; Liu, Z.; Cheng, H.; Falgout, L.; Bajema, M.; Coleman, T.; Gregoire, D.; Larsen, R. J.; Huang, Y.; Rogers, J. A. Fractal Design Concepts for Stretchable Electronics. *Nat. Commun.* **2014**, *5*, 1–8. https://doi.org/10.1038/ncomms4266.

(17) Son, D.; Lee, J.; Qiao, S.; Ghaffari, R.; Kim, J.; Lee, J. E.; Song, C.; Kim, S. J.; Lee, D. J.; Jun, S. W.; Yang, S.; Park, M.; Shin, J.; Do, K.; Lee, M.; Kang, K.; Hwang, C. S.; Lu, N.; Hyeon, T.; Kim, D. H. Multifunctional Wearable Devices for Diagnosis and Therapy of Movement Disorders. *Nat. Nanotechnol.* **2014**, *9* (5), 397–404. https://doi.org/10.1038/nnano.2014.38.

(18) Kim, D. H.; Lu, N.; Ma, R.; Kim, Y.; Kim, R.-H.; Wang, S.; Wu, J.; Won, S. M.; Tao, H.; Islam, A.; Yu, K. J.; Kim, T.; Chowdhury, R.; Ying, M.; Xu, L.; Li, M.; Chung, H.-J.; Keum, H.; Mccormick, M.; Liu, P.; Zhang, Y.; Omenetto, F. G.; Huang, Y.; Coleman, T.; Rogers, J. A. Epidermal Electronics. *Science (80-.).* **2011**, *333* (August), 838–843. https://doi.org/10.1126/science.1206157.

(19) Kim, D. H.; Rogers, J. A. Stretchable Electronics: Materials Strategies and Devices. *Adv. Mater.* **2008**, *20* (24), 4887–4892. https://doi.org/10.1002/adma.200801788.

(20) Khang, D.-Y.; Jiang, H.; Huang, Y.; Rogers, J. A. A Stretchable Form of Single-Crystal.

Science (80-.). **2006**, *311* (January), 208–212.

(21) Segev-Bar, M.; Haick, H. Flexible Sensors Based on Nanoparticles. *ACS Nano* **2013**, *7* (10), 8366–8378. https://doi.org/10.1021/nn402728g.

(22) Tao, L. Q.; Wang, D. Y.; Tian, H.; Ju, Z. Y.; Liu, Y.; Pang, Y.; Chen, Y. Q.; Yang, Y.; Ren, T. L. Self-Adapted and Tunable Graphene Strain Sensors for Detecting Both Subtle and Large Human Motions. *Nanoscale* **2017**, *9* (24), 8266–8273. https://doi.org/10.1039/c7nr01862b.

(23) Tao, L. Q.; Tian, H.; Liu, Y.; Ju, Z. Y.; Pang, Y.; Chen, Y. Q.; Wang, D. Y.; Tian, X. G.; Yan, J. C.; Deng, N. Q.; Yang, Y.; Ren, T. L. An Intelligent Artificial Throat with Sound-Sensing Ability Based on Laser Induced Graphene. *Nat. Commun.* **2017**, *8*, 1–8. https://doi.org/10.1038/ncomms14579.

(24) Xu, R.; Wang, D.; Zhang, H.; Xie, N.; Lu, S.; Qu, K. Simultaneous Detection of Static and Dynamic Signals by a Flexible Sensor Based on 3d Graphene. *Sensors (Switzerland)* **2017**, *17* (5). https://doi.org/10.3390/s17051069.

(25) Wang, L.; Jackman, J. A.; Tan, E. L.; Park, J. H.; Potroz, M. G.; Hwang, E. T.; Cho, N. J. High-Performance, Flexible Electronic Skin Sensor Incorporating Natural Microcapsule Actuators. *Nano Energy* **2017**, *36* (April), 38–45. https://doi.org/10.1016/j.nanoen.2017.04.015.

(26) Ertekin, C.; Pehlivan, M.; Aydoğdu, I.; Ertaşl, M.; Uludağ, B.; Çlelebi, G.; Çlolakoğlu, Z.; Sağduyu, A.; Yüceyar, N. An Electrophysiological Investigation of Deglutition in Man. *Muscle Nerve* **1995**, *18* (10), 1177–1186. https://doi.org/10.1002/mus.880181014.

(27) Ertekin, C.; Yüceyar, N.; Aydoğdu, I.; Karasoy, H. Electrophysiological Evaluation of Oropharyngeal Swallowing in Myotonic Dystrophy. *J. Neurol. Neurosurg. Psychiatry* **2001**, *70* (3), 363–371. https://doi.org/10.1136/jnnp.70.3.363.

(28) Ashida, I.; Miyaoka, S.; Miyaoka, Y. Comparison of Video-Recorded Laryngeal Movements during Swallowing by Normal Young Men with Piezoelectric Sensor and Electromyographic Signals. *J. Med. Eng. Technol.* **2009**, *33* (6), 496–501.

https://doi.org/10.1080/03091900902952691.

(29) Li, Q.; Hori, K.; Minagi, Y.; Ono, T.; Chen, Y. jin; Kondo, J.; Fujiwara, S.; Tamine, K.; Hayashi, H.; Inoue, M.; Maeda, Y. Development of a System to Monitor Laryngeal Movement during Swallowing Using a Bend Sensor. *PLoS One* **2013**, *8* (8), 1–8. https://doi.org/10.1371/journal.pone.0070850.

(30) Schultheiss, C.; Schauer, T.; Nahrstaedt, H.; Seidl, R. O. Evaluation of an EMG Bioimpedance Measurement System for Recording and Analysing the Pharyngeal Phase of Swallowing. *Eur. Arch. Oto-Rhino-Laryngology* **2013**, *270* (7), 2149–2156. https://doi.org/10.1007/s00405-013-2406-3.

(31) Roh, E.; Hwang, B. U.; Kim, D.; Kim, B. Y.; Lee, N. E. Stretchable, Transparent, Ultrasensitive, and Patchable Strain Sensor for Human-Machine Interfaces Comprising a Nanohybrid of Carbon Nanotubes and Conductive Elastomers. *ACS Nano* **2015**, *9* (6), 6252–6261. https://doi.org/10.1021/acsnano.5b01613.

(32) Hwang, B. U.; Lee, J. H.; Trung, T. Q.; Roh, E.; Kim, D. Il; Kim, S. W.; Lee, N. E. Transparent Stretchable Self-Powered Patchable Sensor Platform with Ultrasensitive Recognition of Human Activities. *ACS Nano* **2015**, *9* (9), 8801–8810. https://doi.org/10.1021/acsnano.5b01835.

(33) Zhang, S. H.; Wang, F. X.; Li, J. J.; Peng, H. D.; Yan, J. H.; Pan, G. B. Wearable Wide-Range Strain Sensors Based on Ionic Liquids and Monitoring of Human Activities. *Sensors (Switzerland)* **2017**, *17* (11), 1–10. https://doi.org/10.3390/s17112621.

(34) Kim, M. K.; Kantarcigil, C.; Kim, B.; Baruah, R. K.; Maity, S.; Park, Y.; Kim, K.; Lee, S.; Malandraki, J. B.; Avlani, S.; Smith, A.; Sen, S.; Alam, M. A.; Malandraki, G.; Lee, C. H. Flexible Submental Sensor Patch with Remote Monitoring Controls for Management of Oropharyngeal Swallowing Disorders. *Sci. Adv.* **2019**, *5* (12), 1–10. https://doi.org/10.1126/sciadv.aay3210.

(35) Ramírez, J.; Rodriquez, D.; Qiao, F.; Warchall, J.; Rye, J.; Aklile, E.; Chiang, A. S. C.; Marin, B. C.; Mercier, P. P.; Cheng, C. K.; Hutcheson, K. A.; Shinn, E. H.; Lipomi, D. J. Metallic Nanoislands on Graphene for Monitoring Swallowing Activity in Head and Neck Cancer Patients. *ACS Nano* **2018**, *12* (6), 5913–5922.

https://doi.org/10.1021/acsnano.8b02133.

(36) Schultheiss, C.; Schauer, T.; Nahrstaedt, H.; Seidl, R. O. Automated Detection and Evaluation of Swallowing Using a Combined Emg/Bioimpedance Measurement System. *Sci. World J.* **2014**, *2014*. https://doi.org/10.1155/2014/405471.

(37) Farooq, M.; Sazonov, E. A Novel Wearable Device for Food Intake and Physical Activity Recognition. *Sensors (Switzerland)* **2016**, *16* (7). https://doi.org/10.3390/s16071067.

(38) Shieh, W.-Y.; Wang, C.-M.; Cheng, H.-Y. K.; Wang, C.-H. Using Wearable and Non-Invasive Sensors to Verification , and Clinical Application. *Sensors* **2019**, *19* (11), 2624.

(39) Ramírez, J.; Urbina, A. D.; Kleinschmidt, A. T.; Finn, M.; Edmunds, S. J.; Esparza, G. L.; Lipomi, D. J. Exploring the Limits of Sensitivity for Strain Gauges of Graphene and Hexagonal Boron Nitride Decorated with Metallic Nanoislands. *Nanoscale* **2020**, *12* (20), 11209–11221. https://doi.org/10.1039/d0nr02270e.

(40) Ramírez, J.; Rodriquez, D.; Urbina, A. D.; Cardenas, A. M.; Lipomi, D. J. Combining High Sensitivity and Dynamic Range: Wearable Thin-Film Composite Strain Sensors of Graphene, Ultrathin Palladium, and PEDOT:PSS. *ACS Appl. Nano Mater.* **2019**, *2* (4), 2222–2229. https://doi.org/10.1021/acsanm.9b00174.

(41) Zaretski, A. V.; Root, S. E.; Savchenko, A.; Molokanova, E.; Printz, A. D.; Jibril, L.; Arya, G.; Mercola, M.; Lipomi, D. J. Metallic Nanoislands on Graphene as Highly Sensitive Transducers of Mechanical, Biological, and Optical Signals. *Nano Lett.* **2016**, *16* (2), 1375–1380. https://doi.org/10.1021/acs.nanolett.5b04821.

(42) Marin, B. C.; Root, S. E.; Urbina, A. D.; Aklile, E.; Miller, R.; Zaretski, A. V.; Lipomi, D. J. Graphene-Metal Composite Sensors with Near-Zero Temperature Coefficient of Resistance. *ACS Omega* **2017**, *2* (2), 626–630. https://doi.org/10.1021/acsomega.7b00044.

(43) Vosgueritchian, M.; Lipomi, D. J.; Bao, Z. Highly Conductive and Transparent PEDOT:PSS Films with a Fluorosurfactant for Stretchable and Flexible Transparent Electrodes. *Adv. Funct. Mater.* **2012**, *22* (2), 421–428. https://doi.org/10.1002/adfm.201101775.

(44) Seyedin, M. Z.; Razal, J. M.; Innis, P. C.; Wallace, G. G. Strain-Responsive Polyurethane/PEDOT:PSS Elastomeric Composite Fibers with High Electrical Conductivity. *Adv. Funct. Mater.* **2014**, *24* (20), 2957–2966. https://doi.org/10.1002/adfm.201303905.

(45) Savagatrup, S.; Chan, E.; Renteria-Garcia, S. M.; Printz, A. D.; Zaretski, A. V.; O'Connor, T. F.; Rodriquez, D.; Valle, E.; Lipomi, D. J. Plasticization of PEDOT:PSS by Common Additives for Mechanically Robust Organic Solar Cells and Wearable Sensors. *Adv. Funct. Mater.* **2015**, *25* (3), 427–436. https://doi.org/10.1002/adfm.201401758.

(46) Jin Young, O.; Kim, S.; Baik, H. K.; Jeong, U. Conducting Polymer Dough for Deformable Electronics. *Adv. Mater.* **2016**, *28* (22), 4455–4461. https://doi.org/10.1002/adma.201502947.

(47) Wen, Z.; Yang, Y.; Sun, N.; Li, G.; Liu, Y.; Chen, C.; Shi, J.; Xie, L.; Jiang, H.; Bao, D.; Zhuo, Q.; Sun, X. A Wrinkled PEDOT:PSS Film Based Stretchable and Transparent Triboelectric Nanogenerator for Wearable Energy Harvesters and Active Motion Sensors. *Adv. Funct. Mater.* **2018**, *28* (37), 1–8. https://doi.org/10.1002/adfm.201803684.

(48) Bhattacharjee, M.; Soni, M.; Escobedo, P.; Dahiya, R. PEDOT:PSS Microchannel-Based Highly Sensitive Stretchable Strain Sensor. *Adv. Electron. Mater.* **2020**, *6* (8). https://doi.org/10.1002/aelm.202000445.

(49) Mojsiewicz-Pienkowska, K.; Jamrógiewicz, M.; Szymkowska, K.; Krenczkowska, D. Direct Human Contact with Siloxanes (Silicones) - Safety or Risk Part 1. Characteristics of Siloxanes (Silicones). *Front. Pharmacol.* **2016**, *7* (MAY), 1–8. https://doi.org/10.3389/fphar.2016.00132.

(50) Ertel, S. I.; Ratner, B. D.; Kaul, A.; Schway, M. B.; Horbett, T. A. In Vitro Study of the Intrinsic Toxicity of Synthetic Surfaces to Cells. *J. Biomed. Mater. Res.* **1994**, *28* (6), 667–675. https://doi.org/10.1002/jbm.820280603.

(51) Lee, J. N.; Jiang, X.; Ryan, D.; Whitesides, G. M. Compatibility of Mammalian Cells on Surfaces of Poly(Dimethylsiloxane). *Langmuir* **2004**, *20* (26), 11684–11691. https://doi.org/10.1021/la048562+.

(52) Van Kooten, T. G.; Whitesides, J. F.; Von Recum, A. F. Influence of Silicone (PDMS) Surface Texture on Human Skin Fibroblast Proliferation as Determined by Cell Cycle Analysis. *J. Biomed. Mater. Res.* **1998**, *43* (1), 1–14. https://doi.org/10.1002/(SICI)1097-4636(199821)43:1<1::AID-JBM1>3.0.CO;2-T.

(53) Matsuo, K.; Palmer, J. B. Anatomy and Physiology of Feeding and Swallowing: Normal and Abnormal. *Phys. Med. Rehabil. Clin. N. Am.* **2008**, *19* (4), 691–707. https://doi.org/10.1016/j.pmr.2008.06.001.

(54) Mankekar, G. *Swallowing - Physiology, Disorders, Diagnosis and Therapy*; Springer, 2015.

(55) Pearson Jr., W. G.; Langmore, S. E.; Yu, L. B.; Zumwalt, A. C. Structural Analysis of Muscles Elevating the Hyolaryngeal Complex. *Dysphagia* **2012**, *27* (4), 445–451. https://doi.org/doi:10.1007/s00455-011-9392-7.

(56) Pearson Jr., W. G.; Hindson, D. F.; Langmore, S. E.; Zumwalt, A. C. Evaluating Swallowing Muscles Essential for Hyolaryngeal Elevation by Using Muscle Functional Magnetic Resonance Imaging. *Int. J. Radiat. Oncol. Biol. Phys.* **2013**, *85* (3), 735–740. https://doi.org/doi:10.1016/j.ijrobp.2012.07.2370.

(57) Shaw, S. M.; Martino, R. The Normal Swallow: Muscular and Neurophysiological Control. *Otolaryngol. Clin. North Am.* **2013**, *46* (6), 937–956. https://doi.org/https://doi.org/10.1016/j.otc.2013.09.006.

Chapter 3 External Measurement of Swallowed Volume During Exercise Enabled by Stretchable Derivatives of PEDOT:PSS, Graphene, Metallic Nanoparticles, and Machine Learning

Abstract

Epidermal sensors have the potential to aid in the recovery of a range of conditions and to monitor the performance of healthy individuals (e.g., in sports medicine). However, such devices are typically evaluated under idealized conditions, i.e., without the problematic effects of motion and sweat. Here, we evaluate the use of electrodes based on poly(3,4- ethylenedioxythiophene) (PEDOT) complexed to a stretchable polyelectrolyte block copolymer in concert with strain gauges based on graphene decorated with metallic nanoislands to obtain measurements under the conditions of exercise. In particular, the electrodes are used to obtain surface electromyography (sEMG) and are composed of the common conductive polymer PEDOT electrostatically bound to poly(styrenesulfonate)-b-poly(poly(ethylene glycol) methyl ether acrylate) (PSS-b-PPEGMEA), which is synthesized by controlled radical polymerization. Simultaneously, stretching motions of the surface of the skin are measured using strain gauges comprising single-layer graphene supporting subcontinuous coverage of gold and a highly plasticized composite containing PEDOT:PSS. Together, these materials permit low impedance, high stretchability, high resolution, and resistance to sweat. The sensors were connected to a custom printed circuit board (PCB) that allowed the multicomponent system to acquire data wirelessly. This sensor platform was tested on the swallowing activity of a cohort of 10 subjects while walking and spinning on a stationary bike. Using a machine learning model, it was possible to predict swallowed volume with absolute errors of 36% for walking and 43% for cycling.

3.1. Introduction

Swallowing is a critical function in homeostasis, but its importance is easy to overlook. Healthy individuals swallow 500-700 times per day, often with little attention to the intricacy of the process. Dysfunction in swallowing is known as dysphagia, and has a range of etiologies: traumatic, neurologic, oncologic, or iatrogenic (e.g., due to radiation therapy).[1,2,3,4,5] Dysphagia afflicts 3% of the US population and is a leading proximal cause of death (via aspiration pneumonia) in some populations of afflicted individuals (e.g., the elderly).[6,7,8] The ability to assess swallowing function is possessed by a relatively small group of healthcare providers, specifically, otolaryngologists and speech-language pathologists. These specialists use a range of tools from palpation to videofluoroscopy[9,10,11,12] for diagnosis and measurement. The use of mobile technologies to supplement these approaches—which are often available only in well-equipped healthcare settings—would be highly beneficial. Apart from dysphagia, there are many reasons why individuals may benefit from mobile assessment of swallowing behavior. For example, in the treatment of eating disorders, in patients at risk of dehydration, and in sports medicine. In the case of sports medicine and optimization of the performance of elite athletes, there are no current mobile technologies that permit evaluation of swallowing-associated behavior—especially ingested liquid volume—that have been shown to work under the conditions of exercise. Here, we developed a mobile platform for the estimation of swallowed volume using a wearable patch. The patch is enabled by purpose-synthesized conductive polymers for sEMG, graphene sensors for measuring the movement of the skin while swallowing, and machine learning for estimating swallowed volume from the data obtained externally. Critically, the robust polymeric materials, along with the machine learning, permit this platform to circumvent the confounding effects of motion even in the presence of sweat.

Normal swallowing involves the coordinated movements of a range of structures in the head and neck. These movements work in concert to pass a solid or liquid bolus from the oral cavity to the esophagus. The physiological stages of swallowing are described in detail using well-established models such as the Four Stage Model. Simply, after ingestion of a bolus, the submental muscles contract bringing the larynx upwards to meet the epiglottis allowing the bolus to enter the esophagus towards the stomach.[13,14,15,16,17,18] Many assessment methods for swallowing dysfunctions focus on the two stages of this process, the oral propulsion, and the pharyngeal stages. These two stages occur almost simultaneously for a liquid bolus swallow. The movement of the muscles and structures during a swallow is detectable via sensors placed on the skin. Immediately, each step of the process produces distinctive electrical signals arising from the neuromuscular activity and concomitant bending and stretching of the overlying skin. Attempts to capture this information have thus focused on the use of sensor systems designed to measure EMG, strain, or both. One of the first sensing modalities used for swallow assessment and discerning dysfunctions was intramuscular EMG and/or sEMG.[19,20,21] Due to their convenience and non-invasiveness, the conventional sEMG sensors are the preferred choice between the two. Unlike the needle EMG, sEMG sensors are applied onto the skin over the muscle area of interest. They use silver/silver chloride (Ag/AgCl) as the sensing material and are contacted to the skin with a wet conductive gel that also helps decrease the electrode-skin impedance at the interface. Although the use of the conventional Ag/AgCl is predominant in clinics, with the development of new materials, there has been a shift from gel electrodes to dry electrodes for longevity and conformability to skin.[22] Specifically, dry contact electrodes based on thin metal films[23,24] (such as gold), ionic liquids[25], and intrinsically conductive polymers (ICPs)[26,27,28,29,30] are becoming increasingly popular for applications in acquiring epidermal biopotential signals. Their skin conformability, stretchability,

and longevity with minimum reduction in signal quality ensure better electrical contact with the skin and longer use of the sensors without skin irritation. One example material of ICPs used for sEMG is PEDOT:PSS. Electrodes made only with PEDOT:PSS, although sufficiently conductive, tend to be brittle. To enhance its mechanical properties, it is often combined with plasticizers and other polymers. For example, Zhang et al. demonstrated an ICP-based electrode composed of a PEDOT:PSS, waterborne polyurethane (WPU), and D-sorbitol for this reason.[29] The electrode was capable of a maximum 0.41 N/cm skin adhesion force and an electrode-skin impedance value of 82 $k\Omega.cm^2$ at 10 Hz which was superior compared to Ag/AgCl gel electrode value of 148 $k\Omega.cm^2$ at 10 Hz. The authors also demonstrated that the adhesion force of the electrode was significantly enhanced when contacted with wet skin without compromising the electronic properties. However, D-sorbitol tends to leach from the polymer matrix over time, leaving residues and reducing electrode longevity. ICPs are generally easily processable and can be easily incorporated into noise-reducing electrode geometries. In another example, Wang et al. used PEDOT:PSS as a conformal coating in the fabrication of a stretchable concentric biopotential electrode.[28] They achieved an improved interfacial conductivity which was due to the addition of PEDOT:PSS and the spatial filtering geometry (concentric ring), showing superior noise reduction when compared to various electrodes from the literature. Similarly, Zhao et al. coated a graphene layer with modified PEDOT:PSS (with sodium dodecyl sulfate and bis(trifluoromethane) sulfonimide lithium salt) and transferred it onto an elastomer substrate to use as an sEMG sensor. They also demonstrated good conformability with the skin and electrical properties over long-term monitoring.[30] Even though sEMG has been used in a myriad of wearable and mobile devices for the detection of muscle activation, the biopotential signals can still be distorted due to the inherent noise in the electrode, movement artifacts, electromagnetic noise, crosstalk, and internal noise.[31,32]

Inherent noise can be avoided by using the same conductive material for both electrodes and decreasing the impedance between the electrode and the skin with a skin preparation. The movement artifacts can be the electrode movement at the skin interface or the cable movement and it can be reduced with the use of shielded cables and good conformability of the electrode to the skin. The electromagnetic noise usually refers to the power-line interference which arises from the 60 Hz radiation from the power sources around us. This noise can be eliminated with a notch filter. The crosstalk between electrodes can be reduced with careful placement of the electrodes on the muscle group of interest. Lastly, the internal noise is caused by the subcutaneous tissue between the electrode and active muscles and can be partially reduced with high pass filters. Still, the existing literature on novel sEMG sensors only addressed the noise in the signal when the sensors were used on subjects while they were stationary. Deduction of noise is relatively simpler when the subject's body is still and not moving, however, it becomes a harder task when the subject is in motion during the sEMG measurements. Hence why our choice of intrinsically conductive and stretchable PEDOT:PSS$_{(1)}$-*b*-PPEGMEA$_{(6)}$ ("Block-6") used as the sEMG sensor under non-stationary conditions is novel and justified.

Along with sEMG, orthogonal modalities of sensing such as sound, pressure, bioimpedance, and strain recordings are also used to increase the fidelity of the swallow analysis by correlating mechanical motion with muscle activation.[33,34,35,36,37,38,39,40,41] Specifically, epidermal strain sensors placed on the submental region can detect the motion of the throat during a swallow. For example, Kim et al. developed a wearable patch by incorporating a gold film-based sEMG electrode set for observing muscle activity as well as a piezoresistive strain gauge printed on a conductive adhesive epoxy for detection of laryngeal motion.[33] The authors indicated that the strain signal from the larynx motion allowed them to differentiate sEMG signals from cross-talk

and outperformed a nasal cannula in signal clarity. Roh and Hwang et al. used silver nanowires (AgNWs) or carbon nanotubes (CNTs) mixed with PEDOT:PSS and polyurethane (PU) as strain sensors that can measure the swallowing motion on the throat.[36,37] Another group, Zhang et al., utilized ionic liquids to make strain sensors for swallow detection.[38] They achieved a wide range of strain detection (0.1% - 400%) with their method. Zhu et al. presented a strain sensor made up of PDMS/copper nanowires-water dispersed modified graphene/ PDMS which was able to detect swallowing as well.[40] Similarly, Huang et al. made a fiber-based strain sensor to detect small human motions including swallowing. Their strain sensor was a PU yarn dip-coated with graphene nanoplatelets and carbon black/ single-walled CNTs.[41] This sensor was able to stretch 350% and also detect swallowing. More recently from our group, Ramirez et al. utilized a strain sensor based on graphene/metallic nanoislands to detect swallowing differences between healthy and dysphagic patients.[34] This strain sensor exhibited high sensitivity at a low strain regime however failed above 2% strain. They later incorporated highly plasticized PEDOT:PSS into the sensor complex to bring the dynamic range up to 86%.[42] Our previous work utilized the graphene/gold nanoislands/PEDOT:PSS (Gr/AuNI/PEDOT:PSS) complex alongside a machine learning algorithm to predict different swallowed liquid volumes accurately.[43] During these experiments, the cohorts were seated in a relaxed position and the sensors were connected to a data acquisition board via long cables. Even though all the above-mentioned strain sensors were able to detect the swallowing motion, most of them lacked the sensitivity to minute details in the event except our previous work. Additionally, none of these studies challenged their sensors to detect the swallowing event under non-stationary conditions necessary for real-life wearable devices. Finally, most of the mentioned sensors had data acquisition systems that limited the participant movement due to the tethered connection to a stationary source meter or computer.

With the advancement of this field, the need for wireless data acquisition and removal of motion artifacts from the data became more apparent. Areas of improvement in the field include the form factor of the wearable sensors, correctly identifying and removing the motion artifacts from the data while the participant is not in a stationary condition, and the use of machine learning to have a baseline monitoring of the normal swallowing over time. We can overcome the discrepancies by designing a remote PCB board with wireless capabilities and the use of an algorithm where we can train to look for specific features in the swallowing event. In this paper, we demonstrate how to design and fabricate such a system with materials-enabled strain and sEMG sensors as well as a custom PCB board and a machine learning model to analyze the data from participants swallowing different volumes of water under non-stationary conditions. Our strain sensor was made up of Gr/AuNIs/PEDOT:PSS complex and was able to detect minute differences between different swallowed water volumes and last a long time on the skin even when the participants were moving around and sweating. Similarly, our Block-6 based sEMG sensor showed good conformability and longevity on the skin over an hour period. We also designed and utilized a wireless data acquisition to conduct swallowing experiments under non-stationary conditions to prove the performance of this sensor platform and the machine learning predictions for each swallowed water volume.

3.2 Experimental design

3.2.1 The strain sensor

The strain sensor was based on our previous work that is a monolayer of graphene (Gr) with thermally evaporated gold nanoislands (AuNIs) on top (thickness 8 nm).[43,34,42] The choice to use this strain sensor was made due to its well-studied high sensitivity at small strains (up to 2%)

and its near-zero temperature coefficient of resistance.[44,45] The Gr/AuNIs composition exhibits a high gauge factor of ~17 in the ultralow strain regime (0.001% or 10 ppm) with a limit of detection at 0.0001% strain or 1 ppm (gauge factor ~125) when the metallic film is a percolated subcontiguous film (<10 nm).[44] This is due to the combination of piezoresistive properties of both graphene and the ultrathin gold film. Monolayer graphene is known to have piezoresistive properties due to the changes in its electronic band structure and the electron scattering caused by the defect points in the film.[46,47,48,49,50] The AuNIs exhibit piezoresistive properties mainly due to the nanoscale cracks that occur during mechanical strains.[44] Another advantage of the Gr/AuNIs film comes from its near-zero temperature coefficient of resistance. After an extensive study done by Marin et al, 8 nm thick gold evaporated on graphene was the least affected sample by the temperature change, making it an excellent choice to be used on human skin.[45] Although this combination works very well at detecting strains, it tends to lose its stability in performance above 2% strain due to the thinness of the 2D material and irreversible damage to the film.[42] In order to increase the dynamic strain range of the sensor (up to 86%) and prevent the Gr/AuNIs film from failing due to irreversible fracture, we spray-coated the Gr/AuNIs with a highly plasticized PEDOT:PSS conductive polymer (PEDOT:PSS "dough"). The addition of the plasticized conductive polymer provided another layer of electron transport in the case of a fracture on the Gr/AuNIs, ultimately making it easier for device handling and sensor stability at higher strains.[42] PEDOT:PSS and its variables alone have been used greatly in the field of wearable sensors but here the PEDOT:PSS "dough" assisted with the development of our strain sensor capable of detecting small and large strains. Electrical insulation from the skin was established by sandwiching the sensor film and the wiring with two spin-coated films of polydimethylsiloxane (PDMS) as illustrated in **Figure 3.1a and Figure 3.1c**.

3.2.2 The sEMG sensor

The sEMG sensors were made via a unique formulation of PEDOT:PSS$_{(1)}$-*b*-PPEGMEA$_{(6)}$ block copolymer (also referred to as "Block-6") developed to have fine-tuned electrical and mechanical properties for measuring electromyography signals on-body (**Figure 3.1a-b**). PEDOT:PSS is a conductive polymer used in many different fields of electronics due to its high conductivity with additives and molecular stability.[51,52,53,54,55] However, the additives used to increase the stretchability and the conductivity tend to be toxic and can leach over time while decreasing the performance of the polymer. We used a formulation of PEDOT:PSS$_{(1)}$-b-PPEGMEA$_{(6)}$ (specifically the 1:6 ratio of PSS to PPEGMEA) based on the electrical and mechanical characterization previously published by Blau et al. (**Figure 3.1b**).[56] When the PPEGMEA chains were extended on PSS, the block copolymer exhibited a higher strain at fracture (75%), however, with slightly poor conductivity (0.01 S/cm).[56] The addition of PEDOT rendered the polymer more conductive hence making the overall structure the best of both worlds. In addition, this formulation enabled us to have very stable films of Block-6 which didn't dissolve away when stored in a water bath for 5 days at room temperature.[56] The mechanical properties of Block-6 (elastic modulus around 9 MPa) were also superb and comparable to human skin (elastic modulus varying between 5 kPa-140 MPa[57]).

In order to make suitable sEMG sensors for this study, we made square shape drop-casted films with the dimensions of 1.7 cm x 1.7 cm. The dimensions were determined by the muscle area in the submandibular region. We characterized the sensor films mechanically via stress-strain curve and electrically via resistance change over 400 stretching cycles and the change in impedance on the skin over 1 hour.

3.2.3 Cohort studies

In our previous work, we demonstrated that the Gr/AuNIs strain sensor and conventional Ag/AgCl (3M) sEMG sensors can be used to measure different swallowed volumes while the participants were stationary (i.e., sitting). The collection of signals in stationary conditions had been demonstrated before by many groups. This is relatively a non-trivial task given that the motion artifacts and background noise is minimal in this scenario. We wanted to test our sensor platform with non-stationary conditions to prove that (1) we can detect the swallowing event even with the background motion artifacts coming from the subject's non-stationary position, and (2) we can test this set-up on enough people to have high accuracy predictions of the minute changes in liquid volumes swallowed. Realistically, dysphagia patients and/or athletes would not be interacting with this platform in a completely stationary situation. Therefore, we designed two cohort set-ups: walking and biking on a stationary bike while completing the swallowing event. We reasoned that participant could be walking around their house while completing their exercises for therapy or could be on their exercise machine to get an insight into their swallowing behavior. We tested volumes between 10-30 mL in 5 mL increments. Anything below 10 mL had worse predictions outcomes in the machine learning algorithm due to the low amplitude of the signal as shown in our previous work.[43]

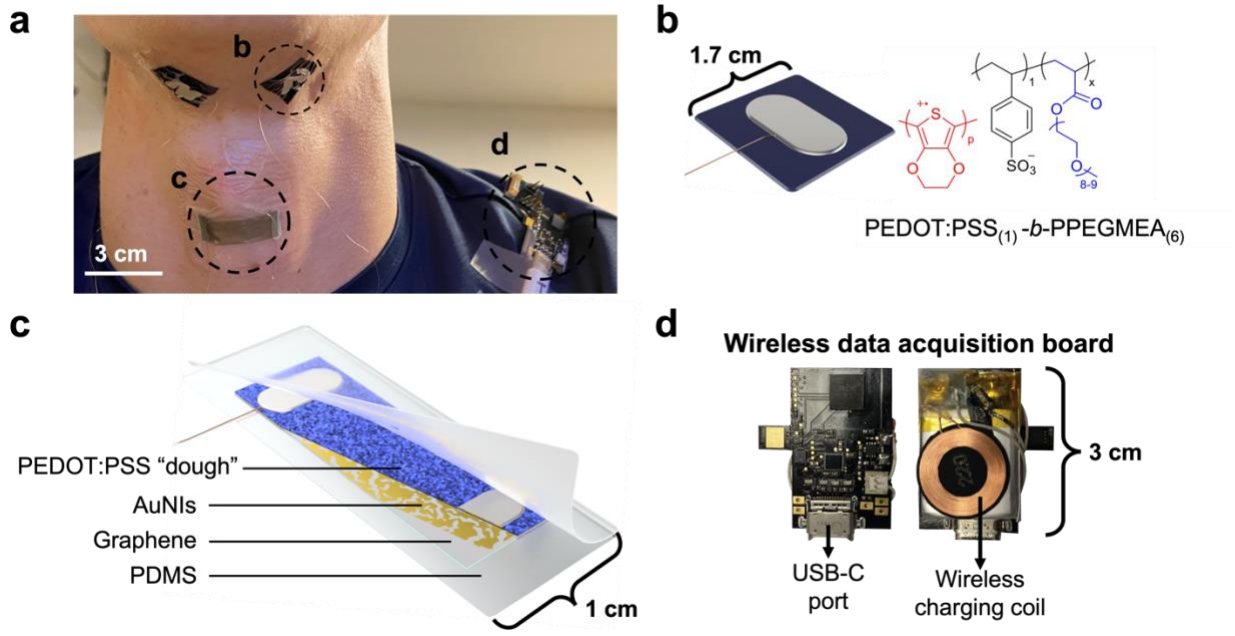

Figure 3.1. Schematic explaining the components of the wireless sensor system. **(a)** The placement of the sEMG and the strain sensors on the participant's neck. **(b)** A schematic and the chemical formula of the PEDOT:PSS$_{(1)}$-*b*-PPEGMEA$_{(6)}$ (Block-6) sEMG electrode film. **(c)** A layer-by-layer schematic of the piezoresistive Gr/AuNI/PEDOT:PSS "dough" strain sensor. **(d)** The front and back side photographs of the wireless PCB board.

3.3 Experimental Methods

3.3.1 The strain sensor fabrication

The strain sensors were fabricated by thermal evaporation (Orion System, AJA International) of gold nanoislands (at 0.03 Å/s with a thickness of 8 nm) onto a single layer of graphene grown on both sides of a 3-inch x 3-inch copper foil (GrollTex, Inc). The excess graphene layer on the backside was etched away in the air plasma cleaner for 5 minutes at 30 W and 250 mTorr. A 200-nm thick film of 4 wt% poly(methyl methacrylate) (PMMA, Alfa Aesar) dissolved in anisole (Sigma Aldrich) was spin-coated on top of the Gr/AuNIs complex at 4000 rpm for 60 seconds and annealed on a hotplate at 150°C for 10 minutes. The PMMA film acted as a supporting layer for the following water transfer process. The underlying copper foil was etched on top of a

0.05 g/mL ammonium persulfate solution (APS, Acros Organics). The floating Gr/AuNIs/PMMA film was later transferred onto a tattoo paper spin-coated with polydimethylsiloxane (Sylgard 184 PDMS, 10:1 base-to-curing agent ratio) at 1000 rpm for 60 seconds and dried completely for 12 hours. Once fully dried, the PMMA film was etched away in an acetone bath for 1 min at 50°C. A PEDOT:PSS "dough" solution was spray-coated on top of the Gr/AuNIs in 8 x 1 second, 4 x 10 seconds, and 4 x 20 seconds intervals, with 1 minute drying period and rotation of sample 90° after each interval. After the last interval, the sample was dried on a hotplate at 150°C for 5 minutes. The copper wiring was attached with silver paint for electrical connection. As the final layer, another PDMS layer (30:1 base-to-curing ratio) was spin-coated on top at 1000 rpm for 60 seconds and cured for 1 hour on a hotplate at 110°C. At this stage, the strain sensors were ready to be cut out of the substrate and placed on the participant's throat with the tattoo paper side facing away from the skin.

3.3.2 The sEMG sensor fabrication

The sEMG sensor films of Block-6 were made by drop-casting in square molds (20 mm x 20 mm x 2 mm depth) that were 3D-printed with Clear V4 resin using FormLabs - Form 3 at 0.025 mm layer height setting. The Block-6 block copolymer was synthesized via controlled radical polymerization using a reversible addition-fragmentation process described in detail in our previous work.[56] Briefly, the PSS-macro-RAFT precursor and the $PSS_{(1)}$-*b*-$PPEGMEA_{(6)}$ were synthesized using a two-step RAFT polymerization. After purification of the $PSS_{(1)}$-*b*-$PPEGMEA_{(6)}$, PEDOT was added onto the block copolymer via oxidative polymerization to make PEDOT:$PSS_{(1)}$-*b*-$PPEGMEA_{(6)}$ (**Figure 3.2a**). The 3-D printed molds were cleaned in a sonication bath for 10 minutes each using deionized water and isopropyl alcohol, successively. Once fully

dried, the molds were cleaned in the air plasma cleaner for 5 minutes at 30 W and 250 mTorr to remove the excess contaminants from the mold surface. A mold release spray (Ease Release 200, Mann Release Technologies) was used to coat the surface of the molds before drop-casting 1 mL of filtered and degassed Block-6. The films were dried on a hotplate at 60°C for 2.5 hours. The molds were cooled down to room temperature before removing the films from the molds (**Figure 3.2b**). Finally, the electrical connections were fixed using copper wiring (36-gauge) and fast-drying silver paint (Ted Pella, Inc). This method produced sEMG electrodes with an area of 2.89 ± 0.23 cm^2 and a thickness of 41 ± 3 µm.

3.3.3 Mechanical and electrical characterization of Block-6 sEMG sensors

We quantified the durability and stability of the Block-6 sEMG sensor films, by measuring the cyclic piezoresistive response as well as the mechanical (tensile) properties using a linear actuator. Block-6 films used for mechanical and electronic testing were prepared using the methods described above. Briefly, a dogbone mold (l = 1.6 cm, w = 0.4 cm, h = 41 µm) was 3D printed and treated with oxygen plasma. The Mann Ease Release 200 mold release spray was applied and let dry. Block-6 solution (1 mL) was drop-casted into each mold before being annealed at 60°C for 2.5 hours until dry, at which point the films were removed using tweezers. Any uneven edges of the dogbones were carefully trimmed before use. For tensile tests, black electrical tape was wrapped around the ends of the dogbones to prevent fracture under the grips of the linear actuator. The dogbones were then placed in 3D printed grips connected to a Mark-10 Series 5 force gauge with 10 N maximum capacity all mounded on a Mark-10 motorized test stand. The samples were pulled until fracture at 1 mm/min and force-elongation data was collected. After the fracture, the thickness of each dogbone was measured using a Dektak XT profilometer. The force-

elongation data was then converted to stress-strain data using the geometry of each dogbone. The linear regime of each set of data was determined by finding the point at which the coefficient of determination (R^2) of each linear regression dropped below 0.98. The modulus was determined from the slope of the linear regime, and the linear elasticity (e.g., a proxy for intrinsic elasticity) was calculated as the strain at which the linear regime ended. For piezoresistive measurements, copper wires (36 gauge) were attached to the ends of each dogbone (underneath the black electrical tape) using carbon paint (Ted Pella, Inc) to ensure a good electrical connection between the wire and the film. These wires were connected to alligator clips attached to a Keithley 2601B Sourcemeter such that the resistance could be measured simultaneously using a custom written LabView program. For piezoresistive measurements, the linear actuator elongated the samples at a rate of 60 mm/min until a certain strain (5%, 10%, 15%, 20% and 30%) was reached before allowing the film to return to its original position (i.e., 0% strain). These cyclic measurements were repeated for 400 cycles.

For electrical characterization, an electrochemical impedance spectroscopy was used to measure the electrode-skin and electrode-electrode impedance of the Block-6 electrodes in the range of 1 Hz to 100 kHz and was compared to the Ag/AgCl (RedDot, 3M) electrodes, and commercial PEDOT:PSS (Clevios, prepared the same way as the Block-6 electrodes) with a potentiostat (Bio-Logic SP-200). The experiment was set up in a two-electrode configuration. A sinusoidal signal of 10 mV without any DC bias was supplied to the electrodes. All the electrodes were placed on the skin of the submandibular area and the impedance spectra were measured over 60 minutes. The Block-6 and Clevios electrode films had an area of 2.89 ± 0.23 cm^2 each and were separated by 2 cm. The Ag/AgCl electrodes had an area of 3.48 cm^2 (3M Datasheet, 2560) and

were separated by 6 cm. Lastly, the conductivities of the Block-6 films were measured with a four-point probe assembly connected to a Keithley 2400 source meter.

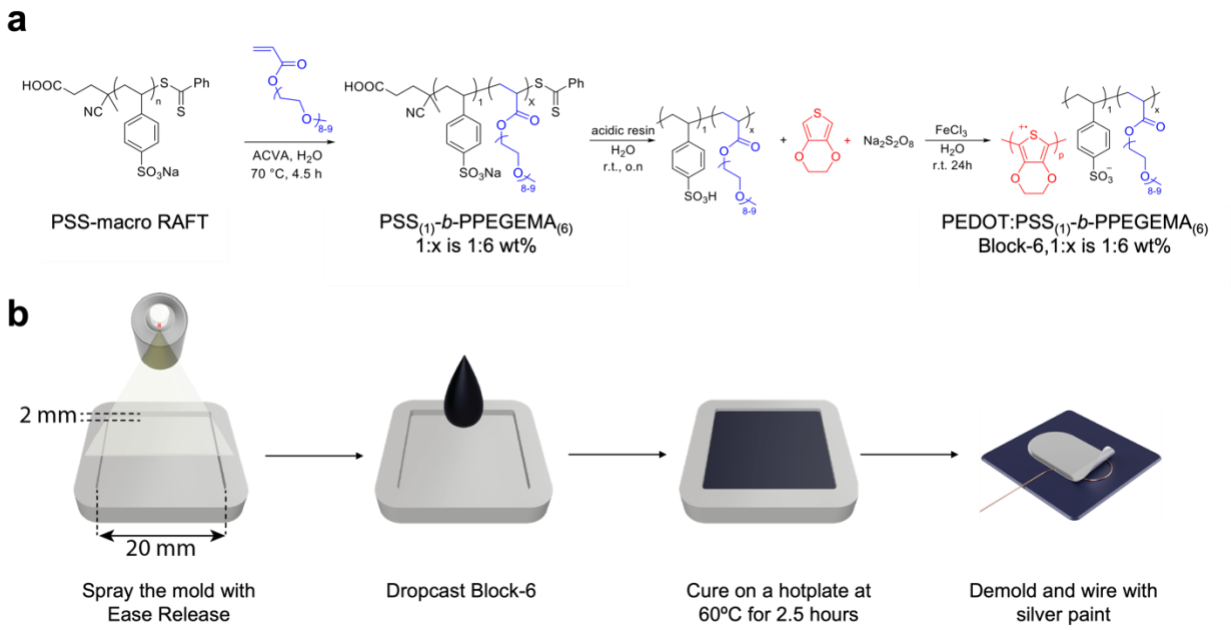

Figure 3.2. A detailed step-by-step fabrication of the Block-6 sEMG sensors. **(a)** The general reaction steps are shown. The procedure was described in an earlier publication.[56] **(b)** The schematic shows the fabrication steps of sEMG electrode films using the synthesized Block-6.

3.3.4 Wireless data acquisition using a PCB board

For a portable experiment setup, a custom printed circuit board (PCB) was designed with the capability of wireless data transfer of the strain and sEMG data to the desired client, a smartphone in our case (**Figure 3.1e**). This design also allowed us to manipulate programmable settings such as filtering, gain setting, and sampling rate. There were two main components on the PCB. The first one was MAX30001 (Maxim Integrated) which was the Analog Frontend (AFE) responsible for the data acquisition and processing of the data. The second one was CYW20736S

(Cypress Semiconductor) which was a Bluetooth Low Energy (BLE) SoC chip responsible for controlling the AFE and other Integrated Circuits on the PCB as well the full wireless communication with the smartphone. The PCB was powered by a 3.7 V (150 mAH) Li-ion battery that was attached to the backside of the board. A charging coil, LTC4124 (Analog Device), was also attached to the battery for wireless charging capability.

A firmware code was written and loaded into the SoC that managed all the BLE communications, the internal data storage, and the transfer from the AFE. For ease of access, a few predefined profiles were set up in the firmware that could be used to quickly set up a working link with the smartphone. We set the sEMG channel to have a sampling rate of 512 samples/second with a gain of 20 V/V, and the strain channel to have a sampling rate of 64 samples/second with a gain of 10 V/V. For the strain channel, we added an analog high-pass filter cutoff of 7.2 kHz, and a current of 48 µA. The digital low pass and high pass filters were bypassed in both channels. To be able to support such a high bandwidth of data (in comparison to other common BLE use-case scenarios) and keep the data accurate (i.e., without dropping any samples), we first maximized the data throughput by changing the connection interval, notification size and only sending the necessary information in packets. Secondly, we utilized the internal FIFO memory of the AFE for temporary data storage and a burst mode was used to send the data to the SoC. The code and the interrupt cycle for the AFE were also set up in such a way that the sEMG and strain data were as time synchronous as possible barring the hardware latency coming from the AFE.

We used a smartphone with the “nRF Connect for Mobile” App (Nordic Semiconductor) to communicate and receive the data from this PCB. This application was a generic one for working with any BLE device. Once we set up the communication link and received the data on the smartphone, we utilized a MATLAB script to clean up and decode the data. This script

converted the information that was stored in notification packets into meaningful voltage samples and assigned a timestamp to each sample. These voltage samples were then finally fed into the machine learning model.

The stable connectivity range of the board once it was connected to the host was around 52 meters and if it wasn't already connected then it was around 16 meters. The battery on the PCB was able to last up to 15 hours when it was fully charged. In order to keep the sensor-PCB interface compact and sturdy, we used a custom-designed USB-C connector on the board. This connector had two electrode cables for the sEMG sensor and two electrode cables for the strain sensor. The size of the whole assembled PCB including the battery was around 2.5 cm x 4.5 cm x 0.5 cm. This allowed us to carry out our experiments in various environments with ease and without the need for any expensive data acquisition equipment.

3.3.5 Cohort studies

We carried out a cohort study of 10 healthy participants (ages between 21 and 34 years old, 6 females, 4 males) with no history of swallowing disorders. Five of the ten cohorts were picked to walk and other five were picked to bike. We used an approved protocol reviewed by the Internal Review Board at the University of California San Diego Human Research Protections Program (Project # 191950S) and collected signed consent forms from each participant prior to the study.

The subjects were instructed to shave well (if applicable) before coming to the study. We placed two Block-6 sEMG sensors symmetrically on the hyoid muscles (mylohyoid and stylohyoid) in the submandibular region and the strain sensor about an inch below the sEMG sensors in the middle of the throat. We attached the PCB to the participant's shoulder directly. We

secured the sensors with additional Tegaderm tape for better adhesion to the curved structure of the throat.

The participants were either instructed to bike on a stationary bicycle or walk while they were given different volumes of water to swallow. The participants were also instructed to swallow the water in their mouth in one go (meaning no piecewise swallowing). We tested the water volumes from 10 mL to 30 mL in 5 mL increments repeating each volume 10 times. We observed in our previous work that 30 mL was the maximum amount on average that participants can swallow comfortably, and the 10 mL was the minimum amount on average where participants felt a difference from a saliva swallow.

3.3.6 Processing sEMG and strain signals

One of the most crucial parts of this sensor platform was signal processing and analyzing the collected data. This step was important for doing experiments under non-stationary conditions where the motion artifacts can overcome the signal to be detected. For this reason, we applied the appropriate filters to the sEMG and strain data after collecting the raw signal from the sensors. For the sEMG signals, we first applied 60 Hz notch filter to reduce the interference noise since we didn't use a third ground electrode on body in our setup for sEMG (the ground was added on the PCB). Then, we employed a high pass filter with a 30 Hz cut-off frequency to filter out most of the artifacts since the main frequency of sEMG signals usually ranges from 30 to 250 Hz.[58,59,60] As for the strain signals, a typical peak of a strain activity lasts around a couple of hundreds of millisecond to 1 second. Therefore, we first applied a band pass filter with a 0.5 Hz low cut-off frequency and a 10 Hz high cut-off frequency. Then, we applied a third order Savitzky-Golay

smoothing filter to remove small variations in resistance that are not related to the swallowing activity. Finally, we used another 16-sample (0.25 seconds) moving window to further smooth the signals so that it was easier to identify local maxima for strain peak detection in our feature extraction stage.

3.3.7 Feature extraction

We extracted three sEMG features out of the processed sEMG signals. The first one was simply the summation of the peak intensities along the swallowing peak in the sEMG signal. The second one was based on the width of the sEMG peak. The width of the sEMG peak was defined as the total length of time when the absolute sEMG signal was above the 99th percentile within the peak. Last, we found that the power of the low-frequency components of the sEMG signal had a good correlation with the swallowed volume. We converted the sEMG signal in frequency-domain with Fast Fourier transform, and then obtained the root mean square (RMS) value between 30-100 Hz as the third feature (**Figure B1**). As for the strain data, two features were extracted out of the processed strain signals. (We used a different feature selection method as in our previous paper[43] because the previous algorithm for fiducial-point detection did not work properly for non-stationary strain signals) The period between 7^{th} and 12^{th} seconds was first extracted. Then local peaks which had the width of at least 250 milliseconds and the prominence of at least the quarter of the (max – min) of the signals were identified. The peak closest to the 10th second and the following peak were selected as the peaks of the swallow. The first strain feature was defined as the peak-to-peak interval between the first and the second peak in the swallow signal. The valley point was further obtained by finding the minimum point between the two peaks. Then the second feature was defined as the difference between the valley point and the middle of the two peaks

(which can be viewed as the skewness of the peaks). Lastly, an additional feature was defined as the offset between the peak of the sEMG power and the first peak point of the strain signal.

3.3.8 Machine learning

We first plotted the distribution of each feature value versus their corresponding swallowed volume to examine the correlation. The features were normalized to zero mean and unit variance within each data set and then pooled together. Then, the scatter plots for each feature were plotted where the color solid lines indicated the mean of each data set, and the thick black line indicated the mean of all samples. We also employed a leave-one-out validation to evaluate the performance of predicting the swallowed volume using the sEMG and strain features we defined. Within a session, each trial took turns to serve as the testing data, and all the other trials in the session were treated as the training data. An outlier detector was applied to filter out outliers in the training samples which had the z-score larger than 2 in any feature dimension. Because the number of samples was relatively small in our data set, we decided to use the support vector regression (SVR) model instead of the linear regression model which was used in our previous publication. The SVR model is known to be more robust when the number of feature dimensions is relatively large in comparison to the number of samples.[61]

3.4 Results and Discussion

3.4.1 Mechanical and electrical properties of Block-6 sEMG sensors

The results of the mechanical and electrical characteristics of the Block-6 sEMG sensor films are shown in **Figure 3.3**. We first compared the electrode-skin impedance spectra of

Ag/AgCl (3M), PEDOT:PSS (Clevios), and Block-6 sEMG sensors over 60 minutes. Over time, the impedance between the skin and the sensor should stay the same with a slightly decreasing trend due to the secretion of sweat from the skin. **Figure 3.3a** shows the initial impedance spectra reading of Block-6, Ag/AgCl, and PEDOT:PSS from 1-10^5 Hz range. The impedance values over time at 10 Hz and 100 Hz for Block-6, Ag/AgCl, and PEDOT:PSS are also shown in **Figure 3.3b.** The electrode-skin impedance of the Block-6 was 483 kΩ at 10 Hz and 85 kΩ at 100 Hz at the beginning of the experiment. Similarly, we measured the Ag/AgCl electrodes to be 97 kΩ at 10 Hz and 13 kΩ at 100 Hz, and PEDOT:PSS to be 2 MΩ at 10 Hz and 197 kΩ at 100 Hz. After 60 minutes, we observed the impedance values stayed around the same for all three sensors with a slight decrease towards the end. This was devoted to the secretion of sweat (includes salts and minerals) from the skin over time. In addition to the impedance spectroscopy, we also measured the average sheet resistance to be 9.4 ± 3.5 kΩ/sq and conductivity to be 0.027 ± 0.022 S/cm which was in accordance with the previously published values for Block-6.[56]

The mechanical properties of a polymer film are a significant determinant in their applicability as a wearable sensor. For example, one consideration is the elastic mismatch between the sensor and the skin. In comparison to commercial formulations of PEDOT:PSS, Block-6 had a modulus closer to that of skin around the neck (16 ± 6 MPa in comparison to 1.78 ± 1.73 MPa[62]), as shown by its tensile response (**Figure 3.3c**). Likewise, while commercial PEDOT:PSS (Clevios) was relatively brittle (~5% fracture strain[56]), Block-6 was both more stretchable (i.e., it has both greater fracture strain at 85% and greater intrinsic elasticity) and tougher (average toughness value at 1.97 ± 0.25 MJ/m^3). Therefore, it was better suited for sensor applications on the skin that were subject to continuous or cyclic strains. Assuming the elastic behavior of Block-6 was Hookean in nature (i.e., in the elastic regime, the change in stress is linear relative to the change in strain), we

determined that the linear elasticity of Block-6 was approximately 10%. Therefore, we conducted cyclic piezoresistance measurements (400 cycles) from 0% strain up to 5, 10, 15, and 20% strain on the Block-6 films (**Figure 3.3d**). **Figure 3.3e** shows the full 400 cycles for 5% strain and **Figure 3.3f** shows a zoomed in section of the 400 cycles. There was essentially no change in baseline resistance over time with the 5% strain cycle and a slight gradual shift in baseline resistance for the 10, 15 and 20% strain cycles (**Figure B2**). The gradual shift was due to the plastic deformation of the films above 10% strain, suggesting that the intrinsic elasticity of these Block-6 films was slightly lower than 10% (e.g., closer to 9%). However, the signal generated by the change in strain from cycle to cycle remained distinct and clearly observable, suggesting that the piezoresistive behavior of Block-6 is quite stable despite constant mechanical deformation and relaxation (**Figure B2**).

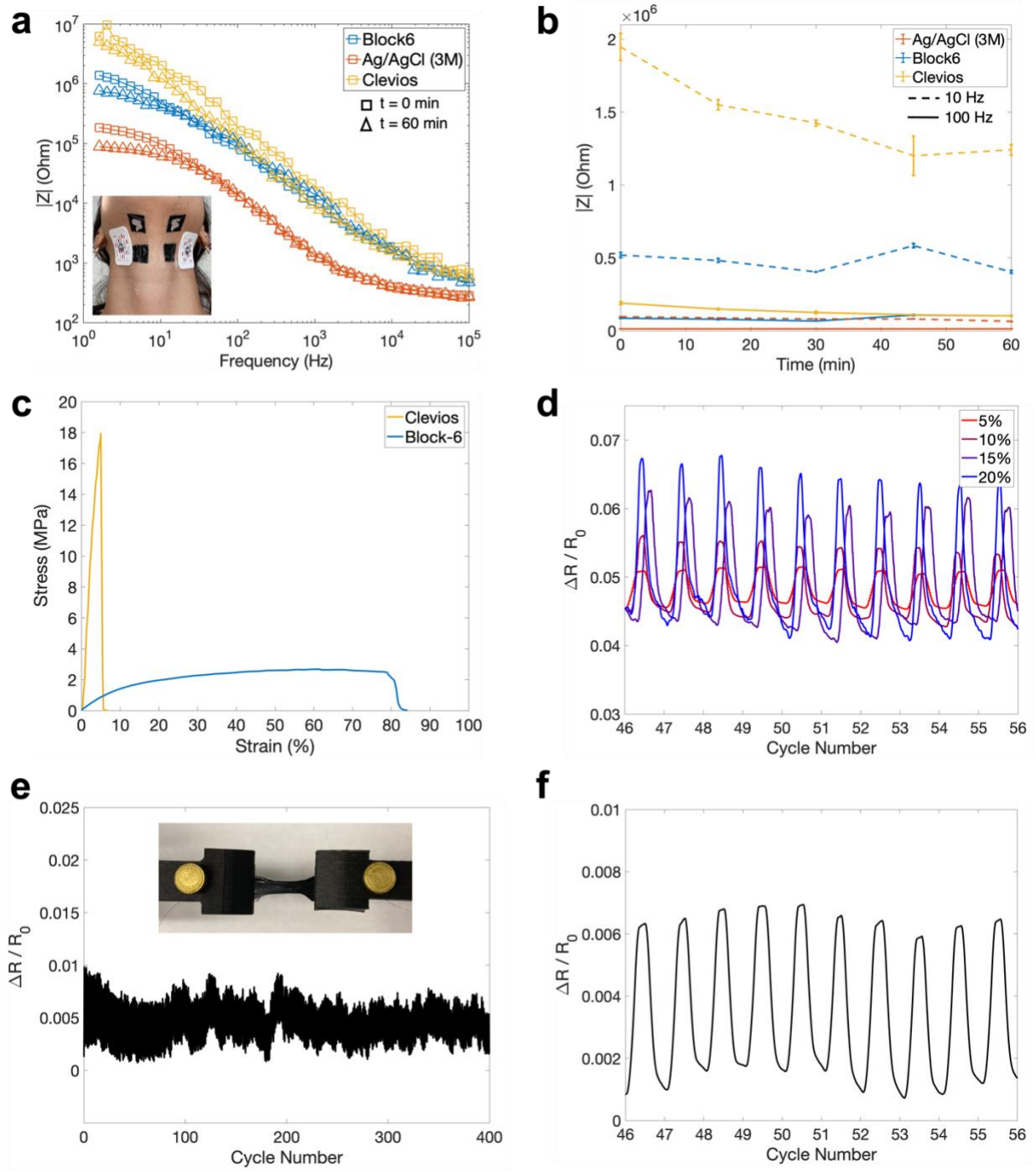

Figure 3.3. Mechanical and electrical characterization of Block-6 sEMG sensor films. **(a)** The plot shows the impedance spectra of Block-6, Ag/AgCl/ (3M) and Clevios on skin over 60 minutes (square: 0 min, triangle: 60 min) and **(b)** the values at 10 and 100 Hz over time. **(c)** A representative stress-strain curve of Block-6 and Clevios films are shown. **(d)** Piezoresistive measurements of Block-6 films were measured at different cyclic strains over 400 cycles (shown only for cycles 46-56). **(e)** Plot shows the full 400 cycles of the 5% cyclic strain experiment whereas **(f)** shows the zoomed-in view of the piezoresistive behavior of Block-6 under continuous strain and relaxation..

3.4.2 Cohort study results

After material characterization, we moved on with the swallow experiments under non-stationary conditions. We collected swallow signals for volumes 10, 15, 20, 25 and 30 mL of water under walking and biking conditions to show that our sensor system was robust enough to distinguish the swallowing event. We asked the participants to walk or bike with the water in their mouth for 10 seconds and then instructed them to swallow the water and keep on the physical activity until the recording was over. In **Figure 3.4a-b**, we plotted representative sEMG and strain signals from a 10 mL water swallow while the participant was walking around. Clearly, the raw signals included low-frequency motion artifacts from the body movement in addition to the swallowing muscle contraction however once we processed the signals, we were able to detect the distinct swallow feature from the signal. We calculated the signal-to-noise (SNR) to be 2.781 for the sEMG signals and 2.989 for the strain signals for the walking experiments. Similarly in **Figure 3.4c-d**, the motion artifacts were even more present in the raw data while the participants were biking but not so much when the data was processed. The calculated SNR for the sEMG signals was 6.935 and 2.633 for the strain signals for the biking experiments.

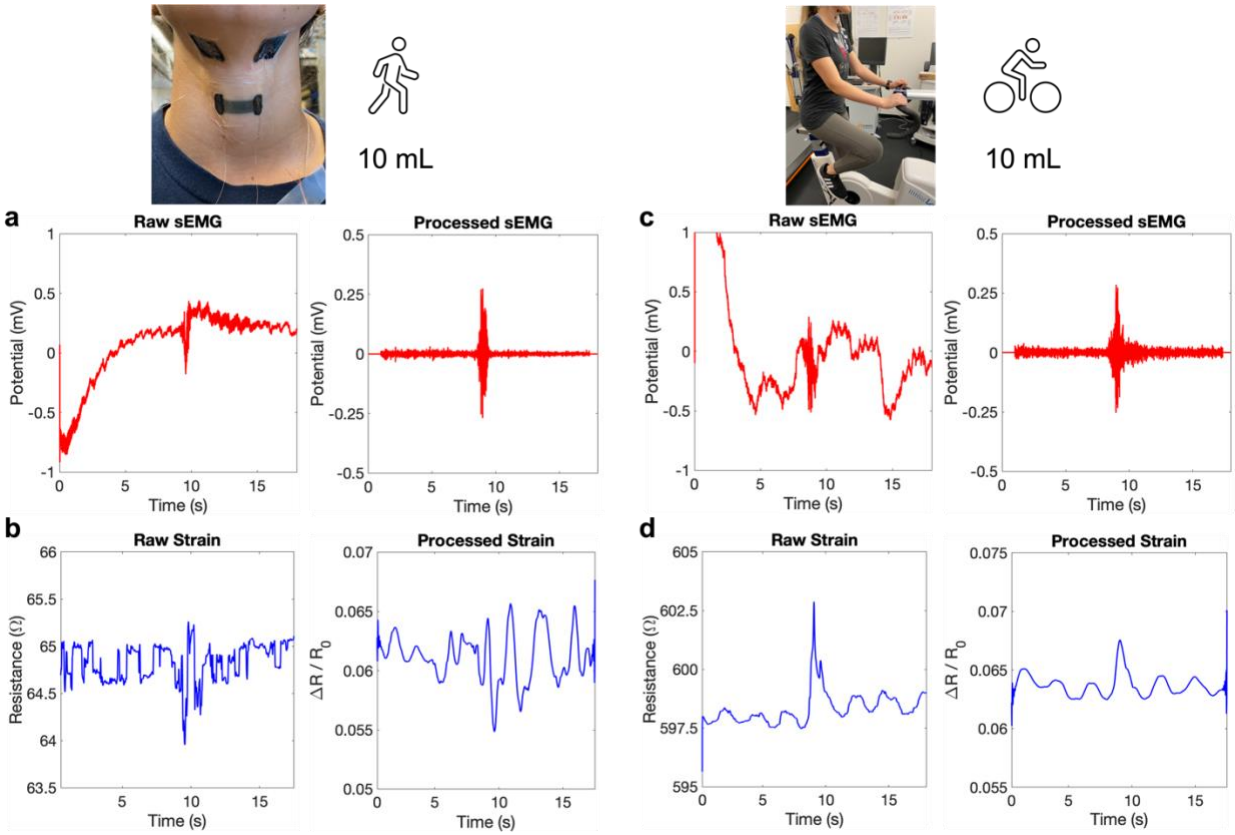

Figure 3.4. A representative processed data of sEMG and strain signals from each type of exercise. Photos show the experimental set-up for the swallowing while walking and biking. Left panel plots show **(a)** of a raw and processed 10 mL swallow sEMG signals and **(b)** strain signals during walking experiments. Right panel plots show raw and processed 10 mL swallow **(c)** sEMG signals and **(d)** strain signals during biking experiments.

3.4.3 Machine learning results

Once the collected swallow data was processed, we extracted the certain features from the swallow peaks in the sEMG and strain signals. From the sEMG signals, we extracted summation, width, and low-frequency power whereas from the strain signals we extracted the peak-to-peak width, peak skewness, and the peak offset between the sEMG and the strain (**Figure 3.5a-b**). **Figure 3.5c** shows the correlation between features and the swallowed volumes for all the experiments (**Figure B5**) shows the correlations for walking and biking experiments separately). On average, there was a trend between the volumes and each feature however it wasn't as distinct

due to the low number of data sets and the non-stationary experimental set-up. In our results, sEMG summation, and low frequency power showed positive correlation whereas the sEMG signal width showed a negative correlation. The highest positive correlation was observed in the low frequency power from the sEMG signals. We observed a positive correlation for the peak-to-peak width for the strain signal and negative correlation for the peak skewness and the peak offset between the sEMG and strain signals. However, overall, these correlations were not enough to distinguish the volumes from each other as clearly as possible due to the low sample size in these experiments. Nevertheless, we proved that it was possible to detect the swallowing peak for each sensor type during exercise conditions and it was possible to extract features from the signals for further machine learning analysis.

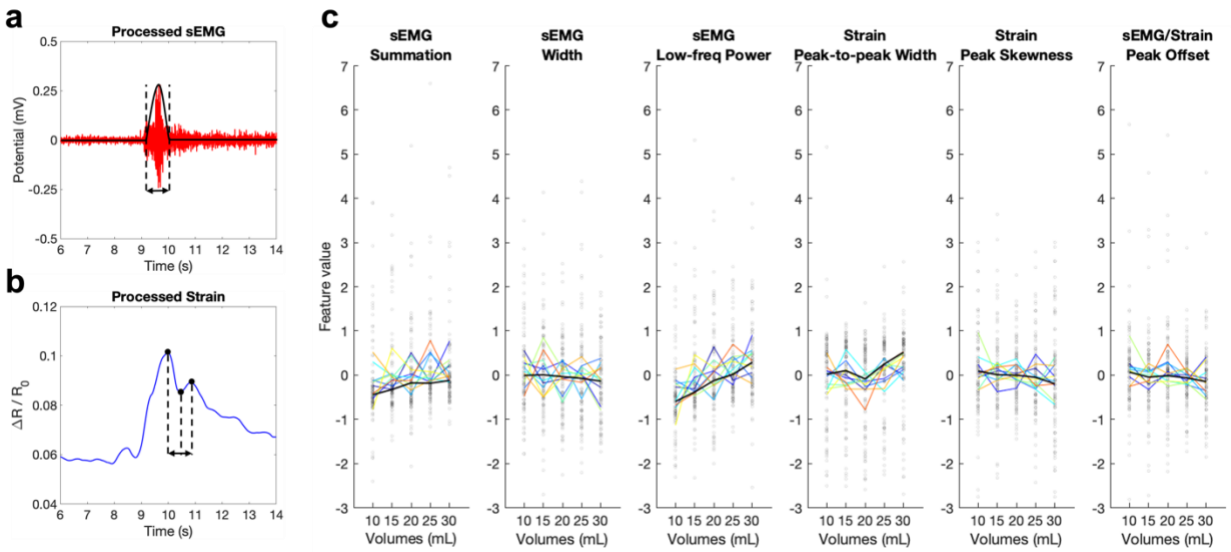

Figure 3.5. The correlation between the volumes and the extracted features for all the walking and biking experiments. The example plots for **(a)** sEMG and **(b)** strain signals from a swallow show the extracted features. **(c)** The correlation between the swallowed volumes and the extracted features for each participant's data (in color) and the overall average (in black) are shown. The vertical dots represent each trial within a volume for all the participants.

Lastly, we utilized a machine learning model using these features to train and predict each swallowed volume. **Figure 3.6** shows the performance of this prediction model. On average, the volume predictions were better for the walking experiments where we also observed less motion artifacts (except for the 15 mL). The model also predicted the middle volumes (15, 20, and 25 mL) better than the smallest (10 mL) and the largest volumes (30 mL). This could be due to the effort participants had to put to be able to hold the 30 mL water in their mouth until they were instructed to swallow. We found 30 mL to be approximately the maximum volume most participants can swallow in one piece. We also observed large prediction error in 10 mL experiments. Although this was not expected, the reason could be that smaller volumes were harder to predict due to the premature movement of the liquid bolus from mouth to larynx (this was also observed in our

previous work[43]). This could cause a change in volume swallowed every time. Regardless, the results of the model were promising, and that this sensor platform can be used to predict the swallowed volumes with more training data even when the participants were moving around and sweating.

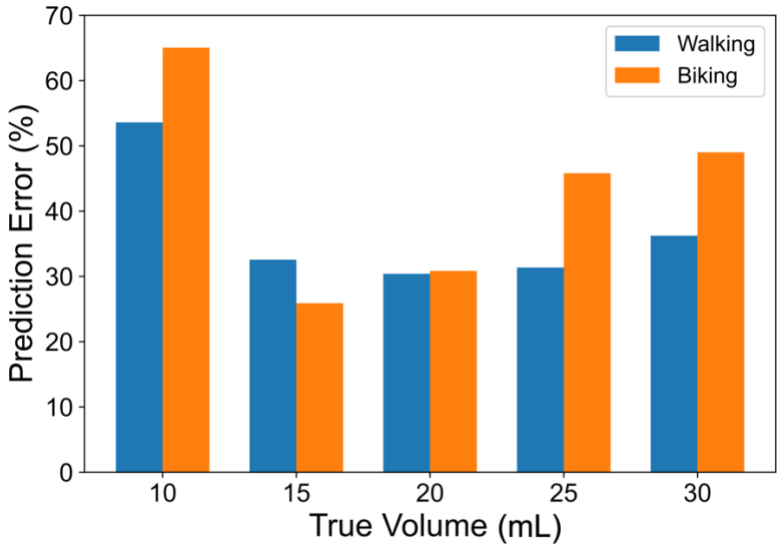

Figure 3.6. Machine learning prediction results. The plot shows the percent error for each volume for the walking and biking experiments.

3.5 Conclusion

In this work, we created a sensor platform capable of collecting sEMG and strain signals from the submandibular area of the neck during a swallow and wirelessly transfer the data from a PCB board attached to the shoulder of the participant to a phone application to be processed via a machine learning algorithm. Both sensors were able to detect minute details about the swallowing maneuvers during a water swallow even when the participants were in a non-stationary condition such as walking and biking. In addition to the wireless portion of the platform, we introduced a

recently published material (Block-6) to be used as the sEMG sensor in our experiments. The mechanical and electrical properties of Block-6 were superior to the conventional PEDOT:PSS (Clevios) and did not need small molecules or toxic additives for better conductivity and stretchability. These properties allowed Block-6 sEMG sensors to last longer on the participants' skin during the exercise experiments compared to the Ag/AgCl (RedDot, 3M) sEMG electrodes which delaminate after 60 minutes. The compact form factor of the sensors and the data acquisition allowed us to use this set-up at various testing locations and provided more comfort of the participants. Although we designed this work to show a proof-of-concept on the detection limits of swallowing with non-stationary conditions, we believe that due to its remote capabilities, it can be used in larger cohort studies at various cancer centers for detection and monitoring of dysphagia as well as exercise physiology labs for hydration monitoring.

Acknowledgments

We would like to thank Prof. Tse (Tina) Nga Ng at UC San Diego for the helpful discussions on sEMG sensor performance. This work was supported by a gift from PepsiCo & the Gatorade Sports Sciences Institute. Additional support was provided by the member companies of the Center for Wearable Sensors in the Jacobs School of Engineering at the University of California, San Diego, including Dexcom, Gore, Honda, Huami, Instrumentation Laboratory, Kureha, Merck KGaA, PepsiCo, Roche, Samsung, and Sony. L.B. acknowledges the support provided by the National Science Foundation Graduate Research Fellowship Program under Grant DGE-2038238. This work was performed in part at the San Diego Nanotechnology Infrastructure (SDNI), a member of the National Nanotechnology Coordinated Infrastructure, which is supported by the National Science Foundation (Grant ECCS-1542148).

Chapter 3 and Appendix B, in part, will be submitted for publication of the material as it may appear in Advanced Healthcare Materials. Beril Polat, Tarek Rafeedi, Laura L. Becerra, Alexander X. Chen, Kuanjung Chiang, Vineel Kaipu, Rachel Blau, Patrick P. Mercier, Chung-Kuan Cheng, and Darren J. Lipomi. 2022. The dissertation author was the primary investigator and author of this paper.

References

(1) Roden, D. F.; Altman, K. W. Causes of Dysphagia among Different Age Groups: A Systematic Review of the Literature. *Otolaryngol. Clin. North Am.* **2013**, *46* (6), 965–987. https://doi.org/10.1016/j.otc.2013.08.008.

(2) Eisbruch, A.; Schwartz, M.; Rasch, C.; Vineberg, K.; Damen, E.; Van As, C. J.; Marsh, R.; Pameijer, F. A.; Balm, A. J. M. Dysphagia and Aspiration after Chemoradiotherapy for Head-and-Neck Cancer: Which Anatomic Structures Are Affected and Can They Be Spared by IMRT? *Int. J. Radiat. Oncol. Biol. Phys.* **2004**, *60* (5), 1425–1439. https://doi.org/10.1016/j.ijrobp.2004.05.050.

(3) Rofes, L.; Vilardell, N.; Clavé, P. Post-Stroke Dysphagia: Progress at Last. *Neurogastroenterol. Motil.* **2013**, *25* (4), 278–282. https://doi.org/10.1111/nmo.12112.

(4) Hutcheson, K. A.; Lewin, J. S.; Barringer, D. A.; Lisec, A.; Gunn, G. B.; Moore, M. W. S.; Holsinger, F. C. Late Dysphagia after Radiotherapy-Based Treatment of Head and Neck Cancer. *Cancer* **2012**, *118* (23), 5793–5799. https://doi.org/10.1002/cncr.27631.

(5) Garon, B. R.; Sierzant, T.; Ormiston, C. Silent Aspiration - Results of 2,000 Video Fluoroscopic Evaluations. *J. Neurosci. Nurs.* **2009**, *41* (4), 178–185. https://doi.org/10.1097/JNN.0b013e3181aaaade.

(6) Sura, L.; Madhavan, A.; Carnaby, G.; Crary, M. A. Dysphagia in the Elderly: Management and Nutritional Considerations. *Clin. Interv. Aging* **2012**, *7*, 287–298. https://doi.org/10.2147/CIA.S23404.

(7) Bhattacharyya, N. The Prevalence of Pediatric Voice and Swallowing Problems in the United States. *Laryngoscope* **2015**, *125* (3), 746–750. https://doi.org/10.1002/lary.24931.

(8) Bhattacharyya, N. The Prevalence of Dysphagia among Adults in the United States. *Otolaryngol. - Head Neck Surg. (United States)* **2014**, *151* (5), 765–769. https://doi.org/10.1177/0194599814549156.

(9) Palmer, J. B.; Kuhlemeir, K. V.; Tippett, D. C.; Lynch, C. A Protocol for the Videofluorographic Swallowing Study. *Dysphagia* **1993**, *8*, 209–214. https://doi.org/https://doi.org/10.1007/BF01354540.

(10) Logemann, J. A. *Manual for the Videofluorographic Study of Swallowing*, 2nd ed.; PRO-ED: Austin, TX, 1993.

(11) Logemann, J. A. Role of the Modified Barium Swallow in Management of Patients with Dysphagia. *Otolaryngol. - Head Neck Surg.* **1997**, *116* (3), 335–338. https://doi.org/10.1016/S0194-5998(97)70269-9.

(12) Martin-Harris, B.; Logemann, J. A.; McMahon, S.; Schleicher, M.; Sandidge, J. Clinical Utility of the Modified Barium Swallow. *Dysphagia* **2000**, *15* (3), 136–141. https://doi.org/10.1007/s004550010015.

(13) Ertekin, C.; Pehlivan, M.; Aydoğdu, I.; Ertaşl, M.; Uludağ, B.; Çlelebi, G.; Çlolakoğlu, Z.; Sağduyu, A.; Yüceyar, N. An Electrophysiological Investigation of Deglutition in Man. *Muscle Nerve* **1995**, *18* (10), 1177–1186. https://doi.org/10.1002/mus.880181014.

(14) Matsuo, K.; Palmer, J. B. Anatomy and Physiology of Feeding and Swallowing: Normal and Abnormal. *Phys. Med. Rehabil. Clin. N. Am.* **2008**, *19* (4), 691–707. https://doi.org/10.1016/j.pmr.2008.06.001.

(15) Jones, B. *Normal and Abnormal Swallowing*, 2nd ed.; Jones, B., Ed.; Springer, New York, NY, 2003. https://doi.org/https://doi.org/10.1007/978-0-387-22434-3.

(16) Shaw, S. M.; Martino, R. The Normal Swallow: Muscular and Neurophysiological Control. *Otolaryngol. Clin. North Am.* **2013**, *46* (6), 937–956. https://doi.org/https://doi.org/10.1016/j.otc.2013.09.006.

(17) Ertekin, C.; Aydogdu, I. Neurophysiology of Swallowing. *Clin. Neurophysiol.* **2003**, *114* (12), 2226–2244. https://doi.org/10.1016/S1388-2457(03)00237-2.

(18) Hiiemae, K. M.; Palmer, J. B. Food Transport and Bolus Formation during Complete Feeding Sequences on Foods of Different Initial Consistency. *Dysphagia* **1999**, *14*, 31–42. https://doi.org/https://doi.org/10.1007/PL00009582.

(19) Schultheiss, C.; Schauer, T.; Nahrstaedt, H.; Seidl, R. O. Automated Detection and Evaluation of Swallowing Using a Combined Emg/Bioimpedance Measurement System. *Sci. World J.* **2014**, *2014*. https://doi.org/10.1155/2014/405471.

(20) Koyama, Y.; Ohmori, N.; Momose, H.; Yamada, S. ichi; Kurita, H. Detection of Swallowing Disorders with a Multiple-Channel Surface Electromyography Sensor Sheet. *J. Dent. Sci.* **2022**, No. xxxx. https://doi.org/10.1016/j.jds.2021.12.015.

(21) Reimers-Neils, L.; Logemann, J.; Larson, C. Viscosity Effects on EMG Activity in Normal Swallow. *Dysphagia* **1994**, *9* (2), 101–106. https://doi.org/10.1007/BF00714596.

(22) Fu, Y.; Zhao, J.; Dong, Y.; Wang, X. Dry Electrodes for Human Bioelectrical Signal Monitoring. *Sensors (Switzerland)* **2020**, *20* (13), 1–30. https://doi.org/10.3390/s20133651.

(23) Nicholls, B.; Ang, C. S.; Efstratiou, C.; Lee, Y.; Yeo, W. H. Swallowing Detection for Game Control: Using Skin-like Electronics to Support People with Dysphagia. *2017 IEEE Int. Conf. Pervasive Comput. Commun. Work. PerCom Work. 2017* **2017**, 413–418. https://doi.org/10.1109/PERCOMW.2017.7917598.

(24) Constantinescu, G.; Jeong, J. W.; Li, X.; Scott, D. K.; Jang, K. I.; Chung, H. J.; Rogers, J. A.; Rieger, J. Epidermal Electronics for Electromyography: An Application to Swallowing Therapy. *Med. Eng. Phys.* **2016**, *38* (8), 807–812.

https://doi.org/10.1016/j.medengphy.2016.04.023.

(25) Velasco-Bosom, S.; Karam, N.; Carnicer-Lombarte, A.; Gurke, J.; Casado, N.; Tomé, L. C.; Mecerreyes, D.; Malliaras, G. G. Conducting Polymer-Ionic Liquid Electrode Arrays for High-Density Surface Electromyography. *Adv. Healthc. Mater.* **2021**, *10* (17). https://doi.org/10.1002/adhm.202100374.

(26) Pani, D.; Dessi, A.; Saenz-Cogollo, J. F.; Barabino, G.; Fraboni, B.; Bonfiglio, A. Fully Textile, PEDOT:PSS Based Electrodes for Wearable ECG Monitoring Systems. *IEEE Trans. Biomed. Eng.* **2016**, *63* (3), 540–549. https://doi.org/10.1109/TBME.2015.2465936.

(27) Ouyang, J. Application of Intrinsically Conducting Polymers in Flexible Electronics. *SmartMat* **2021**, *2* (3), 263–285. https://doi.org/10.1002/smm2.1059.

(28) Wang, K.; Parekh, U.; Pailla, T.; Garudadri, H.; Gilja, V.; Ng, T. N. Stretchable Dry Electrodes with Concentric Ring Geometry for Enhancing Spatial Resolution in Electrophysiology. *Adv. Healthc. Mater.* **2017**, *6* (19). https://doi.org/10.1002/adhm.201700552.

(29) Zhang, L.; Kumar, K. S.; He, H.; Cai, C. J.; He, X.; Gao, H.; Yue, S.; Li, C.; Seet, R. C. S.; Ren, H.; Ouyang, J. Fully Organic Compliant Dry Electrodes Self-Adhesive to Skin for Long-Term Motion-Robust Epidermal Biopotential Monitoring. *Nat. Commun.* **2020**, *11* (1), 1–13. https://doi.org/10.1038/s41467-020-18503-8.

(30) Zhao, Y.; Zhang, S.; Yu, T.; Zhang, Y.; Ye, G.; Cui, H.; He, C.; Jiang, W.; Zhai, Y.; Lu, C.; Gu, X.; Liu, N. Ultra-Conformal Skin Electrodes with Synergistically Enhanced Conductivity for Long-Time and Low-Motion Artifact Epidermal Electrophysiology. *Nat. Commun.* **2021**, *12* (1), 1–12. https://doi.org/10.1038/s41467-021-25152-y.

(31) Clancy, E. A.; Morin, E. L.; Merletti, R. Sampling, Noise-Reduction and Amplitude Estimation Issues in Surface Electromyography. *J. Electromyogr. Kinesiol.* **2002**, *12* (1), 1–16. https://doi.org/10.1016/s1050-6411(01)00033-5.

(32) Chowdhury, R. H.; Reaz, M. B. I.; Bin Mohd Ali, M. A.; Bakar, A. A. A.; Chellappan, K.; Chang, T. G. Surface Electromyography Signal Processing and Classification Techniques.

Sensors (Switzerland) **2013**, *13* (9), 12431–12466. https://doi.org/10.3390/s130912431.

(33) Kim, M. K.; Kantarcigil, C.; Kim, B.; Baruah, R. K.; Maity, S.; Park, Y.; Kim, K.; Lee, S.; Malandraki, J. B.; Avlani, S.; Smith, A.; Sen, S.; Alam, M. A.; Malandraki, G.; Lee, C. H. Flexible Submental Sensor Patch with Remote Monitoring Controls for Management of Oropharyngeal Swallowing Disorders. *Sci. Adv.* **2019**, *5* (12), 1–10. https://doi.org/10.1126/sciadv.aay3210.

(34) Ramírez, J.; Rodriquez, D.; Qiao, F.; Warchall, J.; Rye, J.; Aklile, E.; Chiang, A. S. C.; Marin, B. C.; Mercier, P. P.; Cheng, C. K.; Hutcheson, K. A.; Shinn, E. H.; Lipomi, D. J. Metallic Nanoislands on Graphene for Monitoring Swallowing Activity in Head and Neck Cancer Patients. *ACS Nano* **2018**, *12* (6), 5913–5922. https://doi.org/10.1021/acsnano.8b02133.

(35) Schultheiss, C.; Schauer, T.; Nahrstaedt, H.; Seidl, R. O. Evaluation of an EMG Bioimpedance Measurement System for Recording and Analysing the Pharyngeal Phase of Swallowing. *Eur. Arch. Oto-Rhino-Laryngology* **2013**, *270* (7), 2149–2156. https://doi.org/10.1007/s00405-013-2406-3.

(36) Roh, E.; Hwang, B. U.; Kim, D.; Kim, B. Y.; Lee, N. E. Stretchable, Transparent, Ultrasensitive, and Patchable Strain Sensor for Human-Machine Interfaces Comprising a Nanohybrid of Carbon Nanotubes and Conductive Elastomers. *ACS Nano* **2015**, *9* (6), 6252–6261. https://doi.org/10.1021/acsnano.5b01613.

(37) Hwang, B. U.; Lee, J. H.; Trung, T. Q.; Roh, E.; Kim, D. Il; Kim, S. W.; Lee, N. E. Transparent Stretchable Self-Powered Patchable Sensor Platform with Ultrasensitive Recognition of Human Activities. *ACS Nano* **2015**, *9* (9), 8801–8810. https://doi.org/10.1021/acsnano.5b01835.

(38) Zhang, S. H.; Wang, F. X.; Li, J. J.; Peng, H. D.; Yan, J. H.; Pan, G. B. Wearable Wide-Range Strain Sensors Based on Ionic Liquids and Monitoring of Human Activities. *Sensors (Switzerland)* **2017**, *17* (11), 1–10. https://doi.org/10.3390/s17112621.

(39) Sakaue, Y.; Shimizu, T.; Matsushima, M.; Matsuura, M.; Takahashi, K.; Asahara, K.; Okada, S.; Makikawa, M. Measurement of Swallowing Using Flexible Polymer Sensor. *Proc. Annu. Int. Conf. IEEE Eng. Med. Biol. Soc. EMBS* **2013**, 612–615.

https://doi.org/10.1109/EMBC.2013.6609574.

(40) Zhu, Y.; Hu, Y.; Zhu, P.; Zhao, T.; Liang, X.; Sun, R.; Wong, C. P. Enhanced Oxidation Resistance and Electrical Conductivity Copper Nanowires-Graphene Hybrid Films for Flexible Strain Sensors. *New J. Chem.* **2017**, *41* (12), 4950–4958. https://doi.org/10.1039/c7nj00246g.

(41) Huang, Y.; Zhao, Y.; Wang, Y.; Guo, X.; Zhang, Y.; Liu, P.; Liu, C.; Zhang, Y. Highly Stretchable Strain Sensor Based on Polyurethane Substrate Using Hydrogen Bond-Assisted Laminated Structure for Monitoring of Tiny Human Motions. *Smart Mater. Struct.* **2018**, *27* (3). https://doi.org/10.1088/1361-665X/aaaba0.

(42) Ramírez, J.; Rodriquez, D.; Urbina, A. D.; Cardenas, A. M.; Lipomi, D. J. Combining High Sensitivity and Dynamic Range: Wearable Thin-Film Composite Strain Sensors of Graphene, Ultrathin Palladium, and PEDOT:PSS. *ACS Appl. Nano Mater.* **2019**, *2* (4), 2222–2229. https://doi.org/10.1021/acsanm.9b00174.

(43) Polat, B.; Becerra, L. L.; Hsu, P. Y.; Kaipu, V.; Mercier, P. P.; Cheng, C. K.; Lipomi, D. J. Epidermal Graphene Sensors and Machine Learning for Estimating Swallowed Volume. *ACS Appl. Nano Mater.* **2021**, *4* (8), 8126–8134. https://doi.org/10.1021/acsanm.1c01378.

(44) Ramírez, J.; Urbina, A. D.; Kleinschmidt, A. T.; Finn, M.; Edmunds, S. J.; Esparza, G. L.; Lipomi, D. J. Exploring the Limits of Sensitivity for Strain Gauges of Graphene and Hexagonal Boron Nitride Decorated with Metallic Nanoislands. *Nanoscale* **2020**, *12* (20), 11209–11221. https://doi.org/10.1039/d0nr02270e.

(45) Marin, B. C.; Root, S. E.; Urbina, A. D.; Aklile, E.; Miller, R.; Zaretski, A. V.; Lipomi, D. J. Graphene-Metal Composite Sensors with Near-Zero Temperature Coefficient of Resistance. *ACS Omega* **2017**, *2* (2), 626–630. https://doi.org/10.1021/acsomega.7b00044.

(46) Huang, M.; Pascal, T. A.; Kim, H.; Goddard, W. A.; Greer, J. R. Electronic-Mechanical Coupling in Graphene from in Situ Nanoindentation Experiments and Multiscale Atomistic Simulations. *Nano Lett.* **2011**, *11*, 1241–1246. https://doi.org/10.1021/nl104227t.

(47) Smith, A. D.; Niklaus, F.; Paussa, A.; Vaziri, S.; Fischer, A. C.; Sterner, M.; Forsberg, F.;

Delin, A.; Esseni, D.; Palestri, P.; Östling, M.; Lemme, M. C. Electromechanical Piezoresistive Sensing in Suspended Graphene Membranes. *Nano Lett.* **2013**, *13* (7), 3237–3242. https://doi.org/10.1021/nl401352k.

(48) Couto, N. J. G.; Costanzo, D.; Engels, S.; Ki, D. K.; Watanabe, K.; Taniguchi, T.; Stampfer, C.; Guinea, F.; Morpurgo, A. F. Random Strain Fluctuations as Dominant Disorder Source for High-Quality on-Substrate Graphene Devices. *Phys. Rev. X* **2014**, *4* (4), 1–13. https://doi.org/10.1103/PhysRevX.4.041019.

(49) Skomski, R.; Dowben, P. A.; Sky Driver, M.; Kelber, J. A. Sublattice-Induced Symmetry Breaking and Band-Gap Formation in Graphene. *Mater. Horizons* **2014**, *1* (6), 563–571. https://doi.org/10.1039/c4mh00124a.

(50) Hicks, J.; Tejeda, A.; Taleb-Ibrahimi, A.; Nevius, M. S.; Wang, F.; Shepperd, K.; Palmer, J.; Bertran, F.; Le Fèvre, P.; Kunc, J.; De Heer, W. A.; Berger, C.; Conrad, E. H. A Wide-Bandgap Metal-Semiconductor-Metal Nanostructure Made Entirely from Graphene. *Nat. Phys.* **2013**, *9* (1), 49–54. https://doi.org/10.1038/nphys2487.

(51) Elschner, A.; Kirchmeyer, S.; Wilfried, L.; Merker, U.; Reuter, K. *PEDOT: Principles and Applications of an Intrinsically Conductive Polymer*, 1st ed.; CRC Press: Boca Raton, 2010.

(52) Groenendaal, L.; Jonas, F.; Freitag, D.; Pielartzik, H.; Reynolds, J. R. Poly(3,4-Ethylenedioxythiophene) and Its Derivatives: Past, Present, and Future. *Adv. Mater.* **2000**, *12* (7), 481–494. https://doi.org/10.1002/(SICI)1521-4095(200004)12:7<481::AID-ADMA481>3.0.CO;2-C.

(53) Kirchmeyer, S.; Reuter, K. Scientific Importance, Properties and Growing Applications of Poly(3,4-Ethylenedioxythiophene). *J. Mater. Chem.* **2005**, *15* (21), 2077–2088. https://doi.org/10.1039/b417803n.

(54) Shi, H.; Liu, C.; Jiang, Q.; Xu, J. Effective Approaches to Improve the Electrical Conductivity of PEDOT:PSS: A Review. *Adv. Electron. Mater.* **2015**, *1* (4), 1–16. https://doi.org/10.1002/aelm.201500017.

(55) Wen, Y.; Xu, J. Scientific Importance of Water-Processable PEDOT–PSS and Preparation,

Challenge and New Application in Sensors of Its Film Electrode: A Review. *J. Polym. Sci. Part A Polym. Chem.* **2017**, *55* (7), 1121–1150. https://doi.org/10.1002/pola.28482.

(56) Blau, R.; Chen, A. X.; Polat, B.; Becerra, L. L.; Runser, R.; Zamanimeymian, B.; Choudhary, K.; Lipomi, D. J. Intrinsically Stretchable Block Copolymer Based on PEDOT:PSS for Improved Performance in Bioelectronic Applications. *ACS Appl. Mater. Interfaces* **2022**, *14* (4), 4823–4835. https://doi.org/10.1021/acsami.1c18495.

(57) A, K.; A, L. Mechanical Behaviour of Skin: A Review. *J. Mater. Sci. Eng.* **2016**, *5* (4). https://doi.org/10.4172/2169-0022.1000254.

(58) Stepp, C. E. Surface Electromyography for Speech and Swallowing Systems: Measurement, Analysis, and Interpretation. *J. Speech, Lang. Hear. Res.* **2012**, *55* (4), 1232–1246. https://doi.org/10.1044/1092-4388(2011/11-0214).

(59) Poorjavad, M.; Talebian, S.; Nakhostin Ansari, N.; Soleymani, Z. Surface Electromyographic Assessment of Swallowing Function. *Iran. J. Med. Sci.* **2017**, *42* (2), 194–200.

(60) Stegeman, D.; Hermens, H. Standards for Surface Electromyography: The European Project Surface EMG for Non-Invasive Assessment of Muscles (SENIAM). *Línea). Dispon. en http//www. med. …* **2007**, 108–112.

(61) Drucker, H.; Surges, C. J. C.; Kaufman, L.; Smola, A.; Vapnik, V. Support Vector Regression Machines. *Adv. Neural Inf. Process. Syst.* **1997**, *1*, 155–161.

(62) An, Y.; Ji, C.; Li, Y.; Wang, J.; Zhang, X.; Huang, Y. In Vivo Measurements of Human Neck Skin Elasticity Using MRI and Finite Element Modeling. *Med. Phys.* **2017**, *44* (4), 1402–1407. https://doi.org/10.1002/mp.12154.

Chapter 4 Graphene-based Patterned Strain Sensors for Swallow Detection and Enhanced Machine Learning Performance

Abstract

There has been a vast amount of research done on epidermal sensors to detect swallowing activity over the skin. It has been realized that by studying the signature features in the swallowing signals, we can conclude certain onset of swallowing disorders or understand this extremely well-coordinated physiological event. Luckily, machine learning has been adopted to be used to investigate the collected signals by many groups for this purpose. In order to get meaningful results from the machine learning models, a lot of data needs to be fed into the algorithm. In this chapter, we introduce a re-design of well-established epidermal sensors (sEMG and strain) demonstrated in our previous work. We adopted a similar fabrication method to the strain sensor comprised of graphene/metallic nanoislands/PEDOT:PSS to make an arrayed sensor patch. This arrayed-strain sensor patch is accompanied by a custom-synthesized PEDOT:$PSS_{(1)}$-*b*-$PPEGMEA_{(6)}$ (Block-6) which was also inspired by our previous work. Using these both sensing modalities, it is possible to collect more training data for the machine learning algorithm to increase the analysis performance of this platform. Our vision is the translation of this strain and sEMG-based technology into practical, clinically relevant tools which improve: (i) diagnostic resolution and continuous monitoring of swallowing capability in dysphagic patients and/or (ii) therapy in the form of haptics-driven rehabilitation for patients recovering from facial stroke or paraplegia.

4.1. Introduction

Increasing cost of healthcare, the time that patients have to wait in hospitals for follow-ups or treatments, and the importance of preventative measures pushed scientists to improve the field of wearable sensors. One of these health conditions that needs close monitoring for prevention purposes is swallowing disorder, so called dysphagia. For example, majority of the throat cancer patients suffer from swallowing disorders after radiation therapy.[1,2,3] If not detected and treated early on, it becomes extremely difficult to fully restore the normal function of the swallowing.[4,5] A non-invasive, low-cost wearable sensor could help monitor the changes in the swallowing behavior after radiation therapy closely and report back to the physicians if the patient needs further treatment. This kind of wearable sensor can reduce a trip to the clinic and the cost for an inefficient and expensive follow-up test.

The field of wearable sensors has grown immensely in the past decade with sensors having more compatible mechanical properties and sensitivity to human skin. However, as the field of wearable devices advances, the need for better processability and multiplexing has become more apparent. Addition of a patterned design that can accommodate multiple sensors on one patch can improve spatial resolution, error estimation, and machine learning algorithm performance. There have been multiple studies that investigated the design and fabrication of patterned strain sensors in an array. For example, Feng et al. was able to grow large-scale indium selenide (In_2Se_3) nanosheets in a patterned manner assisted by a template.[6] They used a patterned mica substrate to selectively grow the In_2Se_3 nanosheets in a chemical vapor deposition chamber and later transferred the sensor film onto a polyethylene terephthalate (PET). After supplying electrical connections and insulating the film with polydimethylsiloxane (PDMS), they were able to achieve a gauge factor value of 237 for the strain range up to 0.5%. The mechanical stability was also

confirmed over 120 cycles under 0.39% uniaxial tensile strain. Lastly, they demonstrated the use of the arrayed strain sensor as an electronic-skin (e-skin) sensor by detecting the bend of a finger. As another example, Gao et al. studied the possibility of forming active materials on elastomer substrates directly without using any post-fabrication steps.[7] They used a 532 nm continuous laser beam over an EcoFlex film to convert EcoFlex into silicon carbide (SiC). This conversion was possible due to the localized high temperature created by the laser beam. This patterned SiC-based strain sensor showed a detection limit of 0.05% strain, a small temperature drift, and mechanical durability over 10,000 cycles at 4% strain. The gauge factor was calculated to be 854.7 for strain up to 3.5%. They showed the use of this sensor as a e-skin by recording muscle contractions on arm, carotid arterial pressures, and drinking. Suzuki and coworkers investigated area-arrayed graphene nanoribbons (GNRs) to be used as strain sensor as well.[8] They transferred a patterned layer of GNRs onto a silicon wafer via wet transfer method using polymethyl methacrylate (PMMA) as the support layer. They achieved a gauge factor of 50 for 0.08% strain however they were only able to apply this method on rigid substrates. As another different approach, Pei et al. fabricated a flexible, stretchable, and highly sensitive silver-coated carbon nanotubes (Ag@CNT) as a wearable strain sensor array using 3D printing technologies and material synthesis.[9] First, they synthesized the Ag@CNTs via chemical reduction and then poured this material composite into a PDMS encapsulant made via 3D printed mold. This way, they achieved a gauge factor value of 62.8 in the 0-14.4% strain range with mechanical durability over 500 cycles of stretching and relaxing. They showed simple wearable sensors tasks such as pulse diagnosis on the wrist and gesture recognition on the fingers. Although the idea of patterning active materials of strain sensors has been around for a while, there was no push towards using these arrayed strain sensors on a specific muscle group on body to collect data or create spatial strain mapping.

In this chapter, we demonstrate how to design and fabricate an arrayed, flexible, and wearable strain sensor comprising gold nanoislands (AuNIs) on graphene (Gr) with a highly plasticized elastomer (PEDOT:PSS "dough") for detection of swallowing. The unique piezoresistance of the Gr/AuNI/PEDOT:PSS was proven previously (strain resolution of 0.0001% or 1 ppm) with a high dynamic range (up to 86% strain).[10,11,12] In addition, it was shown that they can be immune to a thermal drift in the signal due to tunable thickness and metal selection unlike the other strain sensors in the literature.[13] In its core, the strain sensor is based on our previous work but in an array form instead of a single strain sensor on the wearable patch.[14] Simply, the strain sensor is made up of gold atoms evaporated and patterned onto a single-layer of graphene via thermal evaporation in an island-like morphology and gold serpentine electrodes were evaporated on top to have a closed circuit data acquisition system. After spray-coating the PEDOT:PSS "dough" for an increase in dynamic range, we sandwiched the sensor film between two PDMS layers for electrical insulation. We believe that the addition of the orthogonal design to our well-established strain sensor will improve the signal accuracy, provide bi-directional strain information, and enhance the machine learning algorithm performance overall. In addition, the processability of this sensor will allow transfer onto many stretchable substrates via wet transfer which makes it convenient for wearable devices.

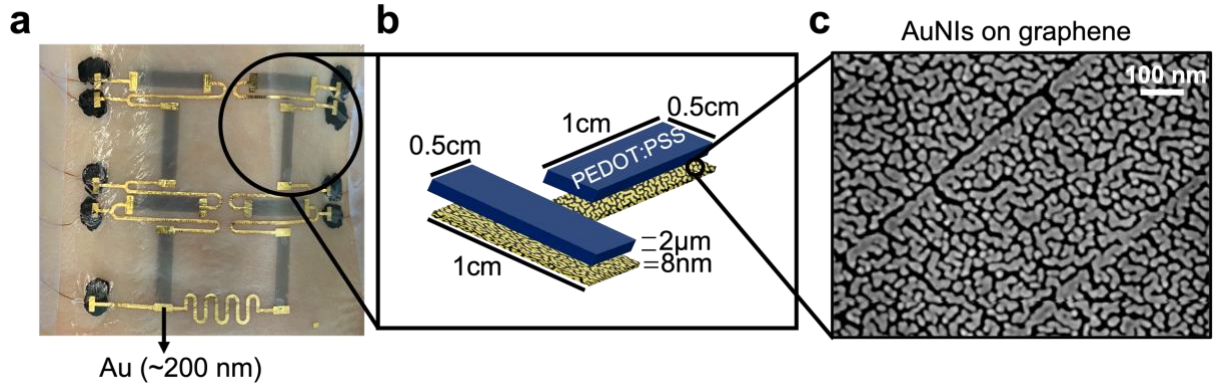

Figure 4.1. The arrayed Gr/AuNI/PEDOT:PSS strain sensor that was used in this work. **(a)** A photograph of the arrayed-strain sensor patch applied onto skin. **(b)** A schematic drawing of the strain sensor patch showing all the stacked material layers. **(c)** A scanning electron microscopy image of the 8-nm AuNIs on graphene.

4.2 Experimental design

4.2.1 The strain sensor

The strain sensor in its basic form is made up of a single-layer graphene sheet with thermally evaporated gold metallic nanoislands on top (thickness of 8 nm) inspired from our previous work (**Figure 4.1a-b**).[14] Graphene has many advantageous properties as a 2D supporting material. It is thin, flexible, and stretchable, which helps with the transferability to many different substrates. More importantly, graphene changes the wetting transparency of the metal substrates. Addition of a single layer of graphene decreases the surface energy and maintains the wettability of the metal substrate throughout the evaporation.[15] In this case, we started with a single layer graphene on a copper foil which we purchased commercially. Evaporating the island-like structures onto graphene added mechanical robustness and increased piezoresistive properties (**Figure 4.1c**). The sensors demonstrated better strain sensitivity (higher gauge factor) at smaller strains, and versatility at larger strain ranges. Due to having low diffusion barrier on graphene at a low deposition rate, our choice of metal for nanoislands was gold. Moreover, previous work from

Marin et al. showed that 8 nm gold has near-zero temperature coefficient of resistance (TCR).[13] This is a distinguishing property of our sensor compared to the ones in the field because it is desirable to remove the sensitivity of the sensor to the temperature changes in the environment. While the metallic nanoislands on graphene exhibit high sensitivity at small strains (0.001%), they tend to fail above 2% strain due to the thinness of the 2D material. In order to increase the dynamic range of the overall sensor, we have chosen to spray coat our metallic nanoislands on graphene with a highly plasticized PEDOT:PSS conductive polymer. PEDOT:PSS acts as a conductive bridge between the nanoislands if a tear or crack on the 2D film occurs during stretching or flexing.

4.2.2 The array design

The importance of an array design comes from a few needs. First, it has been shown in our previous work that there needs to be more data from the sensors for better machine learning algorithm predictions. If only a single sensor is used, there is limitations to how much a participant can swallow in one experiment cycle to collect enough data for algorithm training. Secondly, it is possible to gain a better understanding of the spatial strain mapping of the area that the patch is applied to. Thirdly, this ultimately increases the tolerance for signal deviation due to sensor placement (i.e., “user placement error”). Decreasing these deviations, that are caused by external factors, helps improve the automatic analysis of the data and the performance of machine learning algorithms. For this reason, we designed an array of the Gr/AuNI/PEDOT:PSS strain sensor with a gold serpentine electrode interconnect.

One of the advantages of our sensor patch is having a simultaneous readout of all the sensors on the patch during a strain inducing activity. To do this, we designed a 2 x 2 array patch

as a closed-circuit with resistors in series. This design allowed us to apply a constant current through each sensor and readout the potential difference between the sensors. Since we know the current and potentials, we were able to calculate resistance per sensor. In addition to the ease of data acquisition, this design allowed us to do acquisition of all the sensors simultaneously.

4.3 Experimental Methods

4.3.1 Strain sensor fabrication

The strain sensor was fabricated very similarly to our previous work with the exception of the patterning it into an array (**Figure 4.2**).[14] First, 8 nm gold was evaporated onto a single layer of graphene purchased commercially on a 3x3 inch copper foil piece (GrollTex, Inc.) at a rate of 0.03Å/s. A custom purchased stainless-steel array mask was aligned on top of the graphene before evaporation of the AuNIs (Metal Etch Services, Inc). Within the same evaporation chamber (Orion System AJA International), 20 nm aluminum (Al) was sputter onto AuNIs at ~1Å/s after the evaporation to mask the nanoislands for the next step. Next, the graphene under the masked area was etched away in the air plasma for 5 minutes on high setting at ~250 mTorr. The Al protected the unmasked Gr/AuNI regions during this process. The Al layer was also etched away after this in a 0.025M potassium hydroxide (KOH) solution for 1 minute and rinsed with water immediately after. The sensor film was put back into the thermal evaporation chamber with the second stainless steel mask that had the corresponding serpentine interconnect between the sensors. For the serpentines, ~250 nm Au was evaporated through the mask at 1.0 Å/s. As a support layer for the wet transfer, PMMA was spin-coated onto the film at 4000 rpm for 60 seconds and annealed on a hotplate at 150°C for 5 minutes. The copper foil support was etched away on a 0.05 g/mL ammonium persulfate solution for ~1 hour. At this point, the floating Gr/AuNI/PMMA film was

essentially ready to be transferred onto any substrate. We spin-coated PDMS (Slygard 184, 10:1 base:curing agent ratio) onto a tattoo paper at 1000 rpm for 60 seconds and cured it on a hotplate for 10 minutes at 150°C. After treating the PDMS surface with the air plasma for 2 minutes on high at 250 mTorr, we transferred the sensor film onto the PDMS via wet transfer method and let it air dry for 12 hours in air. We etched off the PMMA support layer on top in a warm acetone bath for 1 minute at 60°C and rinsed the film with isopropyl alcohol. Once completely dry, we spray-coated a mixture of PEDOT:PSS "dough" solution (92 wt% Clevios, 3 wt% Triton X-100, and 5 wt% dimetylsiloxane) diluted with water (1:3 volume ratio) using a custom stencil masking everywhere except the Gr/AuNI regions. The spray-coating was done on a hotplate at 150°C with 8 x 1 second, 4 x 10 seconds and 4 x 20 seconds intervals lifting the stencil off and rotating the sample 90° every time. Copper wires were glued to the Au serpentine electrodes with carbon or silver paint. Lastly, another layer of PDMS (Slygard 184, 30:1 ratio) was spin-coated at 1000 rpm for 60 seconds on top of the whole assembly and cured at 150°C for 10 minutes to ensure electrical insulation from the skin. This whole fabrication process produced eight Gr/AuNI/PEDOT:PSS strain sensors on one wearable patch.

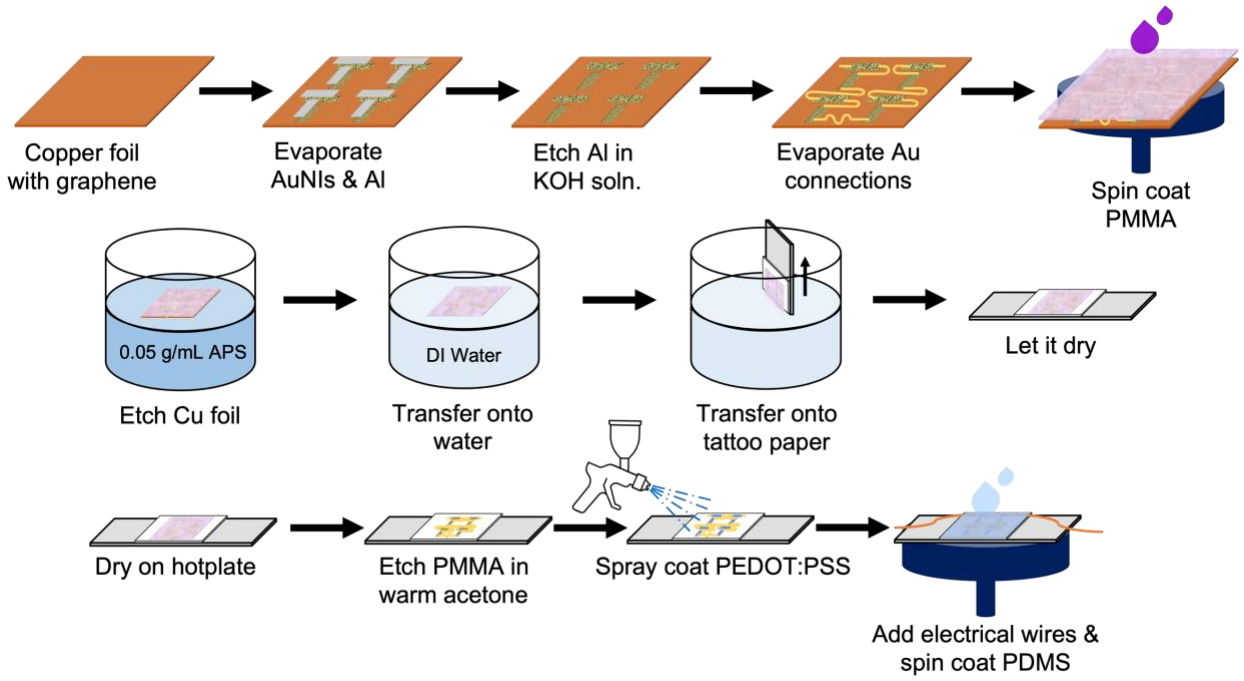

Figure 4.2. The fabrication of arrayed-strain sensor patch is shown in detail.

4.3.2 Data acquisition of the array strain sensor

We designed a closed-circuit supplying constant current throughout all the sensors to collect signals from all sensors simultaneously. The constant current was supplied by a source meter (Keithley 2400, Tektronix) from the first sensor and traveling through each sensor in series (**Figure 4.3a**). We used an 8-channel commercial differential amplifier (DI-1100, DATAQ Instruments) to measure the potential difference across each strain sensor (**Figure 4.3b**).

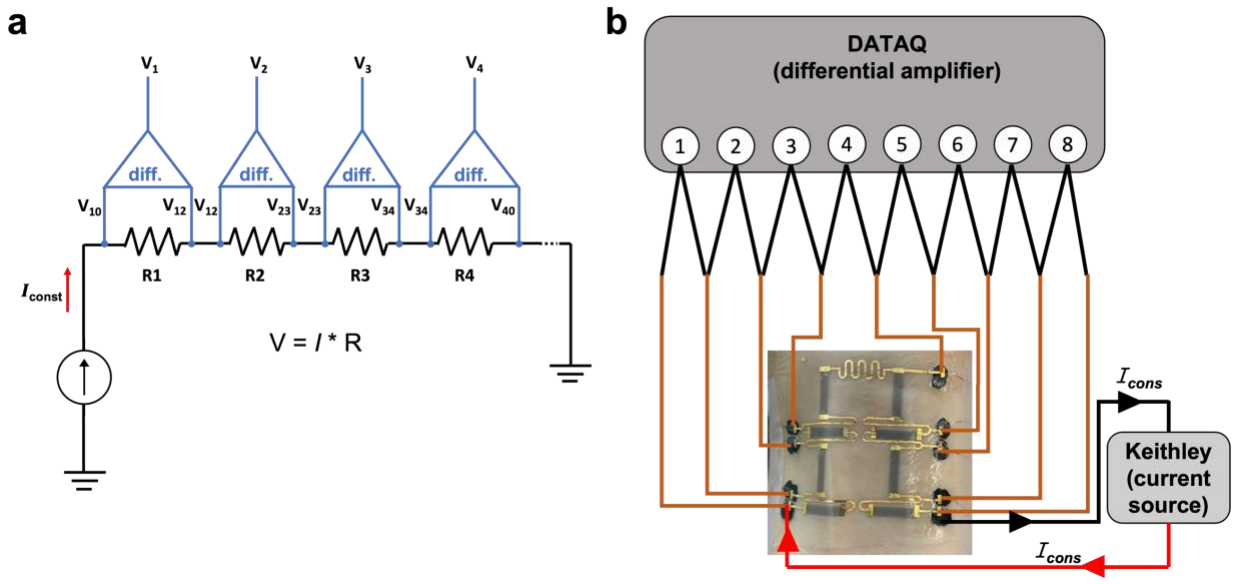

Figure 4.3. Design schematic of the serpentine-connected monolithic strain sensor patch. **(a)** A representative electrical diagram showing the signal acquisition. **(b)** A schematic drawing of the data acquisition set-up using a commercial differential amplifier.

4.4 Results and discussion

Initially, we tested the feasibility of the array design by individually measuring the resistance across each sensor on the wearable patch. We used a design where there were no serpentine interconnects to make a closed-circuit. We attached copper wires to each sensor for resistance measurements via a source meter, Keithley 2400. We applied the array sensor towards to throat of a healthy subject using the tattoo paper and secured the wires with a Scotch tape (**Figure 4.4a**). We asked the participant to swallow a bolus of 10 gr cracker, 10 mL of water, and their saliva 8 times each since we had 8 strain sensors. The strain signals were measured as the change in resistance in the sensor films, one-by-one, using the source meter. Each strain sensor had slightly different detection performance according to this experiment. **Figure 4.4b** shows the signals from the cracker bolus swallow. Similarly, the water and saliva swallows are shown in **Figure 4.4c** and **Figure 4.4d**, respectively. It is clear from the results that each sensor showed a

slightly different response to strain induced by different boluses. This could be due to the placement of these sensors on the throat. It was interesting to note that each bolus had a difference strain effect on the sensor films. This encouraging experiment motivated us to test our array sensor design with serpentine interconnects.

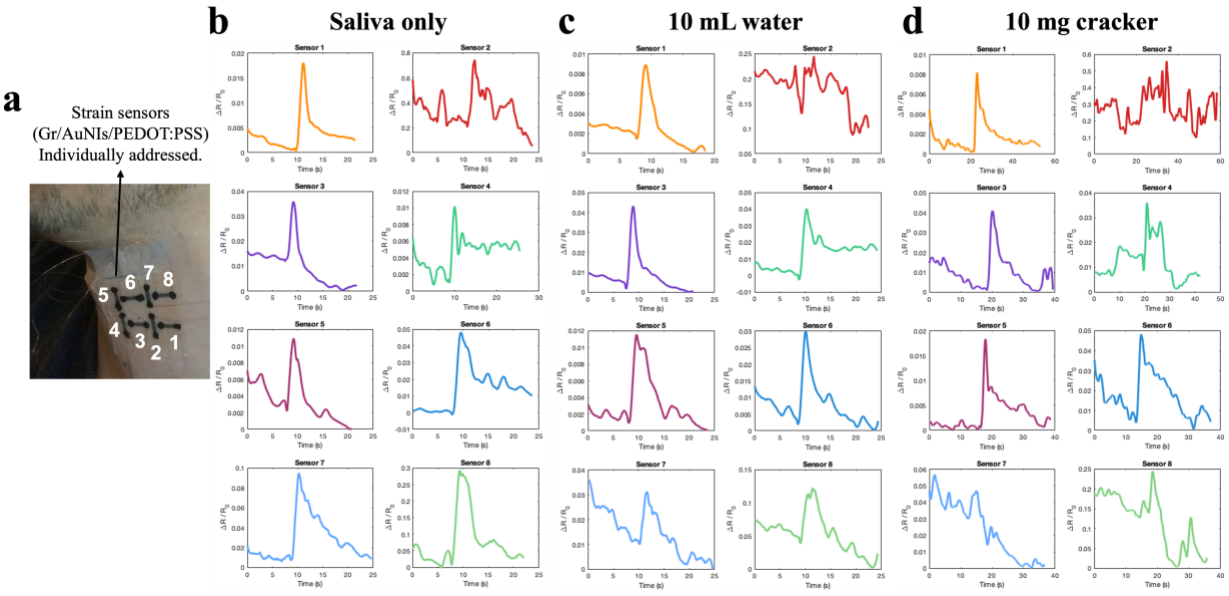

Figure 4.4. On-body experiments performed on a healthy subject without the closed-circuit data acquisition set-up. **(a)** A photograph shows the arrayed-strain sensor placed onto the throat of the subject. **(b)** Detected strain signals from swallowing a 6 gr of cracker, **(c)** 10 mL of water, and **(d)** dry swallow.

Next, we tested the closed-circuit data acquisition design using the Au serpentines on another subject's throat (**Figure 4.5a**). The array sensor patch was applied towards the middle of the participant's throat and secured with a Tegaderm medical tape (**Figure 4.5b**). We first collected the baseline resistance readout from the sensors with a 50 μA supplied current while the participant was in a resting position (**Figure 4.5c**). We then had the participant swallow 10 mL of water 10 seconds after the recording started (**Figure 4.5d**). The response from each strain sensor was varied.

Sensor 1 had a drastic change of resistance during the 10 mL swallow. We suspect that this could have been due to the current source being connected to this sensor. If the resistance between the copper wires and the sensor was too high, the response to any strain was amplified. We concluded that the reason for the large resistance change, which was decided to be unusual for this type of strain sensor, for all the sensor was due to the microcracks and the electrode contacts in the Au serpentine interconnects. This can be avoided in the future by utilizing polyimide (PI) as the support layer for the gold serpentines when using a flexible and soft substrate such as PDMS.

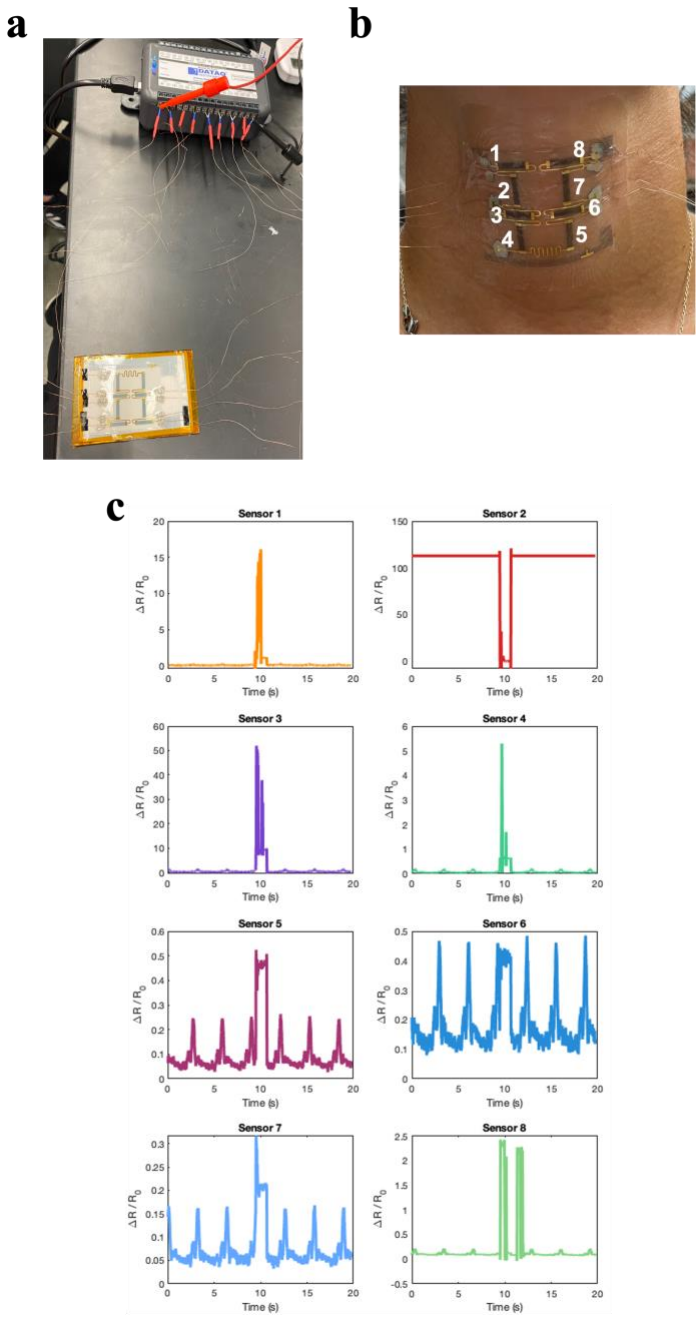

Figure 4.5. On-body experiments performed on a healthy subject with the closed-circuit data acquisition design. **(a)** A photograph showing the array strain sensor on the throat of a subject connected to the 8-channel differential amplifier and the current source. **(b)** A photograph showing the sensor patch placed onto the throat. **(c)** The resistance readout from all the sensors while the participant was swallowing 10 mL of water at around 10 second mark.

4.5 Conclusion

Even with the vast amount of improvement in the epidermal sensors field for detection of swallowing activity, there are still missing areas for a better use of the machine learning algorithms with the data collected. In this chapter, we introduced an alternative arrayed strain sensor design using a previously established fabrication method. The arrayed design allowed for signal collection from all eight strain sensors at the same time on the same wearable patch. We demonstrated this wearable arrayed strain patch on a participant's throat while they were at rest and were swallowing 10 mL of water. Even though this study showed great promise in pursuing an arrayed design, there are still some improvements to be done. We hope this proof-of-concept can inspire the field to create a wearable sensor patch that is able to collect enough samples from a single swallow to be analyzed by a machine learning algorithm that can predict the swallowing conditions of the user.

Acknowledgements

This work was supported by a gift from PepsiCo & the Gatorade Sports Sciences Institute. Additional support was provided by the member companies of the Center for Wearable Sensors in the Jacobs School of Engineering at the University of California, San Diego, including Dexcom, Gore, Honda, Huami, Instrumentation Laboratory, Kureha, Merck KGaA, PepsiCo, Roche, Samsung, and Sony. L.B. acknowledges the support provided by the National Science Foundation Graduate Research Fellowship Program under Grant DGE-2038238. This work was performed in part at the San Diego Nanotechnology Infrastructure (SDNI), a member of the National Nanotechnology Coordinated Infrastructure, which is supported by the National Science Foundation (Grant ECCS-1542148).

Chapter 4, in part, is under preparation for publication of the material. Beril Polat, Tarek Rafeedi, and Darren J. Lipomi. 2023.

References

(1) Eisbruch, A.; Schwartz, M.; Rasch, C.; Vineberg, K.; Damen, E.; Van As, C. J.; Marsh, R.; Pameijer, F. A.; Balm, A. J. M. Dysphagia and Aspiration after Chemoradiotherapy for Head-and-Neck Cancer: Which Anatomic Structures Are Affected and Can They Be Spared by IMRT? *Int. J. Radiat. Oncol. Biol. Phys.* **2004**, *60* (5), 1425–1439. https://doi.org/10.1016/j.ijrobp.2004.05.050.

(2) Hutcheson, K. A.; Lewin, J. S.; Barringer, D. A.; Lisec, A.; Gunn, G. B.; Moore, M. W. S.; Holsinger, F. C. Late Dysphagia after Radiotherapy-Based Treatment of Head and Neck Cancer. *Cancer* **2012**, *118* (23), 5793–5799. https://doi.org/10.1002/cncr.27631.

(3) Cooper, J. S.; Fu, K.; Marks, J.; Silverman, S. Late Effects of Radiation Therapy in the Head and Neck Region. *Int. J. Radiat. Oncol. Biol. Phys.* **1995**, *31* (5), 1141–1164. https://doi.org/10.1016/0360-3016(94)00421-G.

(4) Martin-Harris, B.; McFarland, D.; Hill, E. G.; Strange, C. B.; Focht, K. L.; Wan, Z.; Blair, J.; Mcgrattan, K. Respiratory-Swallow Training in Patients with Head and Neck Cancer. *Arch. Phys. Med. Rehabil.* **2015**, *96* (5), 885–893. https://doi.org/10.1016/j.apmr.2014.11.022.

(5) Ciarambino, T.; Sansone, G.; Para, O.; Giordano, M. Dysphagia: What We Know? A Minireview. *J. Gerontol. Geriatr.* **2021**, *69* (3), 188–194. https://doi.org/10.36150/2499-6564-N241.

(6) Feng, W.; Zheng, W.; Gao, F.; Chen, X.; Liu, G.; Hasan, T.; Cao, W.; Hu, P. Sensitive Electronic-Skin Strain Sensor Array Based on the Patterned Two-Dimensional α-In2Se3. *Chem. Mater.* **2016**, *28* (12), 4278–4283. https://doi.org/10.1021/acs.chemmater.6b01073.

(7) Gao, Y.; Li, Q.; Wu, R.; Sha, J.; Lu, Y.; Xuan, F. Laser Direct Writing of Ultrahigh Sensitive

SiC-Based Strain Sensor Arrays on Elastomer toward Electronic Skins. *Adv. Funct. Mater.* **2019**, *29* (2), 1–9. https://doi.org/10.1002/adfm.201806786.

(8) Suzuki, K.; Nakagawa, R.; Zhang, Q.; Miura, H. Development of Highly Sensitive Strain Sensor Using Area-Arrayed Graphene Nanoribbons. *Nanomaterials* **2021**, *11* (7). https://doi.org/10.3390/nano11071701.

(9) Pei, Z.; Zhang, Q.; Liu, Y.; Zhao, Y.; Dong, X.; Zhang, Y.; Zhang, W.; Sang, S. A High Gauge-Factor Wearable Strain Sensor Array via 3D Printed Mold Fabrication and Size Optimization of Silver-Coated Carbon Nanotubes. *Nanotechnology* **2020**, *31* (30). https://doi.org/10.1088/1361-6528/ab8592.

(10) Ramírez, J.; Rodriquez, D.; Qiao, F.; Warchall, J.; Rye, J.; Aklile, E.; Chiang, A. S. C.; Marin, B. C.; Mercier, P. P.; Cheng, C. K.; Hutcheson, K. A.; Shinn, E. H.; Lipomi, D. J. Metallic Nanoislands on Graphene for Monitoring Swallowing Activity in Head and Neck Cancer Patients. *ACS Nano* **2018**, *12* (6), 5913–5922. https://doi.org/10.1021/acsnano.8b02133.

(11) Ramírez, J.; Rodriquez, D.; Urbina, A. D.; Cardenas, A. M.; Lipomi, D. J. Combining High Sensitivity and Dynamic Range: Wearable Thin-Film Composite Strain Sensors of Graphene, Ultrathin Palladium, and PEDOT:PSS. *ACS Appl. Nano Mater.* **2019**, *2* (4), 2222–2229. https://doi.org/10.1021/acsanm.9b00174.

(12) Ramírez, J.; Urbina, A. D.; Kleinschmidt, A. T.; Finn, M.; Edmunds, S. J.; Esparza, G. L.; Lipomi, D. J. Exploring the Limits of Sensitivity for Strain Gauges of Graphene and Hexagonal Boron Nitride Decorated with Metallic Nanoislands. *Nanoscale* **2020**, *12* (20), 11209–11221. https://doi.org/10.1039/d0nr02270e.

(13) Marin, B. C.; Root, S. E.; Urbina, A. D.; Aklile, E.; Miller, R.; Zaretski, A. V.; Lipomi, D. J. Graphene-Metal Composite Sensors with Near-Zero Temperature Coefficient of Resistance. *ACS Omega* **2017**, *2* (2), 626–630. https://doi.org/10.1021/acsomega.7b00044.

(14) Polat, B.; Becerra, L. L.; Hsu, P. Y.; Kaipu, V.; Mercier, P. P.; Cheng, C. K.; Lipomi, D. J. Epidermal Graphene Sensors and Machine Learning for Estimating Swallowed Volume. *ACS Appl. Nano Mater.* **2021**, *4* (8), 8126–8134. https://doi.org/10.1021/acsanm.1c01378.

(15) Zaretski, A. V.; Root, S. E.; Savchenko, A.; Molokanova, E.; Printz, A. D.; Jibril, L.; Arya, G.; Mercola, M.; Lipomi, D. J. Metallic Nanoislands on Graphene as Highly Sensitive Transducers of Mechanical, Biological, and Optical Signals. *Nano Lett.* **2016**, *16* (2), 1375–1380. https://doi.org/10.1021/acs.nanolett.5b04821.

Appendix A Supporting Information for Chapter 2

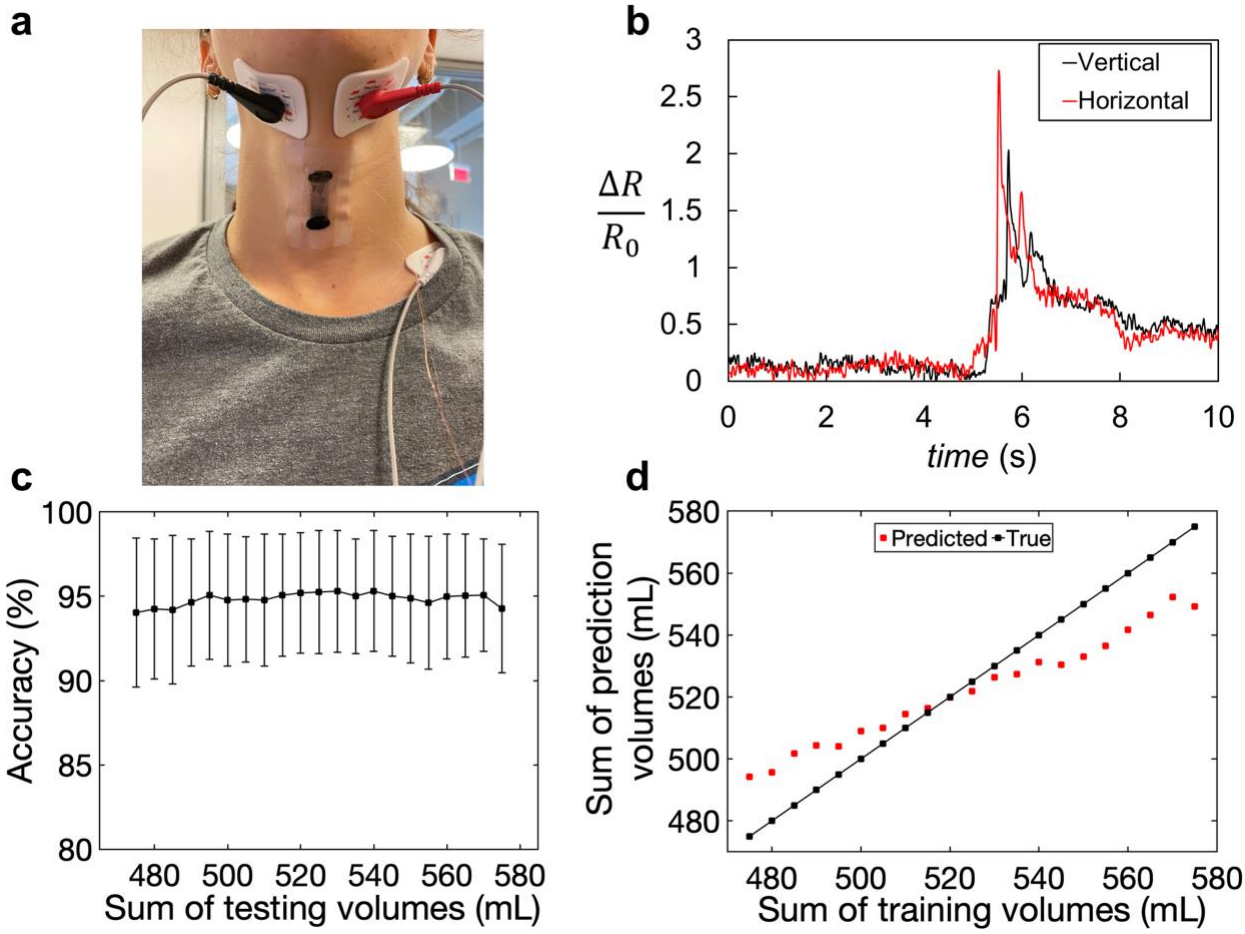

Figure A.1. Evaluation of vertical position for the strain sensor on the throat. **(a)** The picture shows a vertically positioned strain sensor on the participant's throat. **(b)** The plot compares the collected raw swallow data from the same strain sensor placed horizontally and vertically on the same participant. It is important to note that the strain sensor was first tested with the horizontal position and then with the vertical position. **(c)** and **(d)** show the results of the prediction algorithm using the 60 swallows from the vertical position.

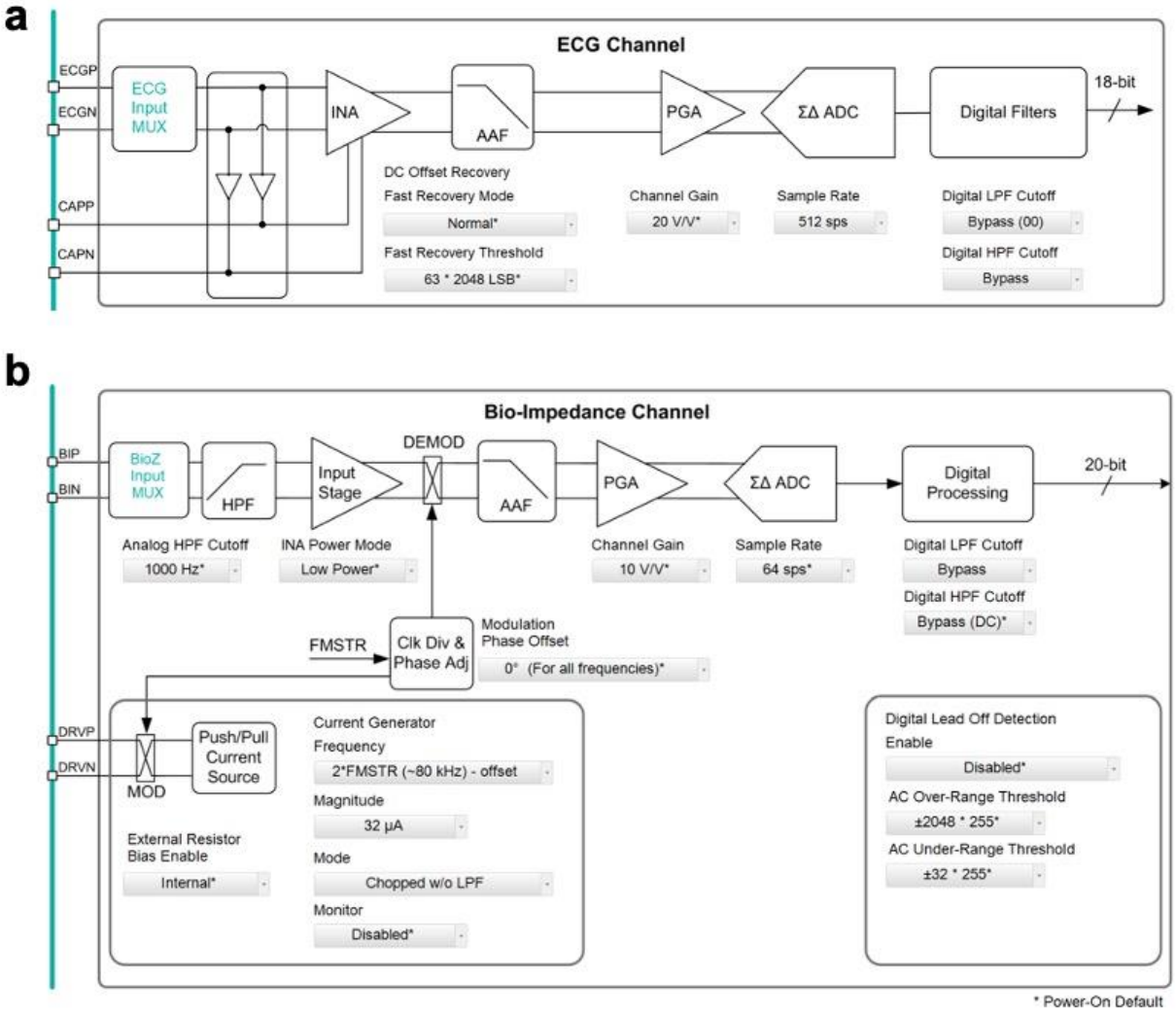

Figure A.2. MAX30001 Evaluation Kit channels (EMG/ECG and BioImpedance/BioZ). **(a)** A detailed functional block diagram of the ECG channel that was used for recording the sEMG signals. **(b)** A detailed functional block diagram of the Bio-Impedance channel that was used for recording the strain signals. Reproduced with permission from the Data Sheet for MAX30001/MAX30002 Evaluation Kit by Maxim Integrated Products, Inc., 2018 (www.maximintegrated.com). Copyright (C) 2018 Maxim Integrated Products, Inc., All Rights Reserved.

Swallow Peak Detection Algorithm

Input: data **y**, time **t**

Output: peak index **mxP**

Start
T = number of time samples
mxI = 1
mxS = $-\infty$

For k = 1 : T
    S = $\frac{\partial y(t_k)}{\partial t}$
    If S > mxS
        S = mxS
        mxI = k
    end If
end For loop
mxP = mxI
For m = mxI : T
    If $y(t_m) \geq y(t_{mxI}) and \ \frac{\partial y(t_m)}{\partial t} \geq 0$
        mxP = m
    else
        break For loop
    end If
end For loop
return mxP
end

Figure A.3. Swallow peak detection algorithm. The algorithm identifies the swallow peak by detecting the largest timing slope in the strain data. We denote the strain data as a function of time t, and we have data $\boldsymbol{y} = \boldsymbol{f}(\boldsymbol{t})$.

Table A.1. Strain sensor features. The table shows some of the representative extracted features from the strain sensor in each swallowed volume. Columns 2-4 show the duration (distance) of each fiducial point. Columns 5-7 show the magnitude (height) of each fiducial point. Columns 8-10 show the slopes between each fiducial point. Columns 11-13 show the curve-fitting parameters.

Volume (mL)	Distance between 1st and 2nd	Distance between 1st and 3rd	Distance between 1st and 4th	Amplitude of 2nd	Amplitude of 3rd	Amplitude of 4th	Slope from 1st to 2nd	Slope from 2nd to 3rd	Slope from 3rd to 4th	Curvature	Kernel 1	Kernel 2
5	0.33	0.48	0.59	0.0266	0.0225	0.0234	-2.35	-1.25	0.39	2.96	-1.18	-1.01
10	0.35	0.51	0.58	0.0218	0.0187	0.0189	-1.50	-0.87	-0.12	1.91	-0.77	-2.26
15	0.34	1.02	1.23	0.0224	0.0073	0.0105	-3.02	0.56	0.57	3.80	-1.54	-0.64
20	0.54	0.80	1.04	0.0246	0.0183	0.0198	0.15	0.32	0.44	0.00	-0.06	-0.17
25	0.34	0.51	0.77	0.0233	0.0194	0.0325	-2.78	-1.61	0.78	3.35	-1.29	-1.27
30	0.30	0.66	0.97	0.0220	-0.0004	0.0172	-4.17	0.82	1.52	4.99	-1.94	-1.42

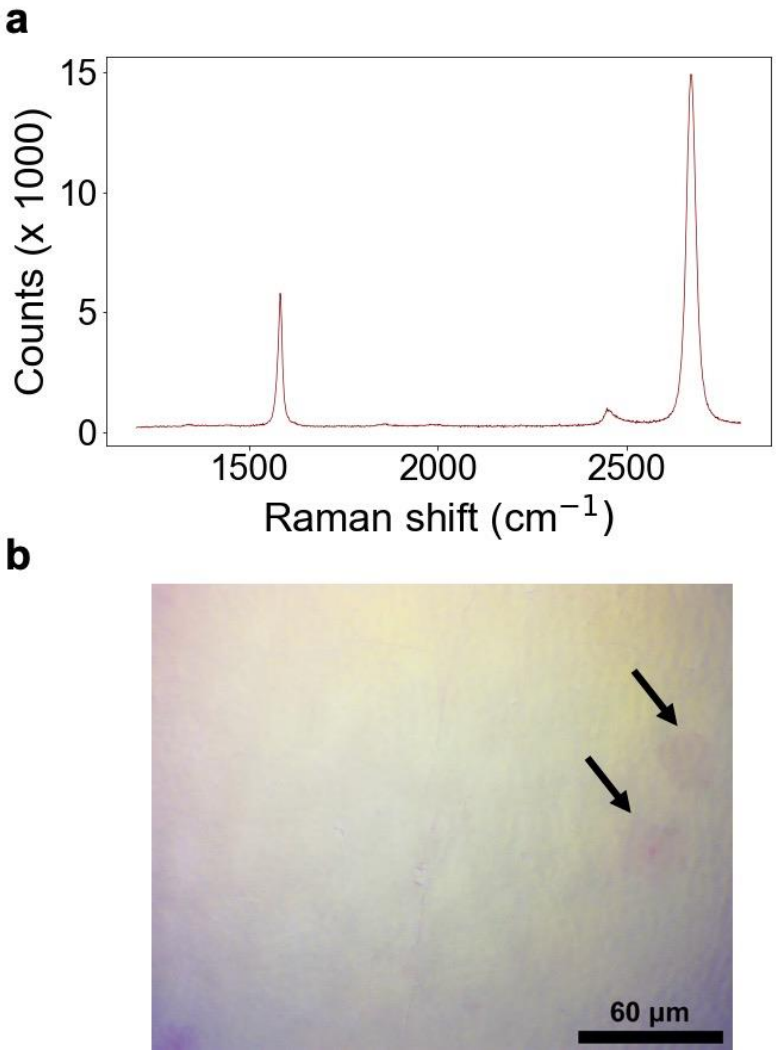

Figure A.4. Material specifications of monolayer graphene. **(a)** Raman spectra of the monolayer graphene. **(b)** Optical microscopy image of the graphene after it was transferred to a silicon wafer with a 90nm layer of SiO_2. The arrows show the darker regions of adlayers in the film. Note: The single-layer graphene used in the strain sensors was purchased commercially from GrollTex, Inc. which specializes in growing high-purity monolayer film of graphene on copper. The graphene is grown via Chemical Vapor Deposition (CVD) on a copper foil. The product specifications can be found on this website (https://grolltex.com/product/monolayer-graphene-on-copper-foil-6-x-6-150-mm-x-150-mm/). We used the batch number SC-200520-2-6x6C. According to the manufacturer's analysis, the monolayer graphene coverage was 100% on the copper foil with sporadic adlayers present (see Figure S4b). The transparency was >97%. The FET mobility was measured to be >2700 $cm^2/(V.s)$ on 90 nm SiO_2 on Si wafer and the sheet resistance was 430 ± 50 Ohm/sq. The process specific grain size was >80 µm. The Raman D/G ratio was 0.03 which confirmed that the sample was single-layer graphene.

Appendix B Supporting Information for Chapter 3

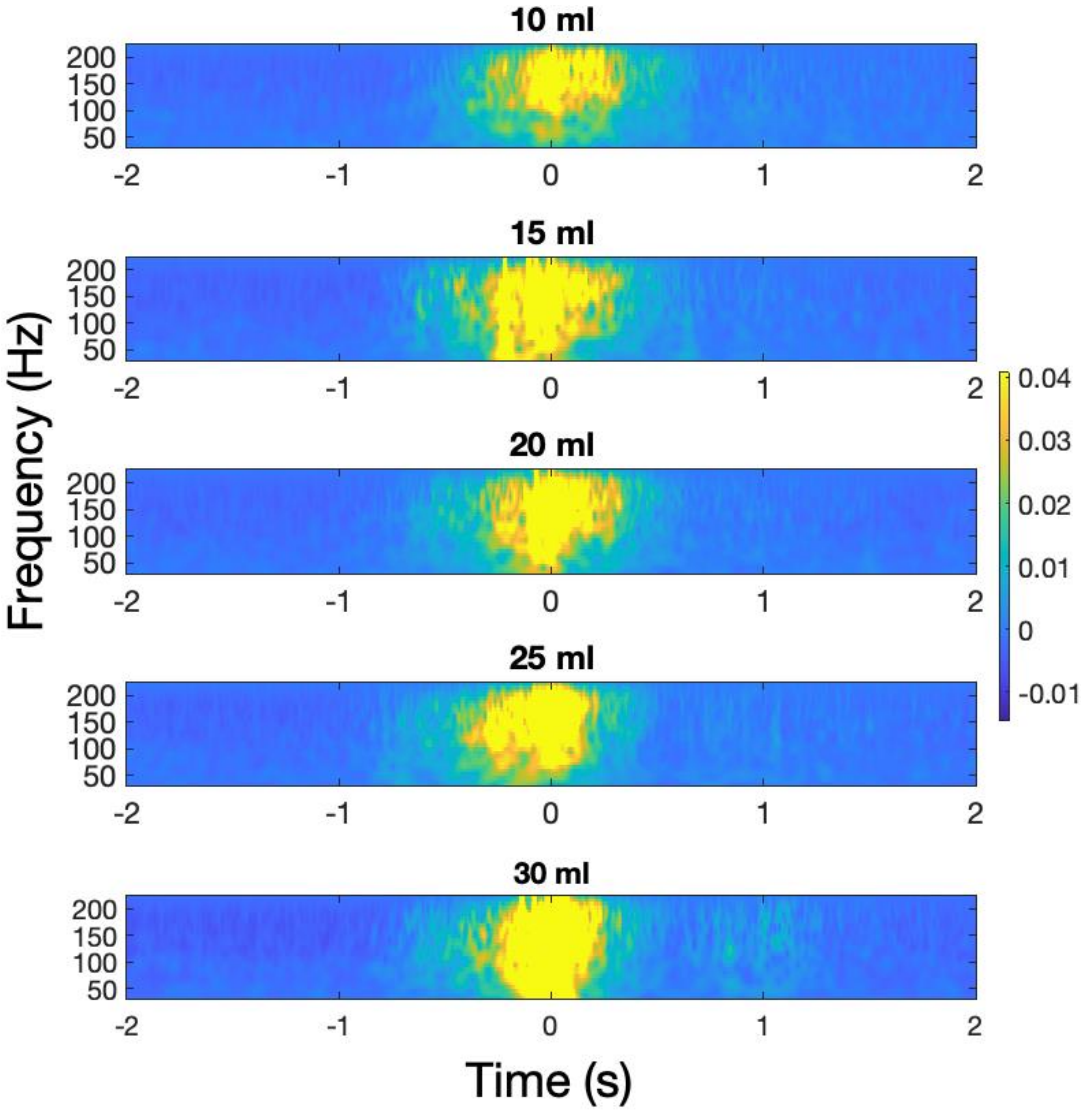

Figure B.1. Wavelet transform analysis of the sEMG signals for each swallowed volume for feature extraction. The colors indicate the power of the frequencies in the signal.

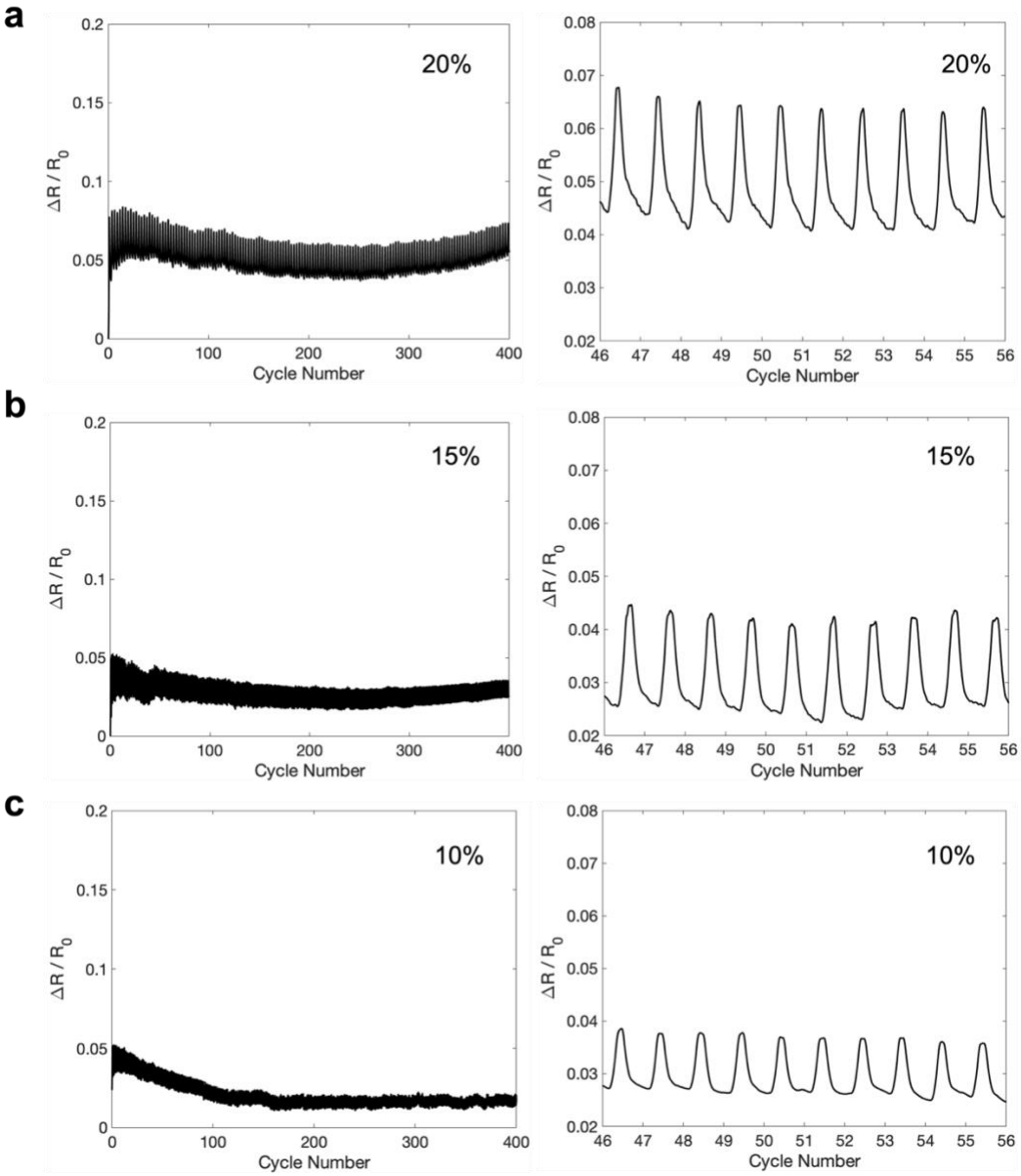

Figure B.2. Cyclic piezoresistive measurements of Block-6 films. The plots show the piezoresistive response for all the cycles stretching up to **(a)** 20% strain, **(b)** 15% strain, and **(c)** 10% strain with a zoomed-in section from the corresponding experiment.

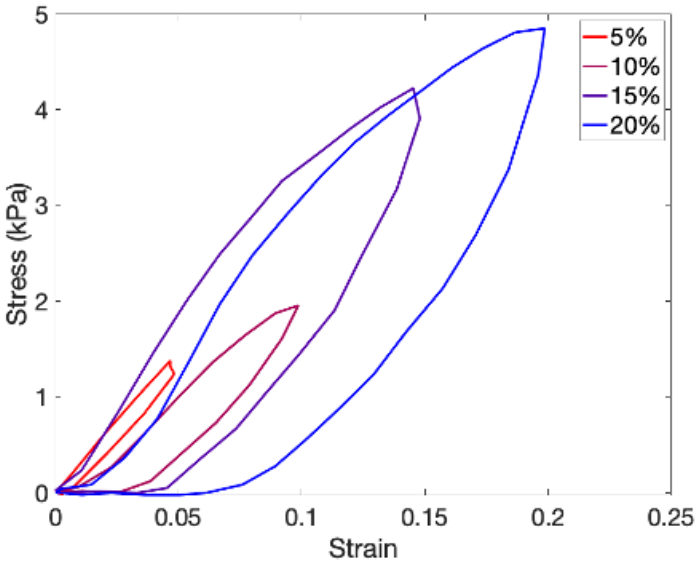

Figure B.3. Stress-strain response of Block-6 films for 5, 10, 15, and 20% strains.

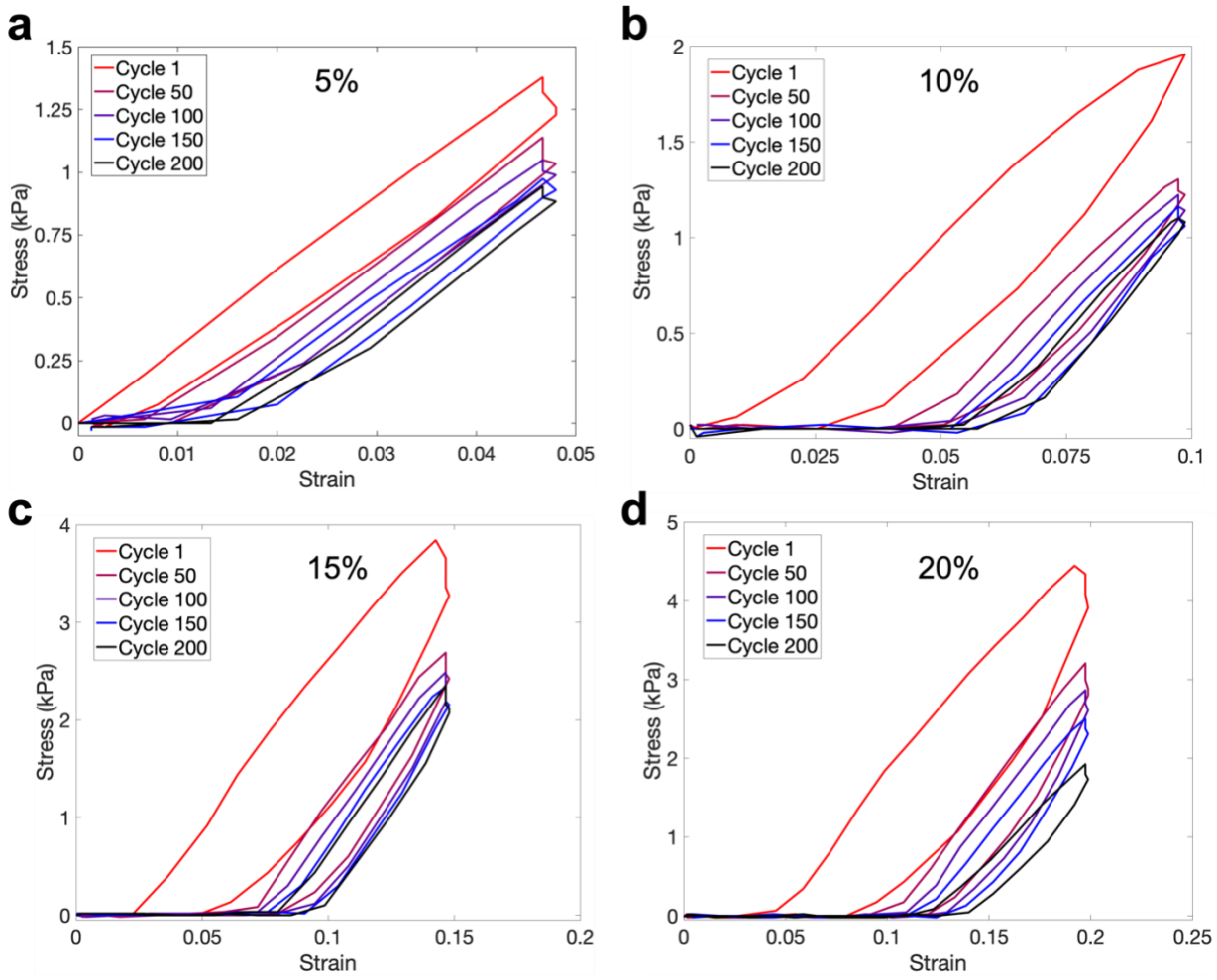

Figure B4. Cyclic stress-strain response of Block-6 films for 10, 15, and 20% strain for cycles 1, 50, 100, 150, and 200.

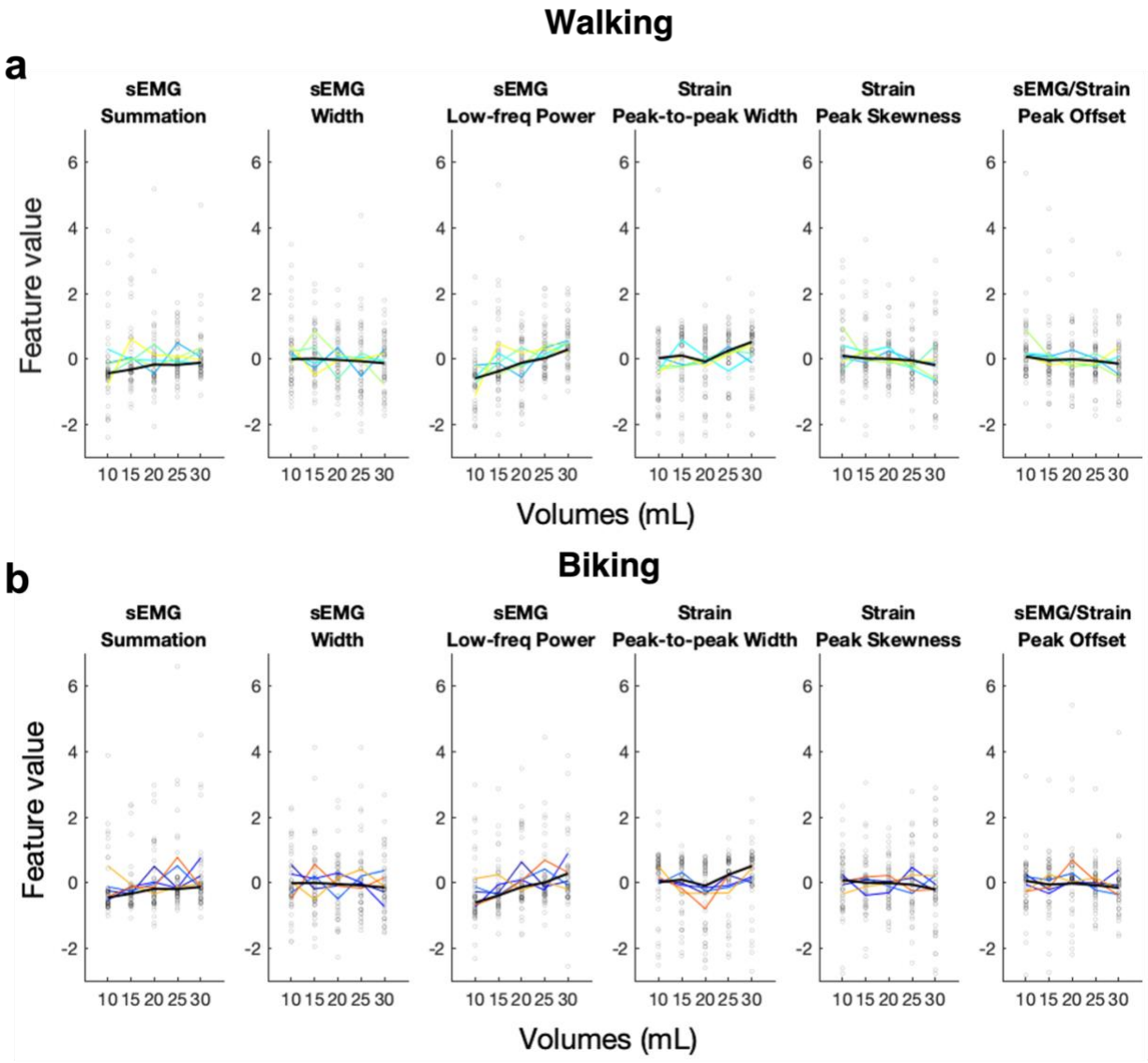

Figure B5. The correlation between the swallowed volumes and the signal features separated for walking and biking experiments.